DOI:10.14753/SE.2015.1828

DEVELOPMENT OF NOVEL SURGICAL, IMAGING AND MOLECULAR METHODS FOR THE IN VIVO MODELING OF PREECLAMPSIA

PhD thesis

Gábor Szalai, MD

Doctoral School of Clinical Medicine
Semmelweis University

Supervisor: Nándor Gábor Than, MD, PhD

Official Reviewers: Péter Tamás, MD, PhD
Sándor Valent, MD, PhD

Head of the Final Examination Committee:
Ferenc Perner, MD, DSc

Members of the Final Examination Committee:
Artúr Beke, MD, PhD
Zorán Belics, MD, PhD

Budapest
2015

DOI:10.14753/SE.2015.1828

TABLE OF CONTENTS

DOI:10.14753/SE.2015.1828

DOI:10.14753/SE.2015.1828

DOI:10.14753/SE.2015.1828

LIST OF ABBREVIATIONS

Ad:	Adenovirus vector
Ad-RGD:	RGD fiber-mutant adenovirus vector
AT1:	Angiotensin II receptor 1
cDNA:	Complementary deoxyribonucleic acid
CMV:	Cytomegalovirus
DHHS:	Department of Health and Human Services
DIC:	Disseminated intravascular coagulation
DLAR:	Division of Laboratory Animal Resources
DSI:	Data Sciences International Inc.
EM:	Experimental mouse
FLT1:	Fms-like tyrosine kinase-1 gene
FW:	Fetal weight
GFP:	Green fluorescent protein
GD:	Gestational day
HELLP syndrome:	Hemolysis, elevated liver enzymes and low platelets syndrome
H&E:	Hematoxylin and eosin
sHLA:	Human leukocyte antigen
hsFlt-1:	Human soluble fms-like tyrosine kinase-1
IACUC:	Institutional Animal Care and Use Committee
IUFD:	Intrauterine fetal demise
IUGR:	Intrauterine growth restriction
KIR:	Killer-cell immunoglobulin-like receptors
LME:	Linear mixed effects
MAP:	Mean arterial blood pressure
mRNA:	Messenger ribonucleic acid
msFlt-1:	Mouse soluble fms-like tyrosine kinase-1
NET:	Neutrophil extracellular trap
NICHD:	National Institute of Child Health and Human Development
NIH:	National Institutes of Health of the USA

DOI:10.14753/SE.2015.1828

NO:	Nitric oxide
NK cell:	Natural killer cell
PAS:	Periodic acid Schiff
PBS:	Phosphate-buffered saline
PE:	Preeclampsia
PFU:	Plaque-forming units
PFR:	Placental/fetal weight ratio
PlGF:	Placental growth factor
PPD:	Postpartum day
PW:	Placental weight
qRT-PCR:	Quantitative real-time reverse transcription polymerase chain reaction
RDS:	Respiratory distress syndrome
SGA:	Small-for-gestational age
sEng:	Soluble endoglin
sFlt-1:	Soluble fms-like tyrosine kinase-1
SMA:	Smooth muscle actin
STBM:	Syncytiotrophoblast microparticle
TMA:	Tissue microarray
VEGF:	vascular endothelial growth factor
VEGFR1:	Vascular endothelial growth factor receptor 1

DOI:10.14753/SE.2015.1828

1. INTRODUCTION

1.1. Preeclampsia is a 'Great Obstetrical Syndrome'

The 'Great Obstetrical Syndromes' are major causes of maternal and fetal morbidity and mortality with various effects on the mother and her fetus. These syndromes are characterized by multiple etiologies, frequent fetal involvement, clinical manifestations which are often adaptive in nature, and gene–environment interactions that may predispose to the syndromes [1-3]. Among the 'Great Obstetrical Syndromes', the most severe maternal and fetal consequences are often observed in preeclampsia, preterm labor, preterm premature rupture of membranes, intrauterine growth restriction (IUGR), and stillbirth [1-3].

Preeclampsia is one of the most severe obstetrical syndrome [2,3], which complicates 3-5% of pregnancies, and has a high incidence of maternal and fetal morbidity and mortality [4-11]. Preeclampsia is a leading cause of maternal (10-15%), perinatal and neonatal (10%) death worldwide [8,9,11]. The clinical diagnosis of preeclampsia is based on new-onset hypertension and proteinuria in formerly normotensive women developing after the 20th week of gestation. The complications of preeclampsia could include multi-organ failure mostly affecting the central nervous system, the kidneys and the liver. The general endothelial damage and multisystem failure caused by preeclampsia is characteristic to human pregnancies, since preeclampsia has not been detected in any other species except some anecdotal cases in a few anthropoid primates (i.e. gorillas and chimpanzees) [12-14]. The central role of the placenta in the pathogenesis of preeclampsia is unquestionable [11], and the definitive treatment of preeclampsia is still the delivery of the placenta [7,9,15,16]. Preeclampsia may be characterized by severe maternal and fetal complications like IUGR, intrauterine fetal demise (IUFD), preterm parturition, low birth weight, hemolysis elevated liver enzymes and low platelets (HELLP) syndrome, and with a very higher incidence of maternal and fetal morbidity and mortality [11]. It should also be emphasized that the long term consequences of preeclampsia may include chronic hypertension, ischemic cardiovascular disease, stroke, metabolic syndrome and diabetes, which could be developed among growth-restricted fetuses and their mothers affected by severe preeclampsia [11,17,18].

1.1.1. Diagnostic criteria for preeclampsia

In our studies we used the diagnostic criteria for preeclampsia proposed by the United States National High Blood Pressure Education Program Working Group on High Blood Pressure in Pregnancy, which has been standardly used in clinical studies for more than a decade [5,9,11,19]. According to this, the clinical definition of preeclampsia included new-onset hypertension and proteinuria after 20 weeks of gestation in women with previously normal blood pressures. Elevated blood pressures were diagnosed in case of systolic and/or diastolic blood pressures of ≥140 and/or ≥90 mm Hg measured at two or more different time points, at least 4 hours but not more than 1 week apart. Proteinuria was diagnosed in case of ≥300 mg protein measured in a 24 hour urine sample, or two random urine specimens obtained at least 4 hours but not more than 1 week apart containing ≥1+ protein on a dipstick [11].

1.1.2. Preeclampsia subforms

Based on the time of the onset of the clinical symptoms, preeclampsia can be divided into early-onset (<34 weeks of gestation) and late-onset (>34 weeks) disease [9,11,20-22]. Most cases are late-onset, with 75% developing after 37 weeks of gestation [9,23,24], and ~6% of cases occurring postpartum [11,25]. Late-onset preeclampsia is typically mild and occurs with less severe maternal and fetal complications than early-onset preeclampsia [20,26,27]. Early-onset preeclampsia has a higher incidence of perinatal and maternal morbidity and mortality, and a more frequent association with HELLP syndrome, IUGR, preterm birth, and stillbirth [6,9,11,20,26,28-40].

1.1.3. Epidemiology

Preeclampsia is one of the leading cause of perinatal morbidity and mortality, as this syndrome has a prevalence of 3-5% worldwide and in developing countries the problem is even more complicated, since there are limited resources for perinatal care which could also have a strong negative effect on perinatal outcomes [9,11,19]. In certain geographic areas (e.g. Africa, Asia) and among certain ethnic or social groups (e.g. African-American women), the incidence of preeclampsia could be three times higher than in the rest of the world [11,41,42]. Moreover, severe seizures – so-called eclampsia – develop in 2-3 cases among every 10,000 patient in Europe, while eclampsia is 10-30 times more frequent in

developing countries [19,43]. Because of these reasons, maternal mortality due to preeclampsia is higher in developing countries than in high-income developed countries [10,19]. The increase in the incidence of pre-existing diseases including chronic hypertension, diabetes and obesity might be the reason why the incidence of preeclampsia has been increasing in developed countries such as the USA [19,44,45].

1.1.4. Risk factors

Several factors could augment the risk of preeclampsia and escalate the symptoms and severity, such as younger or older maternal age (<20 years and >40 years), nulliparity, infections (e.g. urinary tract infection), chronic inflammation, metabolic dysfunctions (e.g. diabetes mellitus), high body mass index, thrombophilias, chronic renal failure or preeclampsia in a previous pregnancy. A new partner may also increase the risk because of the short term exposure of sperm which could hamper the maternal immune tolerance to paternal antigens. Interestingly, "dangerous fathers" who have already fathered a preeclamptic pregnancy have high risk of fathering another pregnancy complicated by preeclampsia with the same woman or with a new partner. Of note, the inhibition of NK cell functions by the combination of maternal inhibitory KIRs (AA genotype) on uterine NK cells and HLA-C2 antigens on trophoblasts also increases the risk of preeclampsia. On the other hand, smoking reduces the risk of preeclampsia [7,9,11,30,31,34,46-48].

1.1.5. Maternal and fetal outcomes

Preeclampsia is a major cause of maternal and perinatal morbidity and mortality, and numerous factors have influence on the outcomes of preeclampsia such as preexisting maternal diseases, the severity and the time of the onset of preeclampsia, and the treatment of the clinical symptoms and complications. The clinical outcomes of preeclampsia are more benign among women with late-onset preeclampsia who have milder symptoms, and these are more severe among women with early-onset preeclampsia with severe symptoms and with pre-existing multisystem disorders like diabetes mellitus, hypertension or renal failure [9,32,37]. The 10-15% of the half million *maternal deaths* worldwide is due to the severe complications of preeclampsia such as seizures (eclampsia), cerebrovascular hemorrhages, renal and liver failure, liver rupture, lunge edema, and disseminated intravascular coagulation (DIC) [11,16,23,49].

Preeclampsia is also the cause of 500,000 *perinatal and neonatal deaths* worldwide in every year. Perinatal mortality mainly results from placental abruption, asphyxia, IUFD, IUGR, preterm birth [9,11]. The incidence of *perinatal and neonatal mortality* caused by preeclampsia is higher when associated with HELLP syndrome and in cases of early-onset syndrome [11]. *Maternal morbidity* is multifarious due to multi-organ failure of the kidneys, brain and liver. The generalized endothelial damage may typically affect the glomeruli of the kidneys, leading to proteinuria, oliguria or anuria. The effects on the brain may range from headache and visual disturbances to a rapid progress to eclampsia, cerebral hemorrhage or encephalopathy. The epigastric pain draws attention to liver failure or could be a sign of subcapsular liver hematoma. Also, generalized endothelial damage may lead to hypertension and development of intravascular coagulation activation [9,11,19,50]. In preeclampsia, *perinatal and neonatal morbidity* primarily depends on the gestational age of the fetus at delivery, the severity of maternal symptoms, and the infrastructure of the neonatal care unit. Preterm birth is the biggest problem in early-onset preeclampsia, particularly the outcome is very poor before 25 weeks of gestation and below a birth weight of 700g. The risk of asphyxia, respiratory distress syndrome (RDS) and neonatal thrombocytopenia associated with HELLP syndrome increases with prematurity and low birth-weight [9,11,31,46,50-52].

1.2. Pathophysiology and molecular mechanisms

1.2.1. Placental pathophysiology

The origins of preeclampsia lie in the placenta, as the clinical symptoms of this syndrome usually diminish within 24-48 hours after the delivery of the placenta, and the presence of the fetus is not required for the development of this obstetrical syndrome [19,46,53-57]. Preeclampsia is associated with placental histopathological lesions consistent with defective invasion of extravillous trophoblasts into the decidua and myometrium [58-66], a phenomenon that may be linked to changes in placental gene expression [67-75] and immune maladaptation [73,76-83]. As a consequence, the failure of physiologic transformation of the spiral arteries by these trophoblasts into low resistance vessels impairs the continuous blood supply of the placenta, leading to hemorheological changes, as well as endoplasmic, nitrosative, and oxidative stress of the placenta [19,56,84-88]. Because of the extensive placental damage and loss of

function, early-onset preeclampsia is frequently associated with IUGR [9,11,20,28,30,47]. On the contrary, placental histopathological changes are less frequent in late-onset preeclampsia [11,30,68,89-93], where IUGR occurs infrequently or even overgrowth of the fetus can be seen [20,27,93,94]. It has recently been suggested that in these late-onset preeclampsia cases the overcrowding of the placental villi may cause placental stress, leading to the "terminal pathway" of preeclampsia [95].

1.2.2. The terminal pathway of preeclampsia

The current hypothesis about the development of preeclampsia implies that the placental stage is followed by a maternal stage, which includes the activation of this terminal pathway [9,16,19,30,33,46,47,50,56,96-104]. It has been shown that the injured placenta can excessively release various factors, such as apoptotic-necrotic trophoblast debris called syncytiotrophoblast microparticles (STBMs), soluble anti-angiogenic molecules, cytokines, and yet unknown factors [16,46-48,68,69,71,74,97,99,104-119], which, in turn, lead to exaggerated maternal immune activation [46,47,118-125] and generalized endothelial cell dysfunction, including the damage of the glomeruli [15,46,47,49,101,103,126-133]. This terminal pathway, characterized by an imbalance of of angiogenic [e.g. placental growth factor (PlGF)] and anti-angiogenic [e.g. soluble fms-like tyrosine kinase-1 (sFlt-1) and soluble endoglin (sEng)] factors has been extensively investigated [15,48,49,75,96,97,104-109,112,117,134-177].

1.2.3. Angiogenic – anti-angiogenic imbalance

Of major interest, the overactivation of anti-angiogenic pathways and inhibited placental angiogenesis in the second half of pregnancy have been identified as central to the pathogenesis of preeclampsia and some others among the 'Great Obstetrical Syndromes' [15,49,96,97,100,102,104-109,112,115,134,137-139,141-147,149-157,159-167,169-174,178,179]. Preeclampsia is characterized by the increased placental expression and maternal systemic concentrations of anti-angiogenic molecules, and decreased maternal concentrations of angiogenic molecules [15,48,49,75,96,97,104-109,112,117,134-177,180,181]. Longitudinal studies have shown that the increase in sFlt-1 and the decrease in PlGF concentrations precede the clinical onset of preeclampsia by several weeks [96,97,145,147,153,157,159,162]. Some studies have even provided evidence for

the placental overexpression of sFlt-1 in preeclampsia, suggesting that the major source of circulating sFlt-1 is the placenta [112,182-184], which would explain why the delivery of the placenta relieves the clinical symptoms of preeclampsia [19,46,53-57,61,109,185]. Since sFlt-1 is a decoy receptor for PlGF and VEGF, its increased concentrations in maternal blood decrease the bioavailability of angiogenic factors, severely inhibiting placental angiogenesis and maternal endothelial functions in the kidneys and in the systemic circulation, leading to an anti-angiogenic state, generalized endothelial dysfunction, hypertension and proteinuria in the second half of pregnancy, preceding the onset of clinical symptoms [15,16,49,56,96,97,104-108,112,135,137-141,143-147,149,150,152-155,157,159-164,166-174,185].

1.2.4. Alterations in the renin-angiotensin system

Besides the anti-angiogenic imbalance, the renin-angiotensin system (RAS) has also been implicated in the development of preeclampsia. Angiotensin II elevates blood pressure due to generalized vasoconstriction by binding to the angiotensin II receptor (AT1) [56,186]. Of note, women with preeclampsia are more sensitive to angiotensin II [56,187], and autoantibodies against AT1, which could elevate blood pressure, were found frequently in women with preeclampsia [188-190]. As a functional evidence of their pathophysiological role, AT1 autoantibodies isolated from sera of women with preeclampsia could induce placental sFlt-1 production, angiogenic imbalance and maternal endothelial dysfunction in pregnant mice [190,191]. Moreover, if persisting beyond pregnancy, AT1 autoantibodies could increase the risk of chronic cardiovascular disease in women with preeclampsia [16,50,192-194].

1.2.5. Systemic inflammatory response, endothelial dysfunction and coagulopathy

Besides the imbalance in angiogenic factors and the role of the RAS, preeclampsia is characterized by an excessive activation of the maternal innate immune system [65,195], including the complement [117,195-200] and neutrophils [195,201-203]. In fact, the extent of neutrophil activation is larger in preeclampsia than in sepsis [66,204-206]. This is due to the excessive release of placental microparticles (STBMs) [67,120], which can trigger the release of neutrophil extracellular traps (NETs) [19,202,203]. Since NETs promote coagulation [68,207], the excessive presence of NETs in the

intervillous space [19,202] could lead to maternal underperfusion of the placenta [20,203], further contributing to ischemic placental stress [48,86,208]. As a result of the exaggerated systemic inflammatory response, increased platelet activation, generalized endothelial damage, and the imbalance of vasodilatative (e.g. NO) and vasoconstrictive (e.g. thromboxane A2) factors, the increased intravascular coagulation may lead to *thrombotic microangiopathy*. Due to the microangiopathy of the small vessels, the damaged endothelial and intimal layers cause fragmentation of erythrocytes, triggering *microangiopathic hemolytic anaemia*. *Thrombocytopenia* is the result of enhanced local platelet consumption at damage sites of the endothelium. *Disseminated intravascular coagulation (DIC),* hemorrhage and multi-organ failure could be the eventual result of intravascular coagulopathy and endothelial dysfunction [11,32,35,37,46,47,118-125,209].

1.3. sFlt-1 isoforms

Since the role of sFlt-1 is unquestionable in the terminal pathway of preeclampsia, it has gained much attention in the past decade. Flt-1 was first characterized in 1990, when Shibuya et al. determined the nucleotide sequence of its encoding cDNA [210-212]. It was revealed that Flt-1 contains seven extracellular Ig-like domains and an intracellular tyrosine kinase domain [210-212] (**Figure 1A**). Later, Flt-1 was shown to bind VEGF and PlGF [211-213] and important for embryonic vascular development [212,214]. It was also revealed that the first three extracellular Ig-like domains of Flt-1 are essential for ligand-binding, while the 4-7th extracellular Ig-like domains for receptor dimerization [211,215-217]. In 1993, a soluble isoform of Flt-1 was identified, which is encoded by the first 13 out of 30 exons of *FLT1*, and is generated by skipped splicing of the Flt-1 mRNA and its premature termination due to intron 13 polyadenylation, hence it is denoted as sFlt-1-i13 (**Figure 1B**) [211,212,218]. sFlt-1-i13 lacks the tyrosine kinase domain of Flt-1, since it only contains the first six extracellular Ig-like domains, corresponding to 1-657 amino acids in Flt-1, along with a unique 31-amino-acid tail which is encoded by Intron 13 (**Figure 1A**) [211,212,219]. Since this unique tail of sFlt-1-i13 is evolutionarily highly conserved among mammals [211,220], it is thought to have an important biological role [212] (**Figure 1A**). Of importance, sFlt-1-i13 is more abundantly

expressed in the placenta than the transmembrane Flt-1 receptor in the second half of the pregnancy in mice [221] and in term gestation in humans [183].

The exact molecular mechanism how the shift from Flt-1 to sFlt-1 production occurs in the placenta is not yet understood [212]. Since sFlt-1-i13 acts as a potent VEGF and PlGF antagonist and a dominant negative inhibitor of angiogenesis [222], it has been suggested to maintain a barrier against extreme VEGF-signaling and vascular hyperpermeability in the placenta [112,212,221].

As an important expansion in the research area, the heterogeneity of human sFlt-1 was described by Thomas et al. in 2007, who discovered a new alternatively spliced sFlt-1 mRNA, which contains the first 14 exon of *FLT1* as well as an alternatively spliced exon (Exon 15a) within an AluSeq retrotransposon, hence it was denoted as sFlt-1-e15a [218,223] (**Figure 1B**). In 2008, Sela et al. published their results on this same sFlt-1 isoform; however, they named it as “sFlt1-14" [112]. Although since then a new terminology was introduced for the sFlt-1 isoforms [182], in our studies we kept with the one described by Thomas et al. reflecting the alternative splicing events during sFlt-1 translation [218,223]. Interestingly, the sFlt-1-e15a mRNA is primate specific, since AluSeq retrotransposons appeared in the primate genome ~40 million years ago [218,223]. The sFlt-1-e15a isoform diverges from Flt-1 after amino acid 706, and contains a unique 28-amino-acid tail (**Figure 1A**) [182]. HsFlt-1-e15a is predominantly expressed in the placenta in humans, and it has a dominant abundance over the hsFlt-1-i13 isoform in the placenta after the first trimester [112,182,183,218,223]. Two additional sFlt-1 isoforms (hsFlt-1-e15b and hsFlt-1-i14) have also recently been described in humans. These are alternatively spliced after exon 14, and contain 13 and 31-amino-acid unique C-termini compared to hsFlt-1-e15a (**Figure 1B**) [182]. These newly described sFlt-1 isoforms have much lower expression in the placenta compared to the two most abundant sFlt-1 isoforms [182,183]. Strikingly, although the transmembrane Flt-1 receptor is the major *FLT1* transcript in most tissues, these four sFlt-1 isoforms account for 95% of all *FLT1* transcripts in the placenta in healthy, term pregnancies [183].

DOI:10.14753/SE.2015.1828

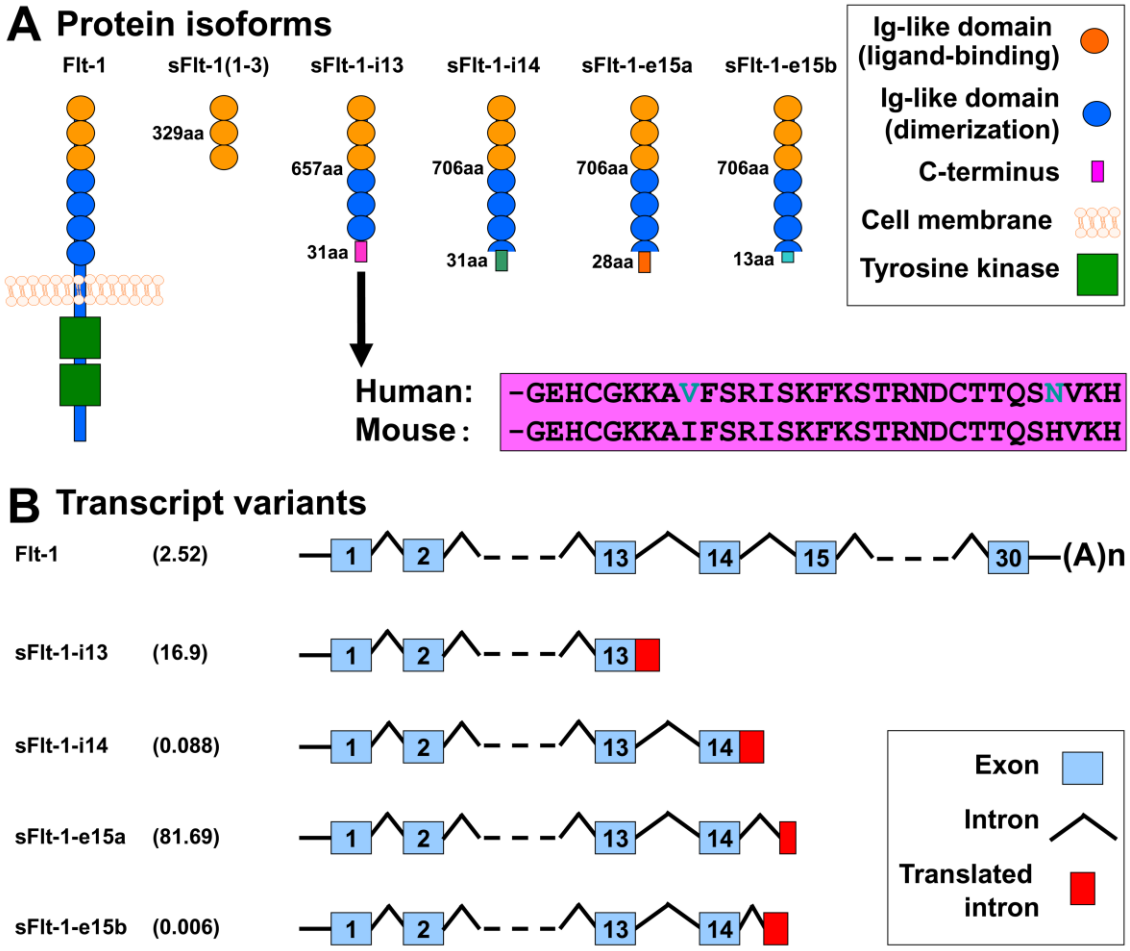

Figure 1. *FLT1* protein isoforms and mRNA transcript variants. (**A**) Flt-1 contains seven extracellular Ig-like domains and an intracellular tyrosine kinase. The first three extracellular Ig-like domains are essential for ligand-binding, while the 4-7th extracellular Ig-like domains for receptor dimerization. The truncated mouse sFlt-1 mutant [msFlt-1(1-3)] contains only 1-329 amino acids of Flt-1, corresponding to the first three Ig-like domains. Mouse and human sFlt-1-i13 contains the first six Ig-like domains corresponding to 1-657 amino acids of Flt-1, as well as a unique 31-amino-acid tail. This unique C-terminus is evolutionarily highly conserved among mammals; the mouse and human amino acid sequences of this tail are only different in two positions (shown with blue letters). Among the human placental expressed sFlt-1 isoforms, hsFlt-1-i14, hsFlt-1-e15a and hsFlt-1-e15b diverge from Flt-1 after amino acid 706, and contain a 31-, 28- and 13-amino-acid unique tails, respectively. (**B**) Among the placental expressed *FLT1* transcripts, the mRNA encoding for the transmembrane receptor is about 2.5% in preeclampsia. *FLT1* transcript expression data was retrieved from Jebbink et al. and is shown as transcript level divided by total *FLT1* transcript level [183]. HsFlt-1-i13, the second most abundant placental *FLT1* transcript in preeclampsia, is generated by skipped splicing and extension of exon 13. Similarly, hsFlt-1-i14 is generated by skipped splicing and extension of exon 14. HsFlt-1-e15a and hsFlt-1-e15b contain alternatively spliced exons derived from intronic sequences (exon 15a and exon 15b, respectively). The most abundant placental transcript, hsFlt-1-e15a contains exon 15a, which is located within a primate-specific AluSeq retrotransposon. The cartoons were adapted with permission from figures in publications of Heydarian et al. [182] and Shibuya M. [212]. Permissions for reuse of these original figures were obtained from Elsevier Ltd. and from the Proceedings of the Japan Academy, Series B, respectively.

In spite of its important role during pregnancy, sFlt-1-i13 is overexpressed in the human placenta in preeclampsia [105,224], and it induces hypertension, proteinuria and glomerular endotheliosis *in vivo* in rats [105]. Interestingly, hsFlt-1-e15a expression was found to be up-regulated in the trophoblast by hypoxia [223], and hsFlt-1-e15a to be the most abundant sFlt-1 isoform in the placenta in healthy pregnant women and in patients with preeclampsia, corresponding to 81.69% of the placental *FLT1* transcripts [112,182-184,211,212]. These findings suggest that hsFlt-1-e15a may have important functions in normal pregnancy; however, its overexpression may promote preeclampsia. It is important in this context that preeclampsia was considered to be a human disease, since only a few cases presenting with preeclampsia-like symptoms have been reported among other primates (pregnant gorillas and chimpanzees), and preeclampsia has not been observed in any other species [12,13,225,226]. Since preeclampsia is specific to primates and sFlt-1-e15a is a primate-specific isoform, it was speculated that hsFlt-1-e15a may have yet unidentified properties which may be critical in the development of preeclampsia [112,223]. Indeed, the unique C-terminus of hsFlt-1-e15a includes a polyserine stretch [112,218], and hsFlt-1-e15a has strong VEGF inhibitor properties [112]. Although it is possible that this primate-specific sFlt-1 isoform has an important role in the development of preeclampsia in humans and in anthropoid primates, the observations on non-human primate pregnancies are limited [227-229]. Although a plethora of studies have implicated placental and maternal blood sFlt-1 overexpression in preeclampsia pathogenesis [96,97,105,107,108,112,139,141,143-147,150,152,153,157,159,163,164,166,167,169,172], none of these had investigated the *in vivo* effects of the hsFlt-1-e15a isoform.

1.4. Animal models of preeclampsia

1.4.1. General overview

Humans have hemochorial placentation with uniquely deep trophoblast invasion that is in certain extent similar to chimpanzees and gorillas, which is not the case in other species [226,230,231]. Because of this and other anatomical and physiological uniqueness of human placentation, it has been impossible to develop adequate animal models to mimic the early placental stages of preeclampsia, especially for early-onset preeclampsia associated with severely impaired placental development. On the other hand, various animal models of preeclampsia could model the terminal

pathway of preeclampsia [232,233]. Most of these models either utilized hypertensive mouse strains [234,235] or were based on impaired uterine perfusion [236-247], nitric oxide synthase function [248-251], metabolic functions [252-254], oxidative and nitrosative stress [255,256], or altered renin-angiotensin system functions [190,194,257,258]. Other preeclampsia models generated systemic maternal inflammatory response [259,260] or utilized the overexpression of anti-angiogenic molecules [105,175,261-267]. Among the various species used in these studies, mice turned to be a good animal model for the study of late-onset preeclampsia, since they have hemochorial placentation similar to humans [268,269]. Although trophoblast invasion is limited in mice, placentation events can be somewhat comparable to those in humans [14,268-272].

1.4.2. Anti-angiogenic animal models with the overexpression of sFlt-1

Most anti-angiogenic preeclampsia models utilized the overexpression of an artificially truncated sFlt-1 mutant [sFlt-1(1-3)] [105,108,177,261,262,264,266,273-277], which is not expressed in any species, lacks the highly conserved sFlt-1 domains important in dimerization, bioavailability and yet unknown functions [211,263], and may induce a stronger preeclampsia phenotype than the full-length sFlt-1-i13 [263]. There was only a recent study that utilized the overexpression of the full-length hsFlt-1-i13, the second most abundant sFlt-1 variant in the human placenta and generated late-onset preeclampsia in mice [265]. However, no study was previously conducted to investigate whether the overexpression of full-length hsFlt-1-e15a may have milder effects in inducing hypertension and proteinuria in mice than the truncated sFlt-1(1-3) [7].

In addition to this limitation, many previous models of preeclampsia in rodents had several technical constraints, which limited follow-up during pregnancy and postpartum, including the: 1) lack of appropriate imaging techniques to determine pregnancy status in early gestation posed by the small size of these rodents; 2) lack of urine protein measurements due to difficulties with urine collection techniques; 3) limitations in continuous and/or non-stressed blood pressure monitoring; and 4) lack of postpartum monitoring.

DOI:10.14753/SE.2015.1828

2. OBJECTIVES

Because of the above listed limitations of earlier animal models of preeclampsia, we designed our studies to overcome these limitations. Accordingly, we set up our aims to:

1. develop a biologically more relevant anti-angiogenic mouse model of preeclampsia by overexpressing the most abundant human placental hsFlt-1-e15a isoform in preeclampsia in order to detect its presumed *in vivo* pathologic effects;

2. use high-frequency ultrasound imaging in early pregnancy determination;

3. utilize high-frequency ultrasound for the detection of telemetric catheter positioning in the aortic arch in order to promote more accurate blood pressure monitoring;

4. utilize non-stressed blood pressure monitoring during pregnancy and postpartum;

5. develop a novel survival cesarean section for enabling postpartum monitoring;

6. develop a novel method for cystocentesis with the use of high-frequency ultrasound to enable accurate urine protein analysis;

7. investigate the tissue distribution of hsFlt-1-e15a viral transgene expression and its relation to the induced clinical symptoms;

8. utilize histopathological, cell- and molecular biological as well as immunological methods for the *in vitro* investigations of the functional effects of hsFlt-1-e15a;

9. compare the biological effects of the full-length hsFlt-1-e15a with that of the truncated msFlt-1(1-3) on the development of preeclampsia in mice;

10. examine the biological effects of full-length hsFlt-1-e15a with that of the truncated msFlt-1(1-3) on the fetus and the placenta.

Aims 1 to 8 were addressed in *Study I*, while Aims 9 to 10 were addressed in *Study II*.

DOI:10.14753/SE.2015.1828

3. METHODS

We conducted two interconnected but separate studies under the same study protocol. In spite of the similar methodologies, certain important differences also existed, and therefore, I separately describe the methods and results of these studies in my Thesis.

3.1. Study I

3.1.1. Ethics statement

The study protocol (A#11-03-11) was approved by the Institutional Animal Care and Use Committee (IACUC) of Wayne State University (Detroit, MI, USA). Animal handling and care followed all standards in strict accordance with the recommendations in the *"Guide for the Care and Use of Laboratory Animals"* of the National Institutes of Health (NIH) [278]. All surgeries were performed under isoflurane anesthesia, and all efforts were made to minimize suffering. Mice were euthanized in accordance with the *"Guidelines on Euthanasia"* of the American Veterinary Medical Association, and the IACUC guidelines at Wayne State University.

3.1.2. Animals and husbandry

Timed-pregnant CD-1 mice arrived from Charles River Laboratories (Wilmington, MA, USA) on gestational day (GD) 5, and then were acclimated for two days before the experiments. Mice were kept separately in standard-size filter top rodent cages and fed with *ad libitum* water and food. Constant temperature (24±1ºC) and humidity (50±5%) were maintained in the animal room with a daily regular 12:12 hour light-dark period. Mice were monitored daily for food and water intake, vital signs, activity, and behavior. Incision sites were examined daily to detect any signs of infection and/or inflammation, and genital regions for signs of vaginal discharge or preterm labor. Animals were excluded from the study in case of miscarriage, surgical complications, or any condition that a veterinarian deemed severe enough to warrant exclusion. (**Figure 2**) shows the experimental procedures performed at certain time-points during Study I.

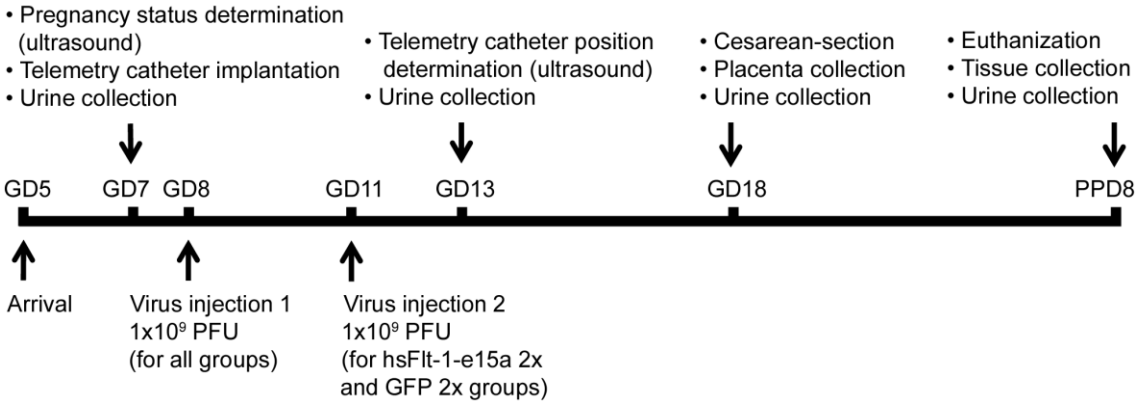

Figure 2. Experimental procedures. The flow-chart shows the experimental procedures performed at certain time-points during the study. GD, gestational day; GFP, green fluorescent protein; PPD, postpartum day; PFU, plaque forming unit.

3.1.3. Determination of pregnancy status with ultrasound

Timed-pregnant CD-1 mice arrived on GD5 (**Figure 2**), when the vendor guarantees only a 75% pregnancy rate. As a methodological development by our study, ultrasound scans were performed on GD6 (n=12) or GD7 (n=35) to determine pregnancy status. Anesthesia was induced by inhalation of 4-5% isoflurane (Aerrane, Baxter Healthcare Corporation, Deerfield, IL, USA) and 1-2 L/min of oxygen in an induction chamber. Anesthesia was maintained with a mixture of 2% isoflurane and 1-1.5 L/min of oxygen. Expired gas from mice and leaking gas from the anesthesia mask were scavenged by a ventilation system connected to a charcoal filter canister. Mice were positioned on a heating pad and stabilized with adhesive tape, and then fur was shaved from the abdomen and neck. Body temperature was supported in the range of 37±1˚C and detected with a rectal probe. Respiratory and heart rates were monitored throughout the ultrasound scans (Vevo Imaging Station, Visual Sonics Inc., Toronto, ON, Canada). After the 55MHz linear ultrasound probe (Vevo 2010, Visual Sonics Inc.) was fixed and mobilized with a mechanical holder, pregnancy status was evaluated while looking for signs of a gestational sac (GD6, **Figure 3A**), as well as an embryo and an advanced endometrial reaction (GD7, **Figure 3B**) [279-287].

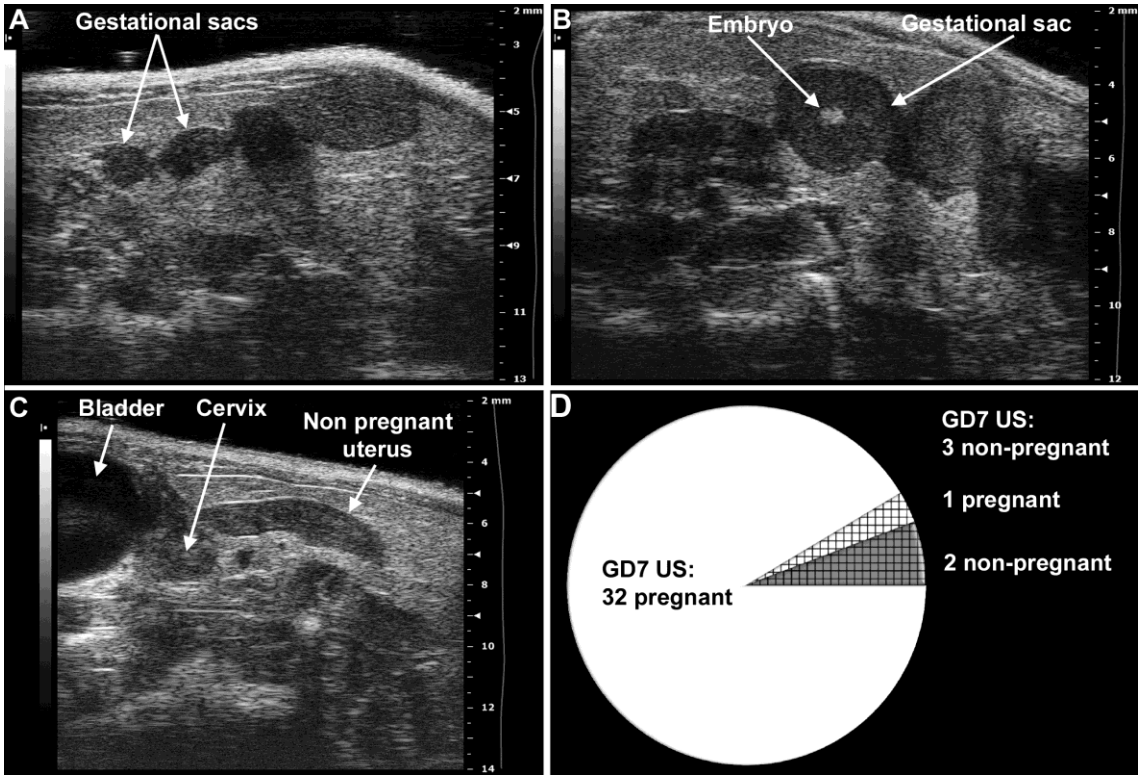

Figure 3. Determination of mouse pregnancy status with a 55MHz ultrasound probe. (**A**) Pregnant uterus on GD6. Gestational sacs of 1.8mm–2.7mm were observed in the proximity of the abdominal surface without visible signs of an embryo. (**B**) Pregnant uterus on GD7. Advanced endometrial reaction and the presence of an embryo were visible in the gestational sacs. (**C**) Non-pregnant uterus of a mouse seven days after mating, equivalent to GD7. (**D**) The pie chart shows that pregnancy could be diagnosed in 32 (white) of the 35 mice with high-frequency ultrasound on GD7. Of three mice diagnosed as non-pregnant on GD7 (shading), two were non-pregnant (grey shading), while one carried a pregnancy to term (white shading).

3.1.4. Implantation of the telemetric blood pressure monitoring system

Only mice with confirmed pregnancies underwent telemetric blood pressure monitoring system implantation on GD7. Isoflurane anesthesia was induced and maintained, and gas was scavenged as previously described. Mice were laid on their backs on the surgical platform, and their upper incisors and limbs were stabilized. Body temperature was controlled by a T/Pump warm-water circulating blanket (Gaymar Industries, Inc. Orchard Park, NY, USA). The incision site was scrubbed with Betadine (Purdue Pharma L.P., Stamford, CT, USA); and 2% lidocaine (0.5 mg/kg, Vedco Inc., St. Joseph, MO, USA) and 0.5% bupivacaine (1.5mg/kg, Hospira Inc., Lake Forest, IL, USA) were injected subcutaneously (s.c.) before the incision, following the rules of aseptic surgery [288]. An approximate 1.5cm midline incision was made on the neck, and the salivary glands were gently dissected and retracted laterally with elastic plastic stay hooks. An approximate space of 1cm of the left common carotid

artery was exposed from the bifurcation in the direction of the heart, with the intention not to injure the vagal nerve. After carotid artery ligation at the level of bifurcation, arteriotomy and cannulation were prepared with the assistance of a 25G tip needle (**Figure 5A**), and the blood pressure monitoring catheter (TA11PA-C10 or HD-X11, Data Sciences International, St. Paul, MN, USA) (**Figure 4**) was positioned into the aortic arch (**Figure 5B**). The catheter was fixed with 6/0 non-absorbable braided surgical silk sutures (Teleflex Medical, Coventry, CT, USA), and the transmitter was placed in a subcutaneous pocket in the left flank, preformed with blind dissection (**Figure 5C**). After repositioning the salivary glands over the catheter, the skin was closed with a continuous 6/0 non-absorbable monofilament polypropylene suture (CP Medical, Portland, OR, USA). Postoperative pain was reduced with s.c. injection of carprofen (5 mg/kg/24h, Rymadil, Pfizer Inc., New York, NY, USA), and with the administration of lidocaine and bupivacaine adjacent to the surgical incision site. In order to avoid post-surgical dehydration, 0.5ml of 0.9% saline solution was s.c. injected. During the postoperative period, mice were kept in their cages, with one-half of each cage placed on a warm water circulating blanket, and vital signs were regularly checked.

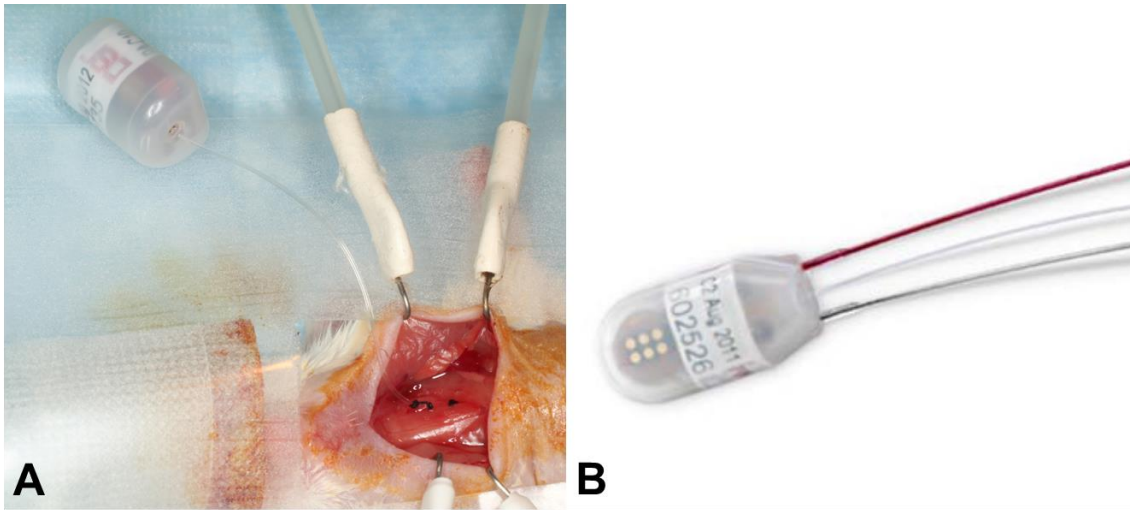

Figure 4. TA11PA-C10 and HDX-11 telemetry blood pressure monitoring device. (**A**) The TA11PA-C10 telemetric blood pressure monitoring device with left carotid artery cannulation in mice. The weight of the TA11PA-C10 device is 1.4 grams, the volume is 1.1 cc, and the battery life is approximately 1.5 months. The photo is courtesy of the Perinatology Research Branch, NICHD, NIH, DHHS. (**B**) The HDX-11 telemetric device can simultaneously record blood pressure, ECG, temperature and activity data from a single mouse. The weight of the HDX-11 device is 2.2 grams, the volume is 1.4 cc, and the battery life is approximately 1 month. The image was downloaded form http://www.datasci.com/products/implantable-telemetry/mouse-(miniature)/hd-x11.

3.1.5. Determination of the telemetry catheter position with high-frequency ultrasound

As another methodological development by our study, transmitter catheter tip positions were examined with the 55MHz linear ultrasound probe (Visual Sonics Inc.) during the routine GD13 ultrasound scans. The ultrasound probe was fixed and mobilized with a mechanical holder, and the transducer was moved downward toward the chest. The left carotid artery, aortic arch, and ascending aorta were visualized, and the position of the catheter tip was determined (**Figure 5D**).

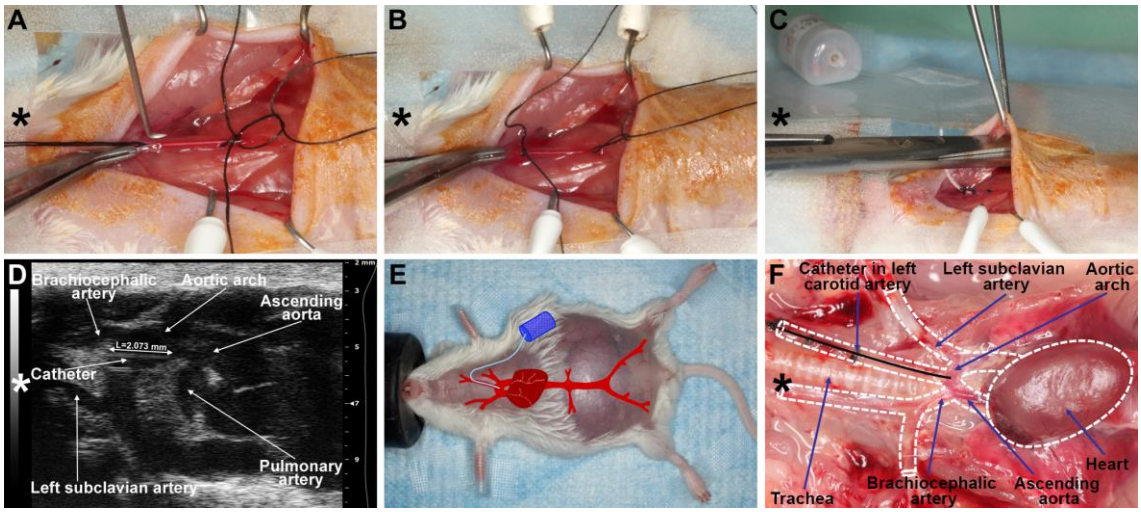

Figure 5. Implantation with a telemetric blood pressure monitoring system. (**A**) On GD8, after isolation and ligation of the left common carotid artery at the level of bifurcation, a small arteriotomy was prepared with a 25G tip needle, (**B**) and the blood pressure monitoring catheter was positioned into the aortic arch with the assistance of the vessel cannulation forceps. (**C**) The transmitter was placed into a subcutaneous pocket in the left flank and preformed with blind dissection. (**D**) On GD13, the position of the telemetry catheter was determined with a 55MHz ultrasound probe. The catheter tip is situated in the aortic arch, and the intra-aortic part of the catheter reaches the optimal 2mm length. (**E**) On GD18, a pregnant mouse is shown before a cesarean section. The incision line of the telemetry surgery healed completely. The projected graph illustrates the position of the intra-aortic catheter and the subcutaneous telemetric blood pressure transmitter. (**F**) On PPD8, the catheter position, aortic arch, and main arterial branches were visualized after autopsy in the mouse mediastinum and chest. The dotted lines show the heart and main arteries of the mediastinum. (**A-F**) Head orientations are shown with asterisks.

3.1.6. Telemetric blood pressure monitoring

As postoperative pain has a strong effect on blood pressure, telemetry monitoring was started on GD10, three days after the catheter implantations on conscious, unrestrained animals, and was continued until postpartum day (PPD) 7 using the Dataquest A.R.T. 4.31 acquisition and analysis system (Data Sciences International) (**Figure 6**). Blood

pressures were recorded for 10s every five minutes for at least 8-12 hours a day during both the light and dark cycles.

Figure 6. Telemetric blood pressure monitoring system. Mice were kept separately in standard-size filter top rodent cages. Blood pressure monitoring was started three days after the catheter implantations on conscious, unrestrained animals, and was continued until postpartum day (PPD) 7 using the Dataquest A.R.T. 4.31 acquisition and analysis system (Data Sciences International). Freely moving mice housed in plastic cages were placed on the top of the receiver, and the implanted telemetric devices transmitted the data to the receiver with radio frequency. The photo is courtesy of the Perinatology Research Branch, NICHD, NIH, DHHS.

3.1.7. Adenoviral gene delivery

As a methodological development by our study, recombinant adenoviruses expressing enhanced green fluorescent protein (GFP) or hsFlt-1-e15a (NP_001153502.1) under the control of a cytomegalovirus promoter (Ad-CMV-GFP and Ad-CMV-hsFlt-1-e15a, respectively) were constructed and titered by Vector BioLabs (Philadelphia, PA, USA). Mice were divided into four groups [hsFlt-1-e15a 1x (n=6), hsFlt-1-e15a 2x (n=5), GFP 1x (n=4), and GFP 2x (n=5)] according to the number of viral construct injections. All mice were injected with adenovirus constructs [$1x10^9$ plaque-forming units (PFU) in 100µl] via the tail vein on GD8, and a subset of mice (GFP 2x and hsFlt-1-e15a 2x) was repeatedly injected with $1x10^9$ PFU adenoviral constructs on GD11. All of these mice underwent the subsequently described procedures.

3.1.8. Ultrasound-guided bladder puncture (cystocentesis)

As another methodological development by our study, ultrasound-guided cystocentesis was performed on GD7, GD13, GD18, and PPD8 under isoflurane anesthesia. Urine samples were obtained using a micro-injection system and a linear 55 MHz high-frequency ultrasound probe (Visual Sonics Inc.) (**Figure 7**).

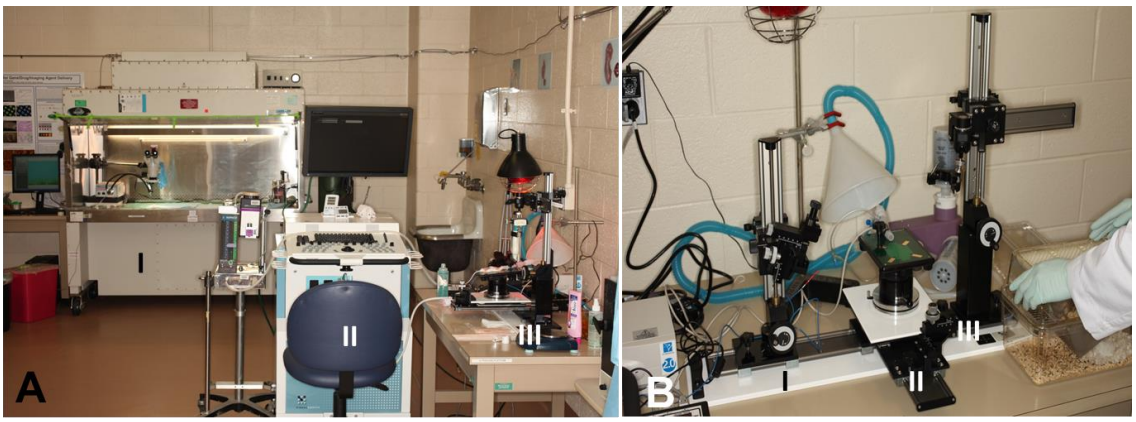

Figure 7. High frequency ultrasound and micro-injection system. (**A**) **I.** Telemetry implantation was done under surgical microscope in a biosafety hood. **II.** 55 MHz high-frequency ultrasound (Vevo 2010, Visual Sonics Inc., Toronto, ON, Canada). **III.** Micro-injection unit. (**B**) **I.** A 1ml insulin syringe with a 30 gauge, 12.7mm long needle was mounted on the micro-injection system, and orientated to target the bladder. **II.** Anesthetized mice were positioned on a heating pad of the imaging unit. **III.** The transcutaneous bladder puncture was performed under continuous ultrasound guidance using the mechanical holder of the micro-injection system. The photos are courtesy of the Perinatology Research Branch, NICHD, NIH, DHHS.

Specifically, the transcutaneous bladder puncture was performed under continuous ultrasound guidance using the mechanical holder of the micro-injection system. The ultrasound probe was aligned and adjusted to obtain a clear view of the maternal bladder; the skin was disinfected with a sterile pad saturated with 70% isopropyl alcohol. A 1ml insulin syringe with a 30 gauge, 12.7mm long needle was mounted on the micro-injection system, and orientated to target the bladder. The procedure was attempted when urine was visualized, disregarding bladder size. The needle was then stopped before entering the skin, and the angle between the needle and the bladder was corroborated. The angle of the scanning pad and the microinjection system was adjusted to allow for a paramedial entrance of the needle through the dome of the bladder in order to avoid damage to the abdominal and pelvic organs**.** After defining the optimal

site for puncture, color Doppler ultrasound was activated for the identification of vascular structures. If vessels were detected, then an alternative site for the bladder puncture was selected. After obtaining the urine sample, a small amount of urine was left in the bladder. Slow forward movements in the micro-injection system allowed the visualization of the tip of the needle in the ultrasound screen. With a fast forward movement of the injection system, the needle was introduced in the bladder without transposing into the posterior wall (**Figures 8**). After obtaining the urine sample, a small amount of urine was left in the bladder. The needle was then retired under continuous ultrasound visualization. After the procedure, the fluid loss was supplemented by subcutaneous injection of pre-warmed 0.9% NaCl (10-15 microliters/g/hour) into the midscapular region of the mice according to the recommendation of the IACUC and the Division of Laboratory Animal Resources (DLAR) of Wayne State University.

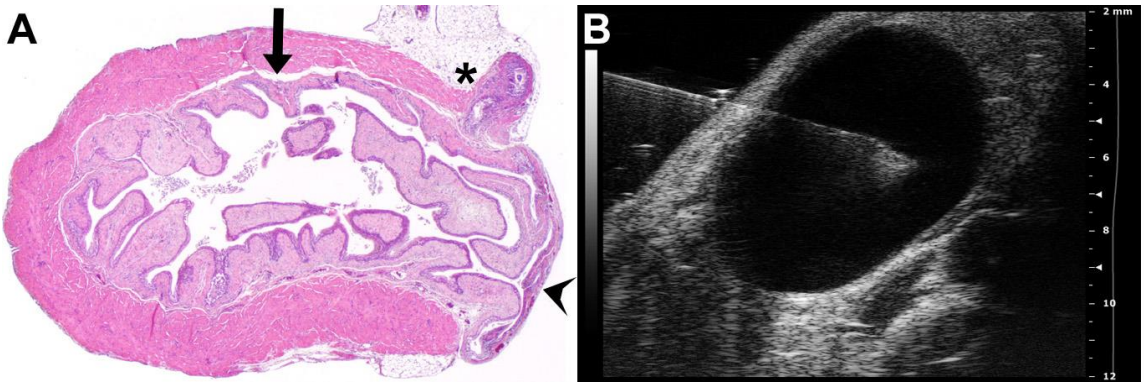

Figure 8. Ultrasound guided cystocentesis. (**A**) A cross-section of a mouse urinary bladder. The urinary bladder can be anatomically divided into two parts: the dome consists of three layers of smooth muscle (arrow), and the thin bladder base (arrowhead) consists of the trigone extending from the urethra (star) to the two ureters. (**B**) An ultrasound image of a filled urinary bladder positioned just underneath the abdominal wall. After image optimization, the urinary bladder is punctured by a 30G needle guided by a high 55MHz ultrasound probe. The images are courtesy of the Perinatology Research Branch, NICHD, NIH, DHHS.

Five µl of urine samples were evaluated for blood contamination using a highly sensitive Urine Chemstrip 5 OB (Roche Diagnostics, Indianapolis, IN, USA). This assay can detect a minimum of 5 erythrocytes/µl [289-291] based on the pseudoperoxidase reaction of erythrocytes and hemoglobin [290]. Then urine samples were stored at -80^{o}C until analysis.

3.1.9. Cesarean section

Utilizing another methodological development, mice underwent survival cesarean section on GD18. Pre- and intra-operative preparation of the mice (i.e. isoflurane anesthesia induction and maintenance, eye protection, surgical stabilization and body temperature control, skin disinfection, and local analgesia) were performed as in the case of the telemetry device implantation. After a short (1-1.5cm) midline abdominal incision in the area where fur had been previously removed, a short segment of one uterine horn was exteriorized at once, and kept moisturized with sterile 0.9% saline. According to the number of pups, two to three exteriorizations and minimal (3-5mm) longitudinal midline hysterectomies were made on each horn, on the opposite side of the mesometrial arterial arcade, while keeping the residual parts of the uterine horn inside the abdominal cavity to avoid contamination (**Figure 9A**). After delivering pups and placentas (**Figure 9B,C**), minimal incisions were closed with a single 4/0 absorbable multifilament polyglycolic acid suture (CP Medical, Portland, OR, USA) (**Figure 9D**). Then, lavage was applied to the abdominal cavity with 2-3ml of 0.9% sterile saline. The abdominal wall was closed with a continuous 4/0 absorbable multifilament polyglycolic acid suture (CP Medical), and the skin was closed with 7mm staples (Braintree Scientific Inc., Braintree, MA, USA) (**Figure 9E**). Body fluids were replenished by an injection of 0.5ml of 0.9% sterile saline subcutaneously. Postoperative pain was reduced with s.c. carprofen (Pfizer Inc.), as well as with the injection of lidocaine and bupivacaine adjacent to the incision line. Postoperative care was similar to that which followed the telemetry system implantation.

DOI:10.14753/SE.2015.1828

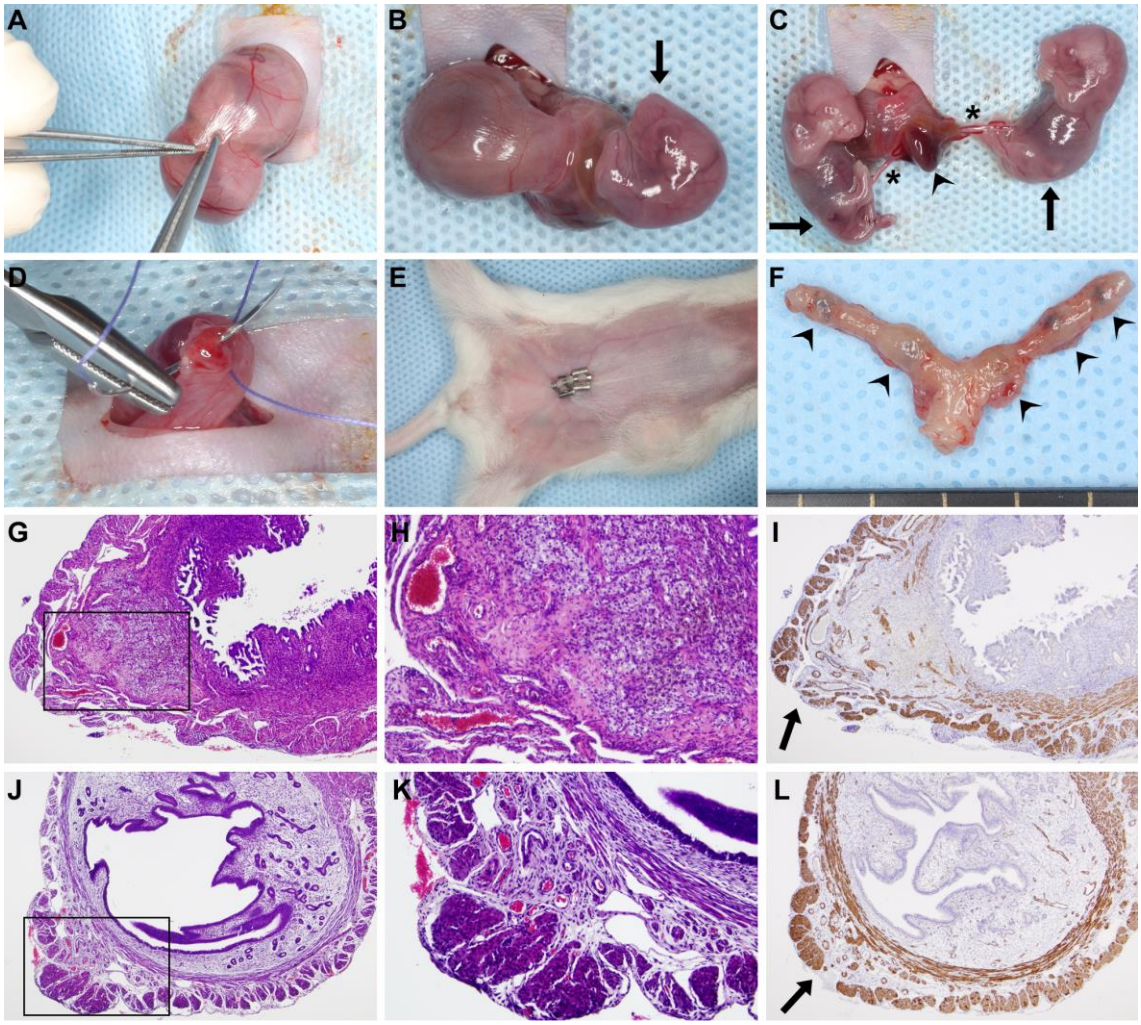

Figure 9. Survival cesarean section. (**A**) After a 1cm–1.5cm midline abdominal incision, a short segment of one uterine horn was exteriorized, and a 3mm–5mm longitudinal hysterectomy was performed on the opposite side of the mesometrial arterial arcade. (**B-C**) As the uterine wall could be easily dilated, this minimal incision enabled the delivery of two to three fetuses and their placentas using gentle fingertip pressure. An arrowhead depicts a placenta, stars depict umbilical cords, and arrows point to the fetuses. (**D**) Hysterectomies were closed with a single 4/0 absorbable multifilament suture. (**E**) After abdominal lavage with 0.9% sterile saline, the abdominal wall was closed with an absorbable multifilament continuous suture, and the skin was closed with 7mm-wide staples. The image shows a surgical field before euthanization on PPD8. (**F**) One uterus harvested after euthanization on PPD8. Arrowheads show hysterectomy sutures. (**G**) H&E staining of a uterine cross-section of a control mouse euthanized on PPD8 shows granulation tissue with enlarged vessels, foam cells, myofibroblasts, macrophages, and hemosiderin deposition. The image inside the black box is magnified in Subfigure H. (**I**) SMA immunostaining of the same uterus. The arrow depicts the cesarean section incision site with the disruption of the two-layered myometrium. (**J**) H&E staining of a uterine cross-section of a control mouse euthanized on PPD77 shows granulation tissue and the complete healing of the two-layered myometrium. The image inside the black box is magnified in Subfigure K. (**L**) SMA immunostaining of the same uterus. The arrow depicts a suture site. (**G, I, J** and **L**: 40x magnifications, **H** and **K**: 100x magnifications).

3.1.10. Tissue collection

Following cesarean section on GD18, each fetus was separated from the placenta and umbilical cord. All fetuses and placentas were weighed with a Scout Pro SP402 digital scale (Ohaus Corp., Pine Brook, NJ, USA). The first placentas adjacent to the uterine cervix in both uterine horns were fixed in 4% paraformaldehyde (PFA) diluted with phosphate buffered saline (PBS, Gibco, Life Technologies Corporation, Grand Island, NY, USA) for 24h, then dehydrated in 70% graded ethanol (Richard-Allan Scientific Dehydrant, Thermo Fisher Scientific Inc., Waltham, MA, USA), and embedded in paraffin for histopathological examinations. The second placentas adjacent to the uterine cervix were collected and homogenized in TRIzol (Invitrogen, Life Technologies Corporation, Carlsbad, CA, USA) and stored at -80˚C until gene expression analyses.

After the euthanization of dams on PPD8, tissues from several organs (spleen, uterus, liver, kidney, and brain) were dissected and sectioned. Tissues were fixed in 4% PFA for 24h, then dehydrated in 70% graded ethanol, and embedded in paraffin for histopathological examinations, or homogenized in TRIzol reagent and stored at -80˚C until gene expression analyses. To evaluate the changes in uterine histology with time after the cesarean sections, additional untreated mice were euthanized on PPD38 (n=3), PPD50 (n=3), and PPD77 (n=3), respectively, and uteri were processed as those on PPD8.

3.1.11. Total RNA isolation, cDNA generation, quantitative real-time RT-PCR

Tissues were homogenized in TRIzol reagent with a homogenizer (Pro Scientific Inc., Oxford, CT, USA) immediately after tissue collection. Total RNAs were isolated using the QIAshredder (Qiagen, Valencia, CA, USA) and the RNeasy Mini Kit (Qiagen), according to the manufacturer's instructions. Complementary DNAs were generated with SuperScript III First-Strand Synthesis System (Invitrogen). Quantitative real-time RT-PCR assays were performed on the Biomark System (Fluidigm, San Francisco, CA, USA) using TaqMan assays (Applied Biosystems, Life Technologies Corporation, Foster City, CA, USA) for *GFP* (Mr04097229_mr) and human *FLT1* (Hs01052961_m1).

3.1.12. Histopathological evaluation of tissues

Five-µm-thick sections of paraffin embedded placenta, kidney, and uterus tissue blocks were serially cut, mounted on silanized slides, deparaffinized, and rehydrated in descending grades of ethanol. Selected levels of all tissues were then stained with hematoxylin and eosin (H&E) to evaluate general morphology, and selected levels of all kidneys were stained with periodic acid Schiff (PAS) reagent for the visualization of basement membranes of glomerular capillary loops and tubular epithelium. Histopathological examination of these tissue sections was performed on an Olympus BX50F light microscope (Olympus America Inc., Melville, NY, USA) by a pathologist (FQ). Kidney sections were evaluated for glomerular endotheliosis (e.g. ballooning of tips of capillary loops, capillary endothelial swelling, occlusion of glomerular capillaries) in at least 20 glomeruli in the inner cortex of one kidney in each animal.

3.1.13. Immunohistochemistry

Selected layers of uteri were immunostained for CD68 and smooth muscle actin (SMA). Immunostainings were performed using a rabbit anti-mouse SMA polyclonal antibody (1:300 dilution; Abcam Inc., Cambridge, MA, USA) and the Bond Polymer Refine Detection Kit (Leica Microsystems, Wetzlar, Germany) on a Leica Bond Max automatic staining system (Leica Microsystems), or using a rabbit anti-mouse CD68 polyclonal antibody (1:150 dilution; Abcam Inc.) and the DAB Map Detection Kit (Ventana Medical Systems, Inc., Tucson, AZ, USA) on a Ventana automatic staining system (Ventana Medical Systems, Inc.).

3.1.14. Aortic ring assays

Aortic ring assays were performed as previously described [292,293]. Briefly, thoracic aortas were dissected from euthanized mice and placed in a Petri dish containing DMEM+GlutaMAX low glucose medium (Gibco, Life Technologies Corporation). The peri-adventitial fibro-adipose tissue was removed, then aortas were sectioned into 1mm-long rings, and incubated in 12-well plates at 37^{o}C in Opti-MEM+GlutaMAX reduced serum medium (Gibco, Life Technologies Corporation) overnight for serum starvation. The serum-starved aortic rings were then placed into 96-well tissue culture plates pre-coated with 50µL of Growth Factor Reduced BD Matrigel Matrix (BD Biosciences,

Bedford, MA, USA). Then, aortic rings were covered with an additional 50µL of Matrigel and 100µL of Opti-MEM medium supplemented with 1% Penicillin–Streptomycin (Gibco, Life Technologies Corporation), 2.5% fetal bovine serum (FBS; Atlanta Biologicals, Lawrenceville, GA, USA), and 30ng/mL of vascular endothelial growth factor (VEGF-A; ProSpec, East Brunswick, NJ, USA). Plates were incubated at 37^{o}C for six days with a change of medium every second day. After six days of incubation, aortic rings were fixed with 4% PFA diluted with PBS, and images were obtained with an Olympus 1X51 inverted microscope equipped with an Olympus DP25 digital camera (Olympus, Tokyo, Japan).

3.1.15. Albumin-creatinine immunoassays

Urine specimens collected on GD6/GD7, GD13, GD18 and PPD8 were examined for murine urinary albumin with the Albuwell kit (Exocell Inc., Philadelphia, PA, USA), and for creatinine with the Creatinine Companion assay employing the alkaline picrate method (Exocell Inc.).

3.1.16. Adenoviral infection of BeWo cells

BeWo cells (American Type Culture Collection, Manassas, VA, USA) were cultured with F12 medium supplemented with 10% FBS and 1% Penicillin/Streptomycin (all from Life Technologies Corporation). Cells were plated on either 6-well plates ($0.5x10^{6}$/well) or 35mm cell culture dishes, and infected with Ad-CMV-GFP or Ad-CMV-hsFlt-1-e15a at a multiplicity of infection of 100. After 16h of infection, cell supernatants were removed, and BeWo cells were washed with PBS and used for Western blotting or confocal imaging.

3.1.17. Protein isolation and Western blot

Total protein from BeWo cell samples was extracted with the RIPA lysis buffer (Sigma-Aldrich Co., St Louis, MO, USA) containing Complete Mini Protease Inhibitor Cocktail Tablets (Roche, Indianapolis, IN, USA). Protein concentrations were determined with the Quick Start Bradford Protein Assay (Bio-Rad, Hercules, CA, USA). Twenty micrograms of total protein from each sample were electrophoresed on 4-12% SDS-PAGE gels (Life Technologies Corporation), and

electro-transferred onto nitrocellulose membranes (Bio-Rad). Membranes were probed with goat anti-human Flt-1 polyclonal antibody (AF321, R&D Systems, Inc., Minneapolis, MN, USA) in a 1:2,000 dilution at 4C^{o} for 16h, and then with peroxidase-conjugated anti-goat IgG (Vector Laboratories, Burlingame, CA, USA) in a 1:5,000 dilution at room temperature for 1h. Protein bands were developed using the ChemiGlow Western Blotting Detection Reagents (Protein Simple, Santa Clara, CA, USA), and then scanned and imaged with a Fujifilm LAS-4000 Image Reader (GE Healthcare, Piscataway, NJ, USA).

3.1.18. Confocal microscopy

BeWo cells infected with adenovirus constructs and cultured in 35mm cell culture dishes were mounted with ProLong Gold Antifade Reagent and 4',6-diamidino-2-phenylindole (DAPI; Invitrogen) followed by confocal microscope imaging using a Leica TCS SP5 spectral confocal system (Leica Microsystems CMS GmbH, Mannheim, Germany). Confocal imaging was performed at the Microscopy, Imaging and Cytometry Resources Core of the Wayne State University School of Medicine.

3.1.19. Data and statistical analyses

Blood pressures: Mean arterial blood pressures (MAP) were calculated from systolic and diastolic blood pressures for each time point and animal, and then were averaged. The mean MAP values on GD10 were subtracted from all MAP values to obtain normalized ΔMAP values. We fitted the MAP and the ΔMAP data with a Linear Mixed Effects (LME) models [294] for the time intervals before and after cesarean delivery, respectively. These models included explanatory variables such as the treatment (GFP or hsFlt-1-e15a) or the dose (1x or 2x), and a continuous measure of time (gestational day or postpartum day) while allowing a random intercept for each animal. An interaction was allowed between the treatment and time, and therefore, we could test if the slope of the MAP or ΔMAP over time was different between the treatments. We relaxed the linear fixed effect patterns to quadratic for the analysis of time intervals after cesarean delivery. Since blood

pressure has a circadian daily rhythm in mice, we also examined blood pressures in 12-hour light and dark cycles separately.

Urine albumin/creatinine ratios: Albumin/creatinine ratios between the hsFlt-1-e15a and GFP groups on different time points were compared with the Student's t-test.

Gene expression profiling: Relative gene expressions were quantified by averaging target (*FLT1* or *GFP*) and reference (*Gapdh*) gene Ct values over technical replicates, and then by subtracting mean target gene Ct values from mean reference gene Ct values within the same sample. The Student's t-test was used to compare gene expression levels between treatments in a given tissue. To examine the dose effect on gene expression for each tissue, we computed the percentage of samples expressing a given gene when over-expressed with a given dose of that gene. Statistical comparison on the percentages across all tissues between the two doses was performed with the one-tailed paired Student's t-test.

Aortic ring assays: The angiogenic response of the aortic rings was analyzed by quantifying the microvessel outgrowth. A ruleset was developed using Definiens Developer XD2 (Definiens, Munich, Germany) to analyze the transmitted light images. A new image layer (or channel) with enhanced local contrast was produced using "contrast to neighbor pixels" to distinguish the newly formed microvessels sprouting from the aortic ring. Next, a series of segmentation and classification operations was performed on the channel to exclude the ring from the area measurements, and the total area of the objects determined to be "outgrowth" was reported. Data were averaged on the picture level for the same ring, then further averaged on the ring level for the same animal, followed by a Student's t-test for group comparisons.

Fetal survival rates, fetal and placental weights: The fetal survival rate (number of live fetuses / number of total fetuses) for each mouse was computed, and the non-parametric Kruskal-Wallis test was used for multiple group comparisons. Fetal weights, placental weights, and placental/fetal weight ratios were compared with the two-way ANOVA test and with a linear mixed effects model.

3.2. Study II.

3.2.1. Ethics statement

The mouse study was approved as part of the animal study protocol (A#11-03-11) similar to that in Study I. Collection and utilization of human samples for research purposes were approved by the Institutional Review Boards of the *Eunice Kennedy Shriver* National Institute of Child Health and Human Development (NICHD), National Institutes of Health (NIH), Department of Health and Human Services (DHHS, Bethesda, MD, USA) and Wayne State University. Written informed consent was obtained from all pregnant women prior to the collection of clinical data and tissue samples. These specimens were coded, and data were stored anonymously.

3.2.2. Animals and husbandry

Timed-pregnant CD-1 mice (n=48) were shipped on gestational day 5 (GD5) from Charles River Laboratories (Wilmington, MA, USA), and were housed, fed and monitored exactly as in Study I. Exclusion criteria were the same as in Study I. (**Figure 10**) shows the experimental procedures performed at certain time-points during the study.

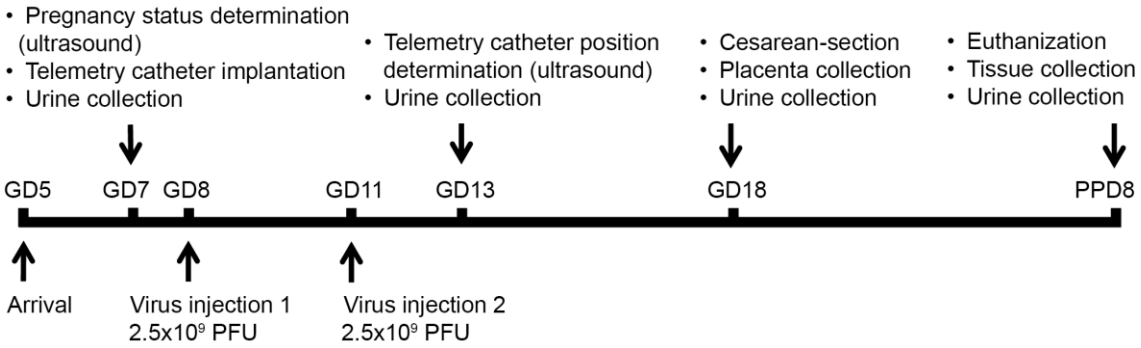

Figure 10. Experimental procedures. The flow-chart shows the experimental procedures performed at certain time-points during the study. GD, gestational day; GFP, green fluorescent protein; PPD, postpartum day; PFU, plaque forming unit.

3.2.3. Evaluation of pregnancy status with high-frequency ultrasound

Ultrasound scans were performed on GD7 to evaluate pregnancy status as described in Study I.

3.2.4. Telemetric blood-pressure catheter implantation and data acquisition

Telemetric blood pressure catheter implantation was done as described in Study I. Telemetric blood pressure monitoring on conscious, unrestrained mice started on GD11 and continued until PPD7 using the Dataquest A.R.T. 4.31 software (Data Sciences International). Telemetry catheter tip positions were verified with a 55MHz linear ultrasound probe (Visual Sonics Inc.) on GD13.

3.2.5. Determination of the telemetry catheter position with high-frequency ultrasound

The telemetry catheter positions were determined as described in Study I.

3.2.6. Telemetric blood pressure monitoring

Telemetric blood pressure monitoring was performed as described in Study I.

3.2.7. Adenoviral gene delivery

In order to test the biological effects of differences in hsFlt-1-e15a expression patterns, we used three different viral vectors constructed from replication deficient adenovirus (Type5, dE1/E3) and an "RGD fiber-mutant" adenovirus with distinct tissue-tropism as well as two different gene promoters that differ in terms of tissue-specific promoter activity (**Figure 11**). The "RGD fiber-mutant" adenovirus that contains an RGD (Arg-Gly-Asp) motif on the fiber knob was developed in conjunction with Vector BioLabs (Philadelphia, PA, USA) according to that described by Mizuguchi et al., 2001 [295]. Adenoviruses and fiber-mutant adenoviruses expressing the full-length hsFlt-1-e15a, the truncated msFlt-1(1-3) or green fluorescent protein (GFP) were constructed and titered by Vector BioLabs. HsFlt-1-e15a was overexpressed by 1) a wild-type adenovirus under the control of the cytomegalovirus promoter (Ad-CMV-hsFlt-1-e15a; n=6), 2) an RGD fiber-mutant adenovirus under the control of the cytomegalovirus promoter (Ad-RGD-CMV-hsFlt-1-e15a; n=6), or 3) an RGD fiber-mutant adenovirus under the control of the human *CYP19A1* promoter (Ad-RGD-CYP-hsFlt-1-e15a; n=5). Truncated msFlt-1(1-3) was overexpressed by the RGD fiber-mutant adenovirus under the control of the cytomegalovirus promoter [Ad-RGD-CMV-msFlt-1(1-3); n=6]. GFP was overexpressed by 1) the RGD fiber-mutant adenovirus under the control of the cytomegalovirus promoter (Ad-RGD-CMV-GFP; n=12), or 2) by the RGD fiber-mutant adenovirus

under the control of the human *CYP19A1* promoter (Ad-RGD-CYP-GFP; n=4). According to the technique described by our parallel study [7], mice in these treatment and control groups were injected via the tail vein with $2.5x10^9$ plaque-forming units (PFU) of adenovirus constructs (in 100µl saline) on GD8 and then repeatedly with $2.5x10^9$ PFU adenoviral constructs or saline on GD11 (**Figure 10**). A group of mice (n=9) that was used only for the expression profiling of endogenous mouse transmembrane Flt-1 and sFlt-1-i13 received only 100µl saline injection on GD8 and GD11 via the tail vein.

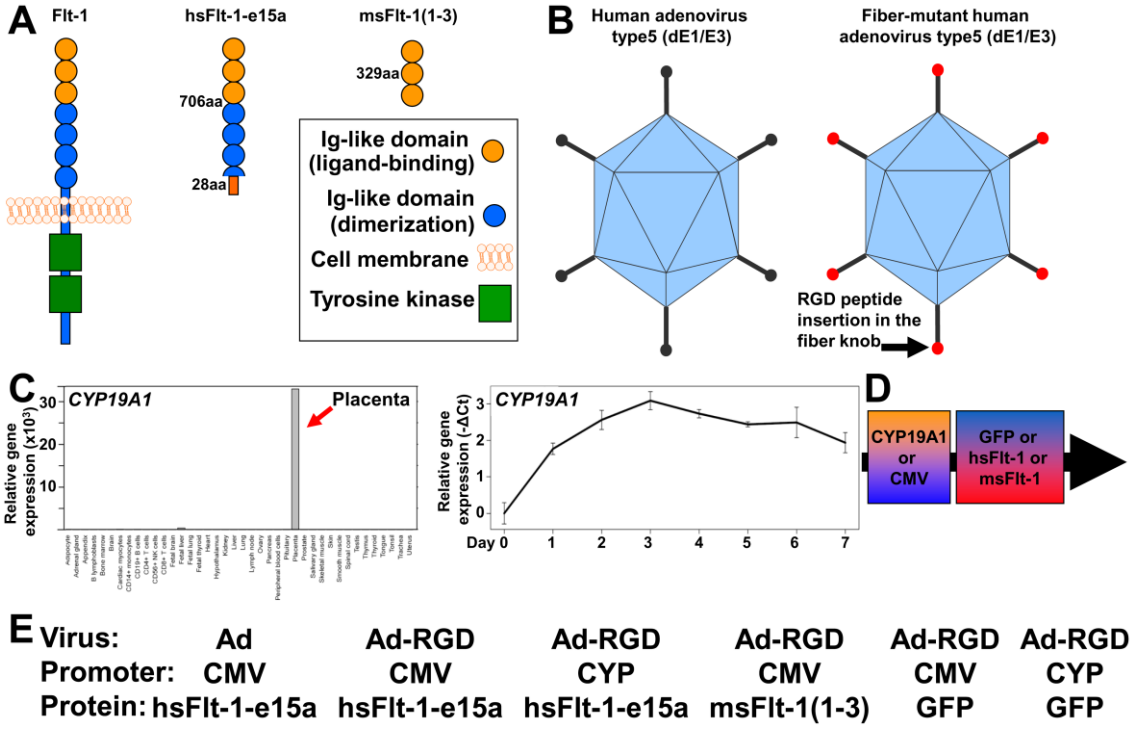

Figure 11. The development of viral constructs for the various treatment groups. (A) Human and mouse Flt-1 contains seven extracellular Ig-like domains and an intracellular tyrosine kinase, from which the first three Ig-like domains are important in ligand-binding, while the 4-7th Ig-like domains in receptor dimerization. The most abundant placental sFlt-1 variant in humans, sFlt-1-e15a, contains six Ig-like domains and a unique C-terminus encoded by exon 15a, which is located within a primate-specific AluSeq retrotransposon. The truncated mouse sFlt-1 mutant [msFlt-1(1-3)] contains only the first three Ig-like domains of Flt-1. **(B)** Besides the replication deficient human adenovirus Type5 (dE1/E3), "RGD fiber-mutant" adenoviruses were also used. **(C)** Besides the CMV promoter that has a strong promoter activity, the human *CYP19A1* promoter was also used. *CYP19A1* is strongly and predominantly expressed in the placenta among 40 human tissues (left), and its expression increases during trophoblast differentiation (right). Relative gene expressions are shown on the Y-axes. **(D-E)** Various combinations of viruses, promoters and transgenes used in this study.

3.2.8. Minimal invasive survival cesarean section

Aseptic survival cesarean section was performed as described in Study.

3.2.9. Tissue collection

Tissue collection was done as described in Study I.

3.2.10. Total RNA isolation, cDNA generation, quantitative real-time RT-PCR

Tissues were homogenized in TRIzol reagent, and total RNA was isolated using the QIAshredder (Qiagen, Valencia, CA, USA) and RNeasy Mini Kit (Qiagen). Total RNA was isolated from primary human trophoblast cultures with TRIzol reagent (Invitrogen) and RNeasy kit (Qiagen) according to the manufacturers' recommendations. Five hundred nanograms of total RNA was reverse transcribed with the SuperScript III First-Strand Synthesis System (Invitrogen). TaqMan assays (Applied Biosystems, Life Technologies Corp., Foster City, CA, USA) for human *FLT1* (Hs01052961_m1), mouse *Flt1* (Mm01210866_m1: exon boundary 1-2; Mm00438980_m1: exon boundary 15-16), *GFP* (Mr04097229_mr), human *CYP19A1* (Hs00903411_m1), as well as the endogenous human and mouse control genes [*RPLP0* (Hs99999902_m1); *Gapdh* (Mm99999915_g1)] were used for quantitative real-time RT-PCR performed on the Biomark System (Fluidigm, San Francisco, CA, USA) according to the manufacturer's recommendation.

3.2.11. Histopathological evaluation

Four-μm-thick sections were cut from paraffin embedded kidney blocks, mounted on silanized slides, deparaffinized and rehydrated. The general morphology was analyzed on selected tissue levels after staining with hematoxylin and eosin (H&E). Selected kidney sections were stained with periodic acid Schiff (PAS) reagent and with the Jones basement membrane reticulum stain (Dako Artisan Link Pro, Dako North America, Inc., Carpinteria, CA, USA) for the evaluation of the glomerular capillary loop basement membranes. Two pathologists (SJ and FQ) blinded to the clinical outcome evaluated 10 glomeruli from each kidney for glomerular endotheliosis (occlusion of glomerular capillaries, capillary tip ballooning, capillary tip swelling, and abnormalities of the capillary loop basement membranes) and changes in the mesangium. Glomerular damage was scored as follows: 0 = no glomerular changes in 10 glomeruli examined;

1+ = 1 to 5 of 10 glomeruli examined with either segmental or diffuse endotheliosis; 2+ = 6 or more glomeruli with segmental or diffuse endotheliosis. Images were taken with an Olympus BX50F light microscope (Olympus America Inc., Melville, NY, USA).

3.2.12. Immunohistochemistry

Selected layers of placentas from control mice were immunostained for CD31 using a rabbit anti-CD31 monoclonal antibody (1:50 dilution; Spring Bioscience, Pleasanton, CA, USA) and the Bond Polymer Refine Detection Kit (Leica Microsystems, Wetzlar, Germany) on a Leica Bond Max automatic staining system (Leica Microsystems).

3.2.13. Aortic ring assays

Aortic ring assays were performed as described in Study I.

3.2.14. Urine collection and albumin-creatinine immunoassays

Urine collection and albumin-creatinine immunoassays were performed as described in Study I.

3.2.15. Primary human trophoblast isolation and cultures

Human placentas (n=4) were collected from normal pregnant women who delivered a healthy neonate at term. Cytotrophoblasts were isolated by a method modified from Kliman et al. [296]. Briefly, villous tissues were cut into pieces, rinsed in PBS, and digested sequentially with Trypsin (0.25%; Invitrogen, Life Technologies Corp.) and DNAse I (60U/ml; Sigma-Aldrich Corp. St. Louis, MO, USA) (90min, 37^{o}C). Dispersed cells were filtered through 100μm Falcon nylon mesh cell strainers (BD Biosciences, San Jose, CA, USA), and then erythrocytes were lysed with NH_4Cl (Stemcell Technologies, Vancouver, BC, Canada). Washed and resuspended cells were layered over Percoll gradients (20-50%) and centrifuged (20min, 1200g). The bands containing trophoblasts were collected; non-trophoblastic cells were excluded by negative selection with anti-CD9 (20μg/ml) and anti-CD14 (20μg/ml) mouse monoclonal antibodies (R&D Systems, Minneapolis, MN, USA) and MACS anti-mouse IgG microbeads (Miltenyi Biotec, Auburn, CA, USA). Trophoblasts were plated on collagen-coated plates (BD Biosciences; $5x10^6$ cells/well) in triplicate and kept in Iscove's modified Dulbecco's medium

[Invitrogen, Life Technologies Corp.; supplemented with 10% fetal bovine serum (FBS), 5% human serum and 1% penicillin/streptomycin (P/S)] for 7 days. Cells were harvested for total RNA isolation in every 24 hours in triplicate.

3.2.16. Confocal microscopy

Five-µm-thick tissue sections were cut from OCT-embedded snap-frozen placentas collected from Ad(RGD)-CMV-GFP and Ad(RGD)-CYP-GFP injected mice, and were mounted on silanized slides. Tissue sections were fixed with -20˚C acetone for 10min and then rinsed three times in ice-cold PBS. Tissue sections were then mounted with ProLong Gold Antifade Reagent and 4',6-diamidino-2-phenylindole (DAPI; Invitrogen, Life Technologies Corp.) and were imaged by a Leica TCS SP5 spectral confocal system (Leica Microsystems CMS GmbH, Mannheim, Germany) at the Microscopy, Imaging and Cytometry Resources Core of Wayne State University School of Medicine. Aortic rings, after fixation, were also mounted with ProLong Gold antifade reagent with DAPI, and image stacks were acquired on the same confocal microscope. To accommodate the size of the aortic rings without sacrificing resolution, 2x2 tiles were acquired using 20x magnification and an open pinhole.

3.2.17. Data and statistical analyses

Gene expression profiling: Relative gene expression levels were quantified by averaging target (human *FLT1*, mouse *Flt1* or *GFP*) and reference (*Gapdh*) gene Ct values over technical replicates, and then subtracting the mean target gene Ct values from the mean reference gene Ct values within each sample. The expression values across different arrays were further adjusted using calibration samples. The Student's t-test was used to compare gene expression levels between treatments in a given tissue. In addition, mouse transmembrane Flt-1 expression was calculated from the data generated by the Mm00438980_m1 TaqMan assay, which is targeted to exon boundary 15-16, and thus, detects only the full-length Flt-1 mRNA expression levels. MsFlt-1-i13 mRNA expression was calculated by subtracting full-length Flt-1 mRNA expression levels from the expression data generated by the Mm01210866_m1 TaqMan assay, which is targeted to exon boundary 1-2, and thus, detects all full-length and alternatively spliced Flt-1 mRNA levels. We used a linear model to estimate the effect of the transgene

(either GFP or hsFlt-1-e15a) and the vector (either the CYP or CMV promoter groups or the two groups merged) on endogenous msFlt-1-i13 expression.

Blood pressure: Mean arterial blood pressure (MAP) was calculated from systolic and diastolic blood pressure at each time point. MAP values for each mouse on a given day (GD or PPD) were averaged. Within the dataset of each mouse, the mean MAP value on GD11 was subtracted from all blood pressure data to obtain a normalized blood pressure, ΔMAP. A separate Linear Mixed Effects (LME) model was fit to the data for the time periods before and after cesarean delivery (GD18). The fixed effect terms in the model included the treatment group, polynomial terms of the gestation day (up to 3^{rd} and up to 2^{nd} degree for the periods before and after cesarean delivery, respectively), and their interaction terms. The random components in the mixed effects models included an intercept term and a quadratic term of gestational day for each animal. A likelihood ratio test comparing the fit quality of the model with and without interaction terms between the group and gestational day was used to test if the blood pressure profile over gestation was different between the groups. The blood pressure levels at specific gestational days were compared between the groups using a t-test.

Glomerular changes, urine albumin/creatinine ratios: Glomerular damage scores were evaluated using a logistic regression model. Albumin/creatinine ratios at different time points were compared with a Student's t-test.

Aortic ring assays: The angiogenic response of the aortic rings was analyzed by quantifying the microvessel outgrowth. A ruleset was developed using Definiens Developer XD2 (Definiens, Munich, Germany) to analyze the 3D confocal microscopy images. A series of segmentation and classification operations was performed on the DAPI channel to exclude the ring from the volume measurements, and the total volume of the objects determined to be "outgrowth" was summed for each image stack and reported. Volume data were averaged for the same ring, and then was further averaged over the multiple rings for the same animal. A t-test was used to compare the volume data between the groups.

DOI:10.14753/SE.2015.1828

Fetal survival rates, fetal and placental weights: The number of total and live fetuses, the fetal survival rate (live/total), the maternal weights, the total (as well as average) fetal and placental weights, and the total placental/total fetal weight ratios were compared between the treatment and control groups using t-tests.

Microarray and qRT-PCR data visualization: Microarray gene expression profiles for human tissues and cells were downloaded from the SymAtlas/BioGPS database [297], and expression data for 40 adult and fetal tissues was visualized via barplots using the R statistical environment (www.r-project.org) (**Figure 11C**). Primary human trophoblast *CYP19A1* expression data were normalized to the reference gene (*RPLP0*) obtained for each sample as - $\Delta Ct_{(gene)}=Ct_{(RPLPO)}-Ct_{(gene)}$ and displayed as a function of time (**Figure 11C**).

DOI:10.14753/SE.2015.1828

4. RESULTS

4.1. Study I

4.1.1. Pregnancy status determination with high-resolution ultrasound

Ultrasound examinations were performed with a 55MHz linear probe to corroborate pregnancy before the implantation of a telemetry catheter. On GD6, only 1.9mm-2.7mm gestational sacs could be visualized (**Figure 3A**). Since an advanced endometrial reaction and the embryo were already visible on GD7, we later decided to perform the ultrasound examinations on GD7 (**Figure 3B**). In non-pregnant animals, none of these signs were visible (**Figure 3C**). In the set of 35 mice scanned on GD7, pregnancy was diagnosed in 32 mice (**Figure 3D**). Among the three mice diagnosed as non-pregnant, two were non-pregnant, and one delivered at term.

4.1.2. Implantation and evaluation of telemetry devices

Telemetry catheter implantations took place only after pregnancy was confirmed with ultrasound, according to the guidelines provided by Data Sciences International Inc. (**Figure 5**). The average length of the implantation surgeries varied between 20-35 minutes, with the TA11PA-C10 device requiring a shorter duration of surgery than the HD-X11 transmitter. Ultrasound examinations on GD13 showed that all animals had a correctly positioned telemetry catheter. The rate of uncomplicated telemetry system implantations was 79% (30/38). According to the type of device implanted, 86% (18/21) were uncomplicated telemetry implantations in cases using the TA11PA-C10 transmitter, and 71% (12/17) in cases using the HD-X11 device. Among these eight cases with complications, three mice implanted with the TA11PA-C10 devices and one mouse implanted with the HD-X11 device had abnormal body posture and seizures, suggesting ischemic brain damage, while four mice implanted with the HD-X11 devices presented with transmitter body exteriorization.

4.1.3. Survival cesarean surgery

We developed a new survival cesarean surgery, in which only a short segment of one uterine horn is exteriorized at a time. In total, two or three short longitudinal hysterectomies were performed on each horn, in which pups and placentas could easily be delivered with a gentle push (**Figure 9A-F**). Due to the minimal invasiveness of this aseptic technique,

administration of appropriate pain medication, and replenishment of lost body fluids, the eight-day survival rate of this new surgery was 100% (30/30) compared to the 85% reported in the literature [298]. Histopathological examination of H&E-stained and SMA-immunostained uterine cross-sections showed granulation tissues with enlarged vessels, foam cells, myofibroblasts, macrophages, and hemosiderin deposits on PPD8 (**Figure 9G-I**). The endometrium was completely healed on PPD77 in all examined cases, and the two-layered myometrium showed complete healing of the inner layer and focal disruption at suture sites in the outer layer. Suture granuloma was observed in the submucosa at the incision site (**Figure 9J-L**).

4.1.4. Overexpression of human placental sFlt-1-e15a isoform and GFP with adenoviral vectors

To compare the expression pattern of hsFlt-1-e15a and GFP mRNAs, total RNAs were isolated from placentas harvested on GD18, as well as from brain, kidney, liver, spleen, and uterus tissues harvested on PPD8. According to the qRT-PCR analysis, hsFlt-1-e15a and GFP mRNA expression was highest in the liver (**Figure 12A,B**).

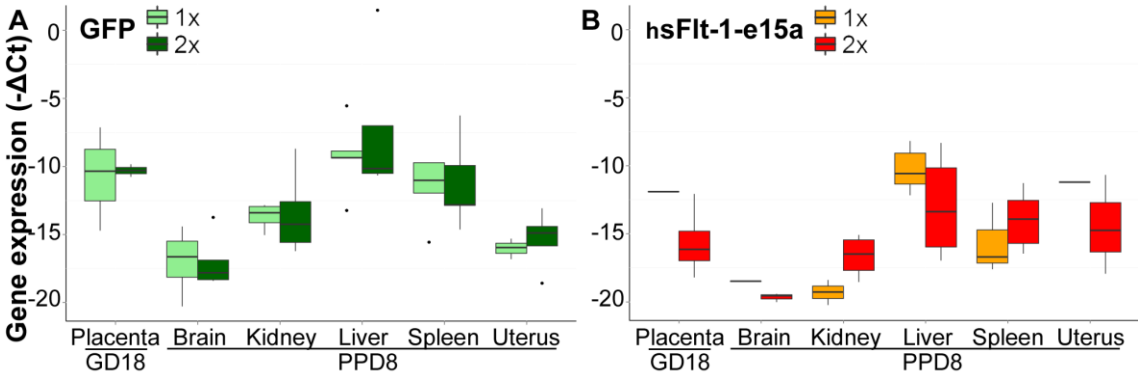

Figure 12. Profiling of hsFlt-1-e15a and GFP expression. Boxplots show the expression profile of GFP (**A**) or hsFlt-1-e15a (**B**) mRNAs in placentas harvested on GD18 and in five tissues harvested on PPD8. Adenovirus doses ($1x10^9$ or $2x10^9$ plaque-forming units) are depicted with different colors. Expression of hsFlt-1-e15a and GFP mRNAs was highest in the liver. Viral dose-effect was not seen in GFP expression; however, there was a dose-effect in hsFlt-1-e15a expression. The number of hsFlt-1-e15a expressing placenta, brain and uterine tissues was low in the hsFlt-1-e15a 1x group.

The placental expression of hsFlt-1-e15a and GFP was not directly comparable with their expression in the five investigated maternal tissues because of the difference in tissue sampling time points (GD18 vs. PPD8). Viral dose-effect ($1x10^9$ PFU vs. $2x10^9$ PFU*)*

DOI:10.14753/SE.2015.1828

was not seen in GFP expression, since there was no difference between the percentage of tissues expressing GFP in the two control groups (GFP 1x: 80.0% vs. GFP 2x: 83.3%; $p=3.5x10^{-1}$). On the contrary, there was a dose-effect in the expression of hsFlt-1-e15a, which had lower expression in all investigated tissues than GFP. For mice in the hsFlt-1-e15a 1x group ($1x10^{9}$ PFU), the average rate of tissue samples with detectable hsFlt-1-e15a expression was 46.7%, and 72.2% in the hsFlt-1-e15a 2x ($2x10^{9}$ PFU) group ($p=9.7x10^{-3}$). The hsFlt-1-e15a mRNA expression was 6.3-fold higher in the kidneys of hsFlt-1-e15a 2x mice than of hsFlt-1-e15a 1x mice ($p=5.3x10^{-2}$). The number of hsFlt-1-e15a expressing placenta, brain, and uterine tissues was low in the hsFlt-1-e15a 1x group.

To confirm the placental overexpression of hsFlt-1-e15a and GFP proteins in the trophoblast *in vitro*, we infected BeWo human trophoblast-like cells with Ad-CMV-GFP or Ad-CMV-hsFlt-1-e15a, and used a human anti-Flt-1 antibody for Western blotting or confocal microscopy for GFP signal detection. Western blotting revealed that non-infected BeWo cells expressed low amounts of the 185kDa Flt-1 membrane receptor as well as 145kDa and 110kDa sFlt-1 variants (**Figure 13A**). Ad-CMV-GFP-infected BeWo cells expressed these proteins to the same extent. Ad-CMV-hsFlt-1-e15a-infected BeWo cells overexpressed the 145kDa and 110kDa sFlt-1 variants. Confocal microscopy revealed cytoplasmic GFP expression in BeWo cells infected with Ad-CMV-GFP (**Figure 13B**), indicating also the efficient transfection of these trophoblastic cells with the adenoviral constructs.

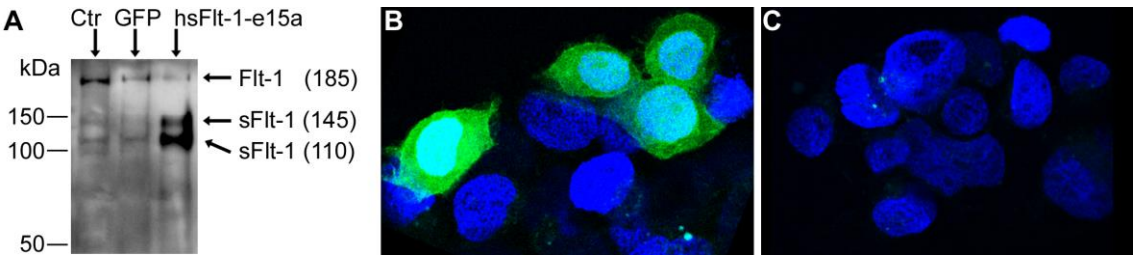

Figure 13. Profiling of hsFlt-1-e15a and GFP expression. (**A**) Western blot shows the expression of the 185kDa transmembrane Flt-1 receptor as well as 145kDa and 110kDa sFlt-1 variants in human BeWo trophoblast-like cells not infected with adenovirus (Ctr), infected with Ad-CMV-GFP (GFP), or infected with Ad-CMV-hsFlt-1-e15a. Ad-CMV-hsFlt-1-e15a enhances the overexpression of 145kDa and 110kDa sFlt-1 variants in BeWo cells. MW markers are depicted in the left; Flt-1 and sFlt-1 variants are depicted on the right. (**B**) A confocal microscopic image shows cytoplasmic GFP expression in BeWo cells infected with Ad-CMV-GFP. (**C**) Control BeWo cells not infected with adenovirus. (B-C) 2000x magnifications.

DOI:10.14753/SE.2015.1828

4.1.5. Blood pressure telemetry monitoring

As our preeclampsia model allowed for postpartum monitoring, blood pressure measurements continued until PPD7. Blood pressures increased until cesarean delivery and then declined until tissue harvest in hsFlt-1-e15a overexpressing mice. Therefore, we fitted the data separately for the time periods before and after cesarean delivery. This analysis revealed that, prior to parturition, there was no significant change in the blood pressure over time in control mice (ΔMAP slope=0.513 mmHg/day; p=0.187) (**Figure 14A,C**).

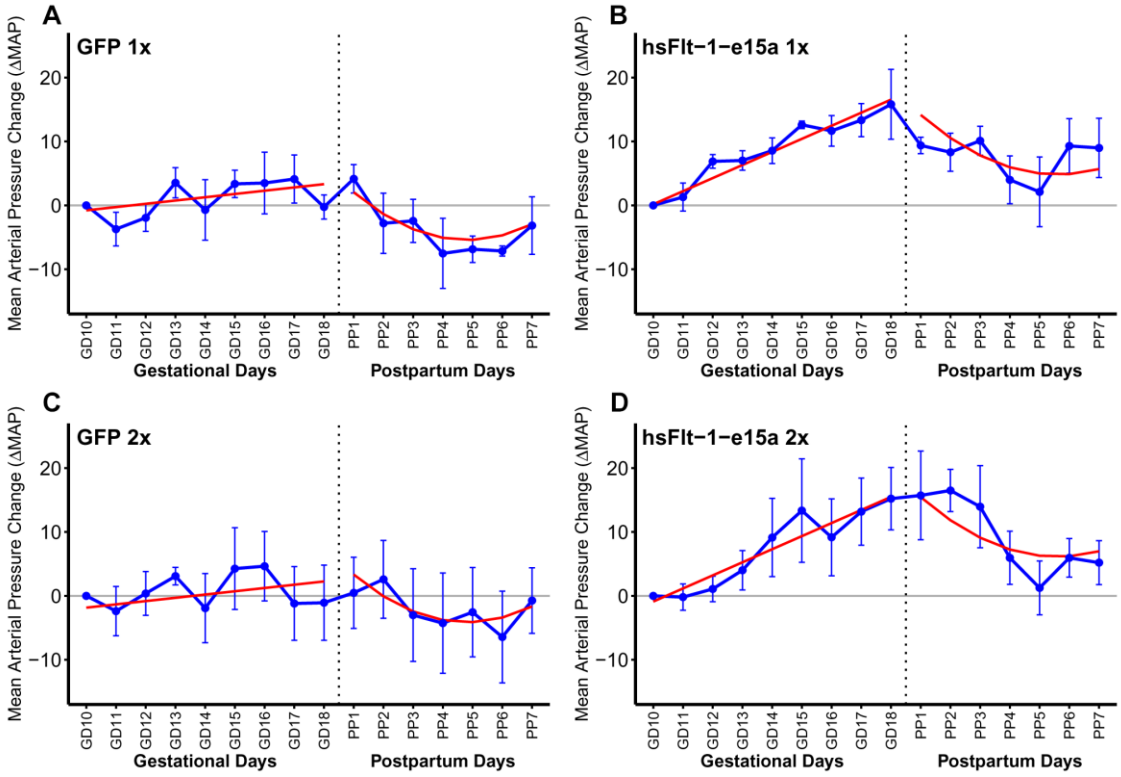

Figure 14. Blood pressure monitoring. X-axes show gestational days (GDs) and postpartum days (PPDs). Mean arterial pressure changes (ΔMAP) are depicted on the Y-axes. Blue dots represent ΔMAP values for given time-points, blue error bars show +/-standard errors. Red lines depict the ΔMAP patterns, fitted from the linear mixed effects models. During pregnancy (left sides of the sub-figures), there was no significant blood pressure elevation in control mice (**A,C**; ΔMAP slope=0.513 mmHg/day; p=0.187), whereas hsFlt-1-e15a treatment significantly increased blood pressure (**B,D**; ΔMAP slope=2.05 mmHg/day; $p=8.09x10^{-8}$). The ΔMAP slope in the hsFlt-1-e15a group was higher compared to the controls (1.53 mmHg/day; p=0.0043). The ΔMAP at parturition (GD18) was 13.2 mmHg higher in hsFlt-1-e15a-treated mice than in the control mice (p=0.00107). After cesarean delivery (right sides of sub-figures), a similar quadratic pattern of ΔMAP was found in both control and hsFlt-1-e15a-treated mice, but ΔMAP dropped below the baseline in control mice (-1.96 mmHg; p=0.560), while it remained above this in hsFlt-1-e15a treated mice (6.88 mmHg; p=0.0346). There was no dose effect of the number of viral construct injections ($1x10^9$ PFU vs. $2x10^9$ PFU*)* in hsFlt-1-e15a-treated or in control mice either before delivery (dose effect: -1.06 mmHg, p=0.693) or in the postpartum period (dose effect: 1.30 mmHg, p=0.763).

However, in response to hsFlt-1-e15a treatment, blood pressures increased over time (ΔMAP slope=2.05 mmHg/day; $p=8.09x10^{-8}$). The ΔMAP slope in the hsFlt-1-e15a group was significantly higher compared to the controls (1.53 mmHg/day; p=0.0043), resembling late-onset preeclampsia in humans (**Figure 14B,D**). The ΔMAP at parturition (GD18) was 13.2 mmHg higher in hsFlt-1-e15a-treated mice than in the control mice (p=0.00107). Interestingly, a similar quadratic pattern of ΔMAP was found in both control and hsFlt-1-e15a-treated mice after cesarean delivery, suggesting a common pattern of drop of blood pressures. However, ΔMAP dropped below the baseline in control mice, while it remained above this in the postpartum period in hsFlt-1-e15a-treated mice. Indeed, ΔMAP on PPD7 was 1.96 mmHg below the baseline in control mice (p=0.560), while it was 6.88 mmHg above the baseline in hsFlt-1-e15a-treated mice (p=0.0346) (**Figure 14A-D**). We did not observe any effect of the number of viral construct injections ($1x10^9$ PFU vs. $2x10^9$ PFU) in hsFlt-1-e15a-treated or in control mice either before delivery (dose effect: -1.06 mmHg, p=0.693) or in the postpartum period (dose effect: 1.30 mmHg, p=0.763).

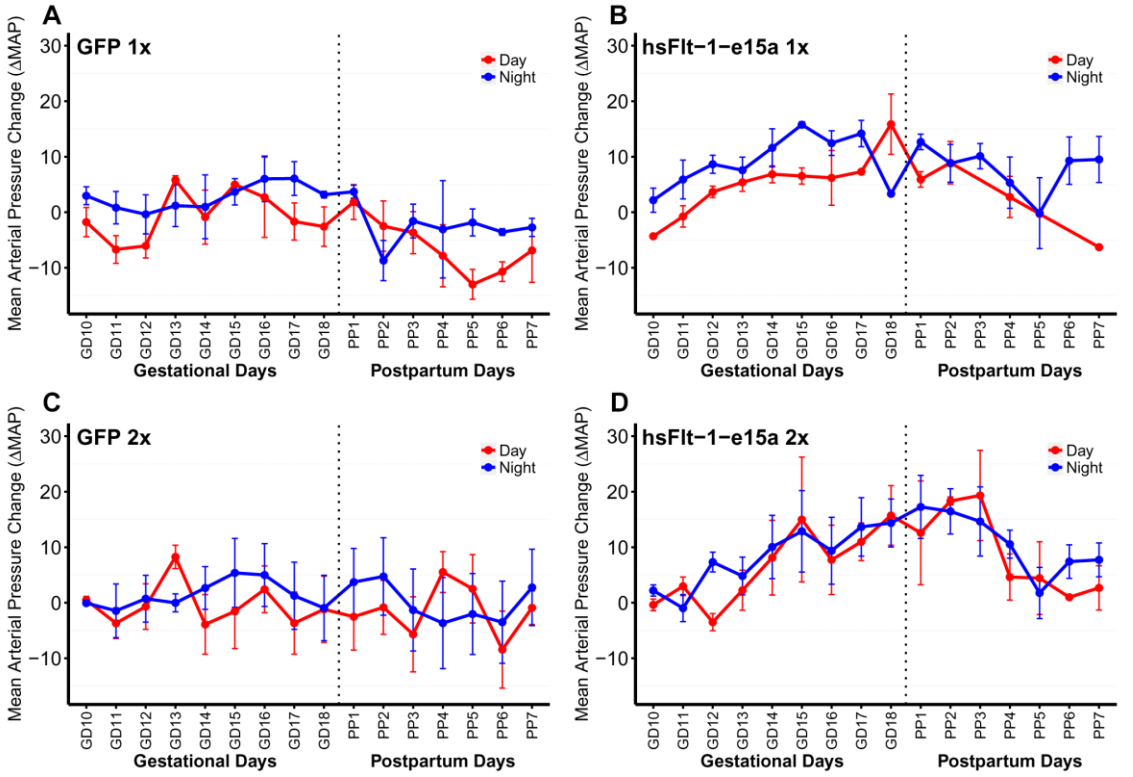

Figure 15. Blood pressure monitoring of day and night cycles. X-axes show gestational days (GDs) and postpartum days (PPDs). Mean arterial pressure changes (ΔMAP) are depicted on the Y-axes. Red and blue dots and standard error bars represent day and night ΔMAP values for given time-points, respectively. Red and blue lines depict the ΔMAP patterns during day and night cycles, respectively. ΔMAP was 2.67 mmHg higher during the night cycles than the day cycles ($p = 2.5x10^{-3}$) before cesarean delivery, and it was 4.37 mmHg higher during the night cycles than the day cycles ($p = 2.7x10^{-6}$) after cesarean delivery.

When examining the day and night cycles separately, we observed that overall the ΔMAP was 2.67 mmHg higher during the night cycles than during the day cycles ($p=2.5x10^{-3}$) before cesarean delivery, and ΔMAP was 4.37 mmHg higher during the night cycles than during the day cycles ($p=2.7x10^{-6}$) after cesarean delivery (**Figure 15**).

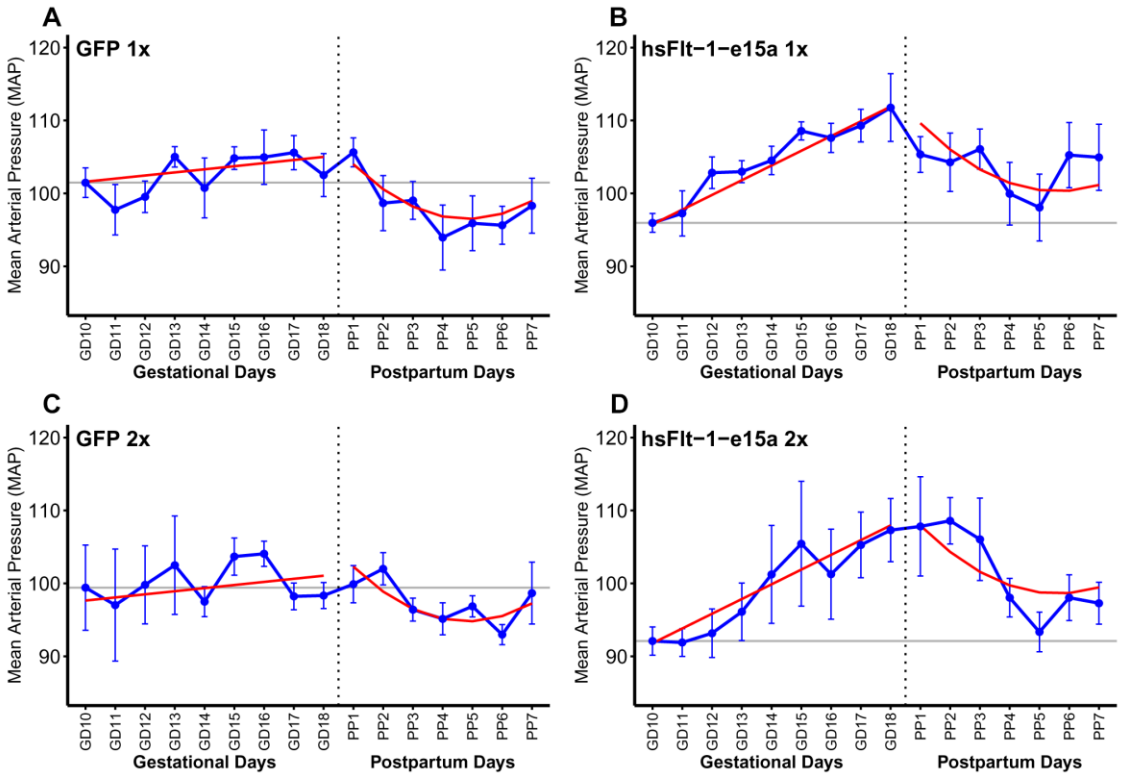

Figure 16. Blood pressure monitoring and mean arterial pressures. X-axes show gestational days (GDs) and postpartum days (PPDs). Mean arterial pressures (MAPs) are depicted on the Y-axes. Prior to parturition, there was no change in the blood pressures over time in control mice (MAP slope = 0.426 mmHg/day; p = 0.174) (**A,C**). However, in response to hsFlt-1-e15a treatment, blood pressures increased over time (MAP slope = 2.02 mmHg/day; $p = 1.13x10^{-10}$). The MAP slope in the hsFlt-1-e15a-treated groups was higher compared to the controls (1.59 mmHg/day; $p = 2.6x10^{-4}$) (**B,D**). The estimated effect of hsFlt-1-e15a treatment on GD18 was 6.90 mmHg (p = 0.0339) in MAP.

In addition to normalizing mean arterial blood pressures to obtain ΔMAPs, we also repeated the above analysis with mean arterial pressures (MAPs). As expected, the conclusions remained the same with regard to the trend before and after parturition for control and hsFlt-1-e15a-treated mice. Prior to parturition, there was no change in the blood pressures over time in control mice (MAP slope=0.426 mmHg/day; p=0.174) (**Figure 16A,C**). However, in response to hsFlt-1-e15a treatment, blood pressures increased over time (MAP slope=2.02, mmHg/day; $p=1.13x10^{-10}$). The difference in the

MAP slope in the hsFlt-1-e15a groups was higher compared to the controls (1.59 mmHg/day; $p=2.6x10^{-4}$) (**Figure 16D**). The only noticeable change was in the estimated effect of hsFlt-1-e15a treatment on GD18, which dropped from 13.2 mmHg in ΔMAP to 6.90 mmHg (p=0.0339) in MAP. This difference could be attributed to the base-line group differences in MAP levels on GD10. Similarly as above, we did not observe any effect of the number of viral construct injections ($1x10^9$ PFU vs. $2x10^9$ PFU) in hsFlt-1-e15a-treated or in control mice either before delivery (dose effect: -3.95 mmHg, p=0.119) or in the postpartum period (dose effect: -1.70 mmHg, p=0.543).

4.1.6. Evaluation of endothelial and kidney functions

An aortic ring assay was utilized to investigate the *in vitro* endothelial functions of aortas collected postpartum. Aortic rings were analyzed after treatment with VEGF-A for six days by light microscopic imaging for the microvessel outgrowth area. We found that the mean microvessel outgrowth area was 46% smaller in hsFlt-1-e15a overexpressing mice than in controls (p=0.012) (**Figure 17**).

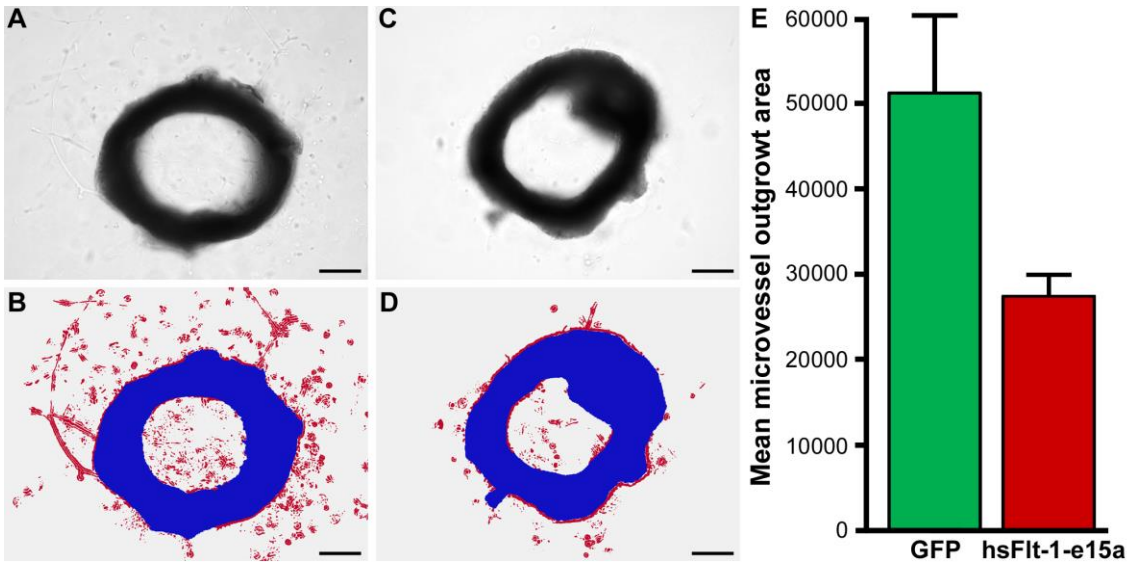

Figure 17. Aortic ring assays. (**A**) A light image of an aortic ring from a mouse injected with Ad-CMV-GFP. (**B**) An image of the same aortic ring, illustrating segmentation and classification, with the aortic ring shown in blue and the red color depicting the microvessel outgrowth area. (**C**) A light image of an aortic ring from a mouse injected with Ad-CMV-hsFlt-1-e15a. (**D**) An image of the same aortic ring, illustrating segmentation and classification, with the aortic ring shown in blue and the red color depicting the microvessel outgrowth area. (**A-D**) Scale bars depict 500µm. (**E**) The bar chart depicts the differences in mean microvessel outgrowth areas (pixels) between the GFP and hsFlt-1-e15a groups.

Histopathological examinations of the kidneys showed focal glomerular changes, including swollen capillary endothelial cells and occlusion of glomerular capillaries in mice overexpressing hsFlt-1-e15a (**Figure 18**). In addition, rare glomeruli appeared sclerotic. In contrast, there were no significant morphological changes in the glomeruli of control mice.

As *in vivo* functional evidence of kidney damage, we also determined albumin/creatinine ratios in urine samples obtained at GD6/GD7, GD13, GD18 and PPD8. Mean urine albumin/creatinine ratios did not change in control mice; however, these increased by GD18 and then dropped postpartum in hsFlt-1-e15a overexpressing mice. Mean (±2SE) urine albumin/creatinine ratio on GD18 was five times higher in hsFlt-1-e15a-treated (109.3±51.7µg/mg) than in control mice (19.3±5.6µg/mg; $p=4.4x10^{-2}$). The mean urine albumin/creatinine ratio on PPD8 was still marginally significantly higher in hsFlt-1-e15a-treated (36.6±9.0µg/mg) than in control mice (18.0±4.9µg/mg; p=0.06) (**Figure 18**).

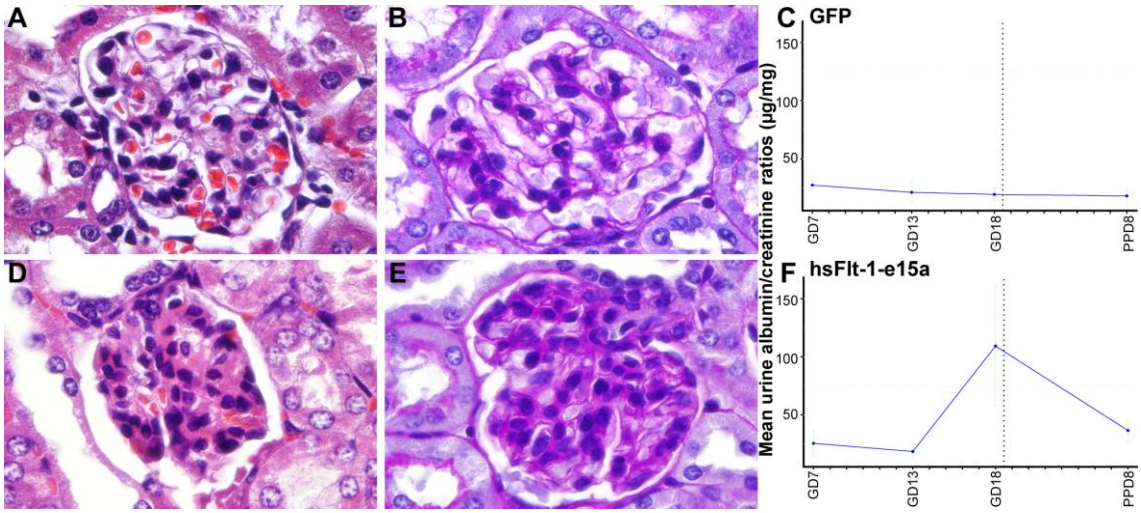

Figure 18. Histopathological and functional evaluation of the kidneys. Representative H&E (**A**) and PAS (**B**) stained sections show a morphologically normal glomerulus in a control animal. Representative H&E (**D**) and PAS (**E**) stained sections show a glomerulus with signs of swollen capillary endothelial cells and occlusion of glomerular capillaries in a mouse overexpressing hsFlt-1-e15a. (**C,F**) Charts depict albumin/creatinine ratios in urine specimens collected on GD7, GD13, GD18, and PPD8 from mice in the GFP (**C**) and hsFlt-1-e15a (**F**) groups. Mean urine albumin/creatinine ratios did not change in control mice; however, these increased by GD and then dropped postpartum in hsFlt-1-e15a overexpressing mice. Mean urine albumin/creatinine ratio on GD18 was higher in hsFlt-1-e15a-treated than in control mice ($p=4.4x10^{-2}$). The mean urine albumin/creatinine ratio on PPD8 was marginally significantly higher in hsFlt-1-e15a-treated (36.6±9.0µg/mg) than in control mice (18.0±4.9µg/mg; p=0.06).

4.1.7. Evaluation of fetal survival rate, placental and fetal weights

Fetal survival rate was not affected by hsFlt-1-e15a treatment, as no differences (p=0.38) were found in the groups (GFP 1x: 100%; hsFlt-1-e15a 1x: 100%; GFP 2x: 96.43%; hsFlt-1-e15a 2x: 100%). Also in agreement with most studies, fetal weight (FW), placental weight (PW), and placental/fetal weight ratios (PFR) were not affected by hsFlt-1-e15a treatment (**Figure 19**). Mean (±2SE) PWs, FWs, and PFRs were as follows: GFP 1x (PW: 0.109±0.009g; FW: 1.03±0.097g; PFR: 0.107±0.014g), hsFlt-1-e15a 1x (PW: 0.117±0.015g; FW: 1.08±0.059g; PFR: 0.109±0.017g), GFP 2x (PW: 0.098±0.014g; FW: 1.07±0.064g; PFR: 0.092±0.009g), and hsFlt-1-e15a 2x (PW: 0.102±0.010g; FW: 1.00±0.133g; PFR: 0.102±0.008g).

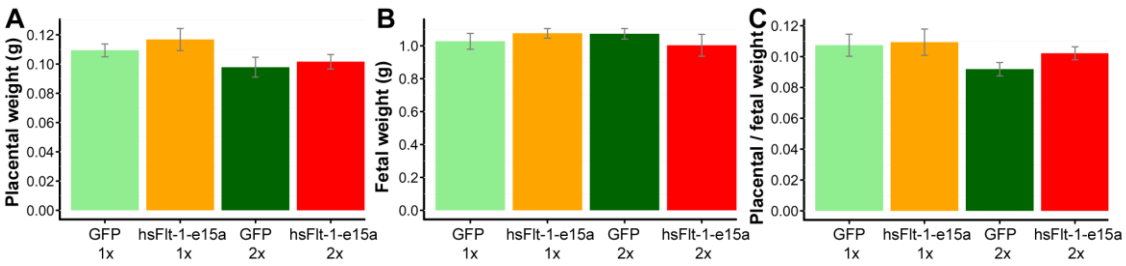

Figure 19. Placental weights, fetal weights and placental/fetal weight ratios. (**A**) Placental weights [mean±2 standard error (SE)] were not different between the groups (GFP 1x: 0.109±0.009g; hsFlt-1-e15a 1x: 0.117±0.015; GFP 2x: 0.098±0.014g; hsFlt-1-e15a 2x: 0.102±0.010g). (**B**) Fetal weights (mean ±2SE) were not different between the groups (GFP 1x: 1.03±0.097g; hsFlt-1-e15a 1x: 1.08±0.059g; GFP 2x: 1.07±0.064g; hsFlt-1-e15a 2x: 0.102±0.010g). (**C**) Placental/fetal weight ratios (mean±2SE) were not different between the groups (GFP 1x: 0.107±0.014g; hsFlt-1-e15a 1x: 0.109±0.017g; GFP 2x: 0.092±0.009g; hsFlt-1-e15a 2x: 0.102±0.008g).

4.1.8. Evaluation of a mouse with early-onset preeclampsia-like symptoms

It is noteworthy that one mouse in the hsFlt-1-e15a 2x group showed a different biological response despite receiving the same treatment (dosage and timing) as others in the group. The “EM35” mouse had a markedly higher and earlier (GD15) blood pressure peak than other hsFlt-1-e15a-treated mice (**Figure 20A**). This was followed by the normalization of blood pressures and by a second blood pressure peak on PPD1. To investigate whether the extreme blood pressure elevation in this mouse could bias the effects estimated for hsFlt-1-e15a-treated mice, we re-analyzed ΔMAPs in the hsFlt-1-e15a group with or without including "EM35" mouse. This re-analysis showed that in the period before delivery the ΔMAP slope

was 2.05 ($p=8.09x10^{-8}$) before and 2.01 ($p=1.13x10^{-8}$) after removing "EM35" mouse. The ΔMAP difference between the slopes was 1.53 before (p=0.00430) and 1.49 (p=0.00173) after removing "EM35" mouse. The difference in ΔMAPs at GD18 was 13.2 mmHg before (p=0.00107) and 11.9 mmHg (p=0.00130) after removal of "EM35" mouse. We obtained similar results when analyzing MAPs (data not shown).

The urinary albumin/creatinine ratio on GD18 was higher in the "EM35" mouse than in other hsFlt-1-e15a-treated mice (**Figure 20B**). Surprisingly, hsFlt-1-e15a expression in the liver was lower in the "EM35" mouse than in other hsFlt-1-e15a-treated mice (**Figure 20C**). Histopathological examination of the liver showed that the "EM35" mouse had multiple cystic biliary hyperplasia and recent and remote thrombotic infarcts in the hepatic parenchyma, suggesting decreased functionality (**Figure 20D-E**). Aortic ring assays revealed the lowest endothelial outgrowth area in the "EM35" mouse among hsFlt-1-e15a-treated mice (**Figure 20F**). Moreover, mean fetal weights (0.749±0.029g) and placental weights (0.080±0.006g) of the "EM35" mouse were significantly lower than in other hsFlt-1-e15a-treated mice (fetal weight: 1.06±0.023g, $p=2.017x10^{-15}$, placental weight: 0.111±0.004g, $p=2.05x10^{-6}$) (**Figure 20G,H**). Histopathological examination of the "EM35" mouse placenta showed multiple thrombi in the decidual vessels (**Figure 20I,J**).

DOI:10.14753/SE.2015.1828

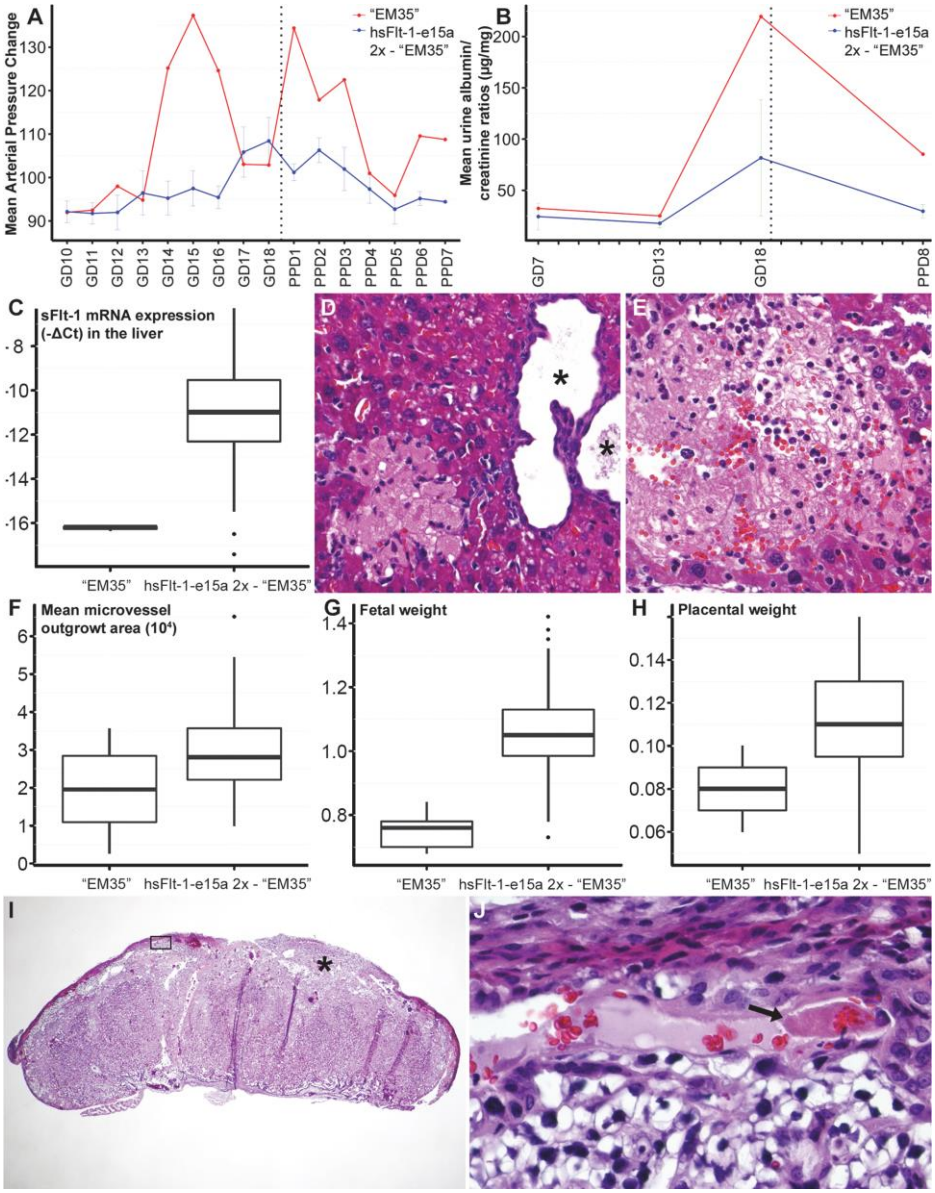

Figure 20. "EM35" mouse had early-onset preeclampsia-like symptoms associated with fetal growth restriction. (**A**) "EM35" mouse had a higher and earlier blood pressure peak than other hsFlt-1-e15a-treated mice, followed by the normalization of blood pressures and a second blood pressure peak on PPD1. (**B**) The urinary albumin/creatinine ratio on GD18 was higher in "EM35" mouse than in other hsFlt-1-e15a-treated mice. (**C**) HsFlt-1-e15a expression in the liver was lower in "EM35" mouse than in other hsFlt-1-e15a-treated mice. (D-E) Histopathological examination of the liver found a multiple cystic biliary hyperplasia in the liver (*** in D**), and multiple recent (**D**) and remote (**E**) infarcts in the parenchyma of liver. H&E stainings, 200x magnifications. (**F**) The endothelial outgrowth area was the lowest in "EM35" mouse among hsFlt-1-e15a-treated mice. (**G-H**) Mean fetal (**G**) weights (0.749±0.029) and placental (H) weights (0.080±0.006) in "EM35" mouse were significantly lower than in other hsFlt-1-e15a-treated mice (fetal weight: 1.06±0.023, $p=2.017x10^{-15}$, placental weight: 0.111±0.004, $p=2.05x10^{-6}$). (**I**) Histopathological examination of a placenta from "EM35" mouse showed multiple thrombi in maternal decidual vessels (star and black box). H&E staining, 20x magnification. The image inside the black box is magnified to 800x in Subfigure I. (**J**) The arrow shows one of the thrombi.

4.2. Study II

4.2.1. The development of various transgene delivery systems

In order to compare the effects of the full-length hsFlt-1-e15a with that of the truncated msFlt-1(1-3), viral constructs containing these two transgenes were constructed (**Figure 11A**)**.** Since previous studies demonstrated that an "RGD fiber-mutant" adenovirus has a tissue tropism distinct from the replication deficient (Type5, dE1/E3) adenovirus [295,299], we used both to investigate the effect of varying tissue expression profiles of hsFlt-1-e15a on its biological effects (**Figure 11B**). BioGPS data located the major and predominant expression of human *CYP19A1* to the placenta, and we observed that the expression of this gene strongly increased during villous trophoblast differentiation (**Figure 11C**). Since previous data showed that the 501bp placenta-specific promoter of human *CYP19A1* is able to drive placenta-specific gene expression in transgenic mice [300], we tested the effect of this 501bp *CYP19A1* promoter besides the CMV promoter in our viral constructs. **Figure 11D** and **Figure 11E** show the various combinations of viruses, promoters and transgenes used in this study.

4.2.2. Unique placental expression of msFlt-1

First, we aimed to detect the expression profile and levels of msFlt-1 in mice that had not received any viral injection. Total RNAs were isolated from placentas harvested on GD18, as well as from brain, kidney, liver, spleen, and uterine tissues harvested on PPD8. The expression of the endogenous transmembrane mFlt-1 mRNA was the highest in the placentas among the six tissues of mice that had not received virus injection (**Figure 21A**); msFlt-1-i13 mRNA expression was solely detected in the placentas of these non-treated animals (**Figure 21B**). Of note, the placental expression of msFlt-1-i13 mRNA was the highest among all tissues, genes and transcripts investigated in this study (**Figure 21B**). When we injected mice with the viral construct overexpressing the truncated msFlt-1(1-3), we observed the appearance of msFlt-1 mRNA expression in the liver (**Figure 21B**). The placental transcript levels of msFlt-1-i13 mRNA were not evidently increased in animals injected with the viral construct overexpressing truncated msFlt-1(1-3) compared to saline-treated mice, suggesting that the endogenous placental msFlt-1-i13 mRNA expression is higher than that of the transgene expressed msFlt-1(1-3) mRNA (**Figure 21B**).

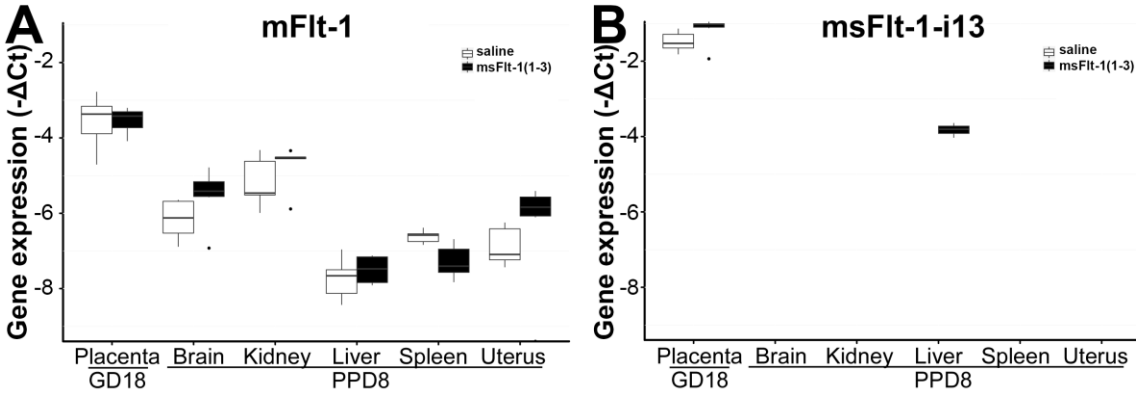

Figure 21. Profiling of mFlt-1 and msFlt-1-i13 expression. (**A**) Boxplots show the endogenous expression profile of the mouse transmembrane Flt-1 mRNA in placentas harvested on gestational day (GD) 18 and in five tissues harvested on postpartum day (PPD) 8. Endogenous Flt-1 mRNA expression was highest in the placenta in both the non-treated (saline) and the msFlt-1(1-3)-treated mice. (**B**) Boxplots show the endogenous expression profile of the msFlt-1-i13 mRNA in placentas harvested on GD18 and in five tissues harvested on PPD8. Endogenous msFlt-1-i13 mRNA expression was restricted to the placenta in control animals, and transgenic msFlt-1(1-3) expression was detected in the placenta and the liver.

4.2.3. Expression patterns of various viral transgenes

To compare the expression patterns of hsFlt-1-e15a and GFP, total RNAs were isolated from tissue samples harvested from virus-infected mice. Human sFlt-1-e15a and GFP mRNA expression varied according to the viral constructs (adenovirus or fiber-mutant adenovirus) and promoters (CMV or CYP). The fiber-mutant adenovirus supported a higher hsFlt-1-e15a mRNA expression in the kidney and liver compared to the adenovirus, while the CYP promoter restricted hsFlt-1-e15a mRNA expression in the liver compared to the CMV promoter (**Figure 22A**). Similarly, the CYP promoter restricted GFP mRNA expression in the liver (49.8-fold down-regulation, p=0.005), kidney (9.3-fold down-regulation, p=0.02) and spleen (13.5-fold down-regulation, p=0.01) compared to the CMV promoter, leading to the highest GFP mRNA expression in the placenta (**Figure 22B**). GFP expression was mainly restricted to the labyrinth zone of the placenta irrespective of the promoter in RGD fiber-mutant virus injected mice (**Figure 22C-E**).

DOI:10.14753/SE.2015.1828

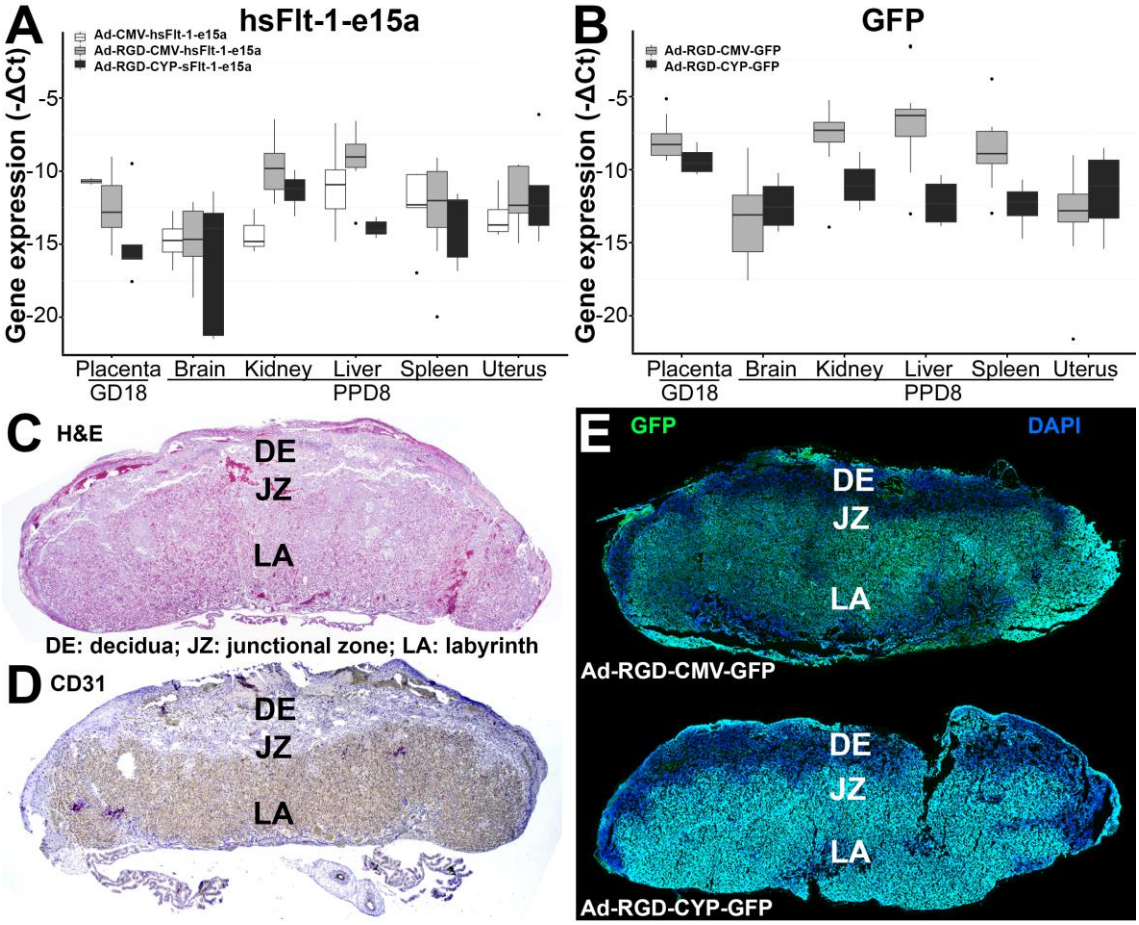

Figure 22. Profiling of hsFlt-1-e15a and GFP expression. (**A**) Boxplots show the expression profile of the transgenic hsFlt-1-e15a mRNA overexpressed by three different adenoviral vectors (Ad-CMV-hsFlt-1-e15a; Ad-RGD-CMV-hsFlt-1-e15a; Ad-RGD-CYP-hsFlt-1-e15a) in placentas harvested on gestational day (GD) 18 and in tissues harvested on postpartum day (PPD) 8. (**B**) Boxplots show the expression profile of GFP mRNA overexpressed by two different vectors (Ad-RGD-CMV-GFP; Ad-RGD-CYP-GFP) in placentas harvested on GD18 and in tissues harvested on PPD8. (**C**) Control placenta, H&E staining, 20x magnification. (**D**) Control placenta, anti-CD31 immunostaining, 20x magnification. The CD31 immunopositivity of the labyrinthine vessels are clearly seen. (**E, F**) Confocal microscopic images of placentas from GFP-treated mice. The placental expression of adenoviral GFP was the strongest in the labyrinth in both the Ad-RGD-CMV-GFP and Ad-RGD-CYP-GFP treated groups.

Since it is important to know whether the transgene affects endogenous gene expression, we have tested the impact of the transgene and the vector on endogenous msFlt-1-i13 expression. Importantly, we did not find any significant effect of either the transgene (GFP or hsFlt-1-e15a) or the vector (either the CYP or CMV promoter groups or the two groups merged) on the endogenous expression of msFlt-1-i13.

4.2.4. Blood pressure telemetry monitoring

The blood pressure profile over gestation was different in msFlt-1(1-3)-treated mice from that in GFP-treated mice ($p=3.7x10^{-5}$) prior to cesarean delivery. The ΔMAP at GD15 was 11.1mmHg higher (p=0.0008) in msFlt-1(1-3)-treated mice than in control mice, and this difference was even larger on GD18 (ΔMAP: 12.8mmHg, p=0.005) (**Figure 23A-B**).

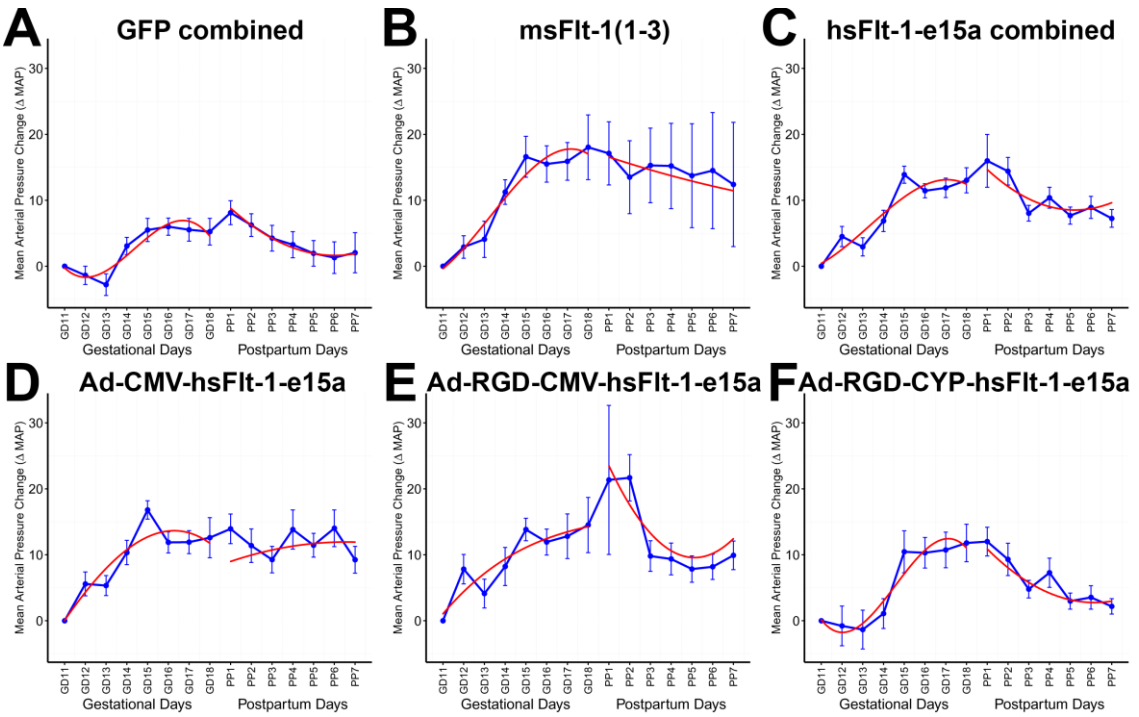

Figure 23. Blood pressure monitoring. X-axes show gestational days (GDs) and postpartum days (PPDs). Mean arterial pressure changes (ΔMAP) are depicted with blue curves. Blue lines show +/-standard errors. Red curves depict the ΔMAP patterns, fitted from the linear mixed effects model. (**A,B**) The blood pressure profile over gestation was different in msFlt-1(1-3)-treated mice from that in GFP-treated mice prior to cesarean delivery ($p=3.7x10^{-5}$; ΔMAP at parturition: 12.8mmHg, p=0.005). (**A,C**) The blood pressure profile over gestation in hsFlt-1-e15a-treated mice (all subgroups combined) was different from that in GFP-treated controls prior cesarean delivery ($p=4.3x10^{-4}$; ΔMAP at parturition: 7.8mmHg, p=0.009). (**D-F**) Among the three sub-groups of hsFlt-1-e15a-treated mice, those that received Ad-CMV-hsFlt-1-e15a and Ad-RGD-CMV-hsFlt-1-e15a had the highest increase in ΔMAP on GD15 (Ad-CMV-hsFlt-1-e15a: 11.3mmHg, p=0.0007; Ad-RGD-CMV-hsFlt-1-e15a: 8.3mmHg, p=0.009) and on GD18 (Ad-CMV-hsFlt-1-e15a: 7.4mmHg, p=0.09; Ad-RGD-CMV-hsFlt-1-e15a: 9.3mmHg, p=0.04) compared to controls. The blood pressure was 5mmHg (GD15) and 6.6mmHg (GD18) higher in Ad-RGD-CYP-hsFlt-1-e15a-treated mice than in control mice; however, p-values did not reach statistical significance (0.14 and 0.16, respectively).

Of interest, one mouse in this group had a very high ΔMAP and a blood pressure of 175/135mmHg on GD18. In contrast to all other mice in this group, this animal had constantly increasing blood pressure until PPD7 with a peak of 182/146mmHg, resembling

chronic hypertension following preeclampsia. The very high blood pressure values in this mouse skewed the mean MAPs in the postpartum period, causing the increased variance observed in **Figure 23B**.

Similarly, the blood pressure profile over gestation in hsFlt-1-e15a-treated mice (all subgroups combined: Ad-CMV, Ad-RGD-CMV, Ad-RGD-CYP) was different from that in GFP-treated controls ($p=4.3x10^{-4}$) prior to cesarean delivery. The ΔMAP at GD15 was 8.4mmHg higher (p=0.0005) in hsFlt-1-e15a-treated mice than in control mice, and it was 7.8mmHg higher on GD18 (p=0.009) (**Figure 23C**). Among the three sub-groups of hsFlt-1-e15a-treated mice, those that received Ad-CMV-hsFlt-1-e15a and Ad-RGD-CMV-hsFlt-1-e15a had the highest increase in ΔMAP on GD15 (Ad-CMV-hsFlt-1-e15a: 11.3mmHg, p=0.0007; Ad-RGD-CMV-hsFlt-1-e15a: 8.3mmHg, p=0.009) and on GD18 (Ad-CMV-hsFlt-1-e15a: 7.4mmHg, p=0.09; Ad-RGD-CMV-hsFlt-1-e15a: 9.3mmHg, p=0.04) compared to controls (**Figure 23D,E**). The blood pressure was 5mmHg (GD15) and 6.6mmHg (GD18) higher in Ad-RGD-CYP-hsFlt-1-e15a-treated mice than in control mice; however, p-values did not reach statistical significance (0.14 and 0.16, respectively) (**Figure 23F**).

4.2.5. Morphological and functional changes in the kidneys in sFlt-1 treated mice

The kidneys from GFP-treated mice showed widely open capillary loops which had thin delicate walls, and no segmental thickening or hypercellularity was noted (**Figure 24A,B**). These findings were confirmed using the Jones basement membrane reticulum stain, in which the capillary basement membranes were thin and delicate, and no mesangial thickening was seen (**Figure 24G**). In contrast, the most consistent histopathological changes seen in the kidneys of mice overexpressing hsFlt-1-e15a or msFlt-1(1-3) were focal and segmental, with swollen capillary endothelial cells, occlusion of glomerular capillaries, and focal mesangial thickening (**Figure 24C-F**). Scattered glomeruli appeared sclerotic. Glomerular capillary changes were further confirmed by PAS staining and Jones basement membrane reticulum stain, which showed thickened capillary loops and focal expansion of the mesangium (**Figure 24H**).

DOI:10.14753/SE.2015.1828

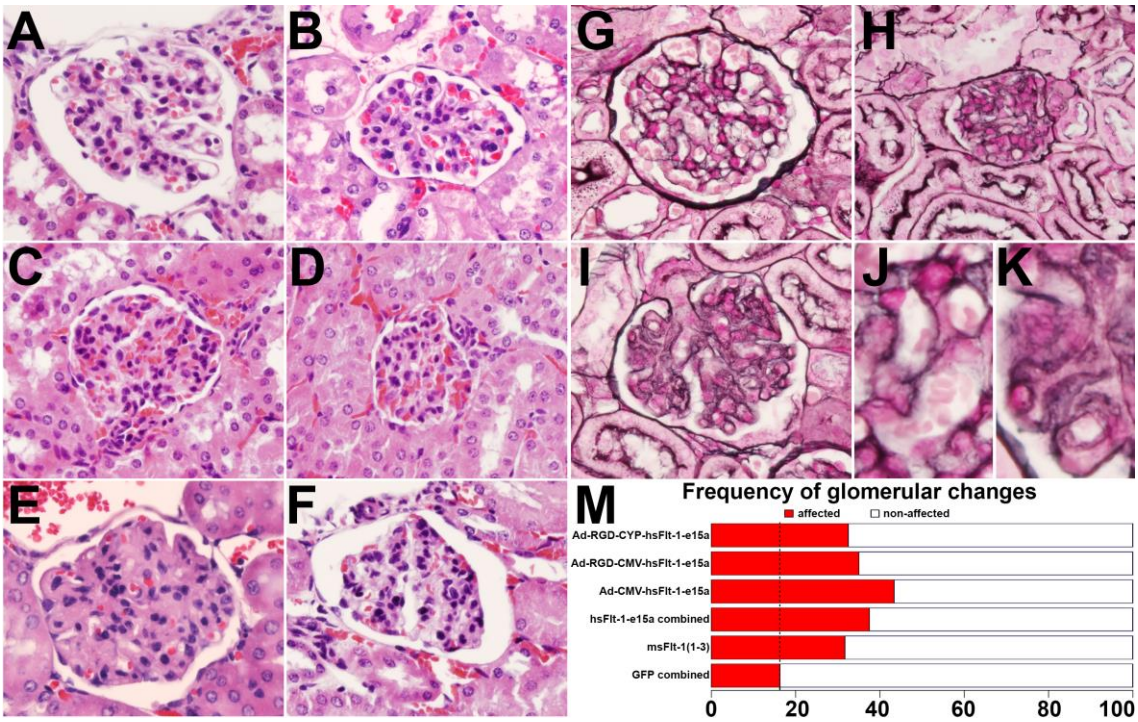

Figure 24. Histopathological evaluation of the kidneys. (**A,B,G**) Representative H&E (**A**: Ad-RGD-CMV-GFP, **B**: Ad-RGD-CYP-GFP) and Jones (**G**: Ad-RGD-CMV-GFP) stained sections show morphologically normal glomeruli in control animals. (**C,D,F,H**) Representative H&E (**C**: Ad-RGD-CMV-sFlt-1-e15a, **D**: Ad-RGD-CYP-sFlt-1-e15a, **F**: Ad-CMV-sFlt-1-e15a) and Jones (**H**: Ad-RGD-CMV-sFlt-1-e15a) stained sections show glomeruli with signs of swollen capillary endothelial cells and occlusion of glomerular capillaries in mice overexpressing sFlt-1-e15a. (**E,I**) Representative H&E (**E**) and Jones (**I**) stained sections show glomeruli with signs of swollen capillary endothelial cells and occlusion of glomerular capillaries in the dam overexpressing msFlt-1(1-3) with chronic hypertension. 400x magnifications. (**J**) High magnification image (1200x) from sub-image G shows a normal capillary structure. (**K**) High magnification image (1200x) from sub-image I shows thickened capillary loops. (**M**) The glomerular damage score was significantly higher in all treatment groups compared to the combined control group. Mice treated with msFlt-1(1-3) had an odds ratio (OR) of 2.4 for glomerular damage (p=0.01). The OR for glomerular damage was 3.1 in hsFlt-1-e15a-treated mice ($2.8x10^{-5}$). Among hsFlt-1-e15a-treated mice, mice in the Ad-CMV-hsFlt-1-e15a group had the largest OR (3.9, $p=4.8x10^{-5}$) for glomerular damage.

The dam in the msFlt-1(1-3)-treatment group with the constantly increasing blood pressure had dramatic changes in kidney histology, with extensive glomerular lesions seen in all glomeruli examined. These glomeruli appeared to be somewhat enlarged with marked thickening and expansion of the mesangium, and marked occlusion of capillaries and thickened capillary loops (**Figure 24E**). In this mouse, Jones basement membrane reticulum stain showed marked thickening and reduplication of the capillary loop basement membranes (**Figure 24I**). **Figure 24K** shows severe capillary loop damage with reduplication of the capillary loop in this mouse at high

magnification. A normal capillary loop stained with Jones basement membrane reticulum stain is shown in **Figure 24J** at high magnification.

Histopathological evaluations revealed that the glomerular damage score was significantly higher in all treatment groups compared to the combined control group. Mice treated with msFlt-1(1-3) had an odds ratio (OR) of 2.4 for glomerular damage (p=0.01). The OR for glomerular damage was 3.1 in hsFlt-1-e15a-treated mice ($p=2.8x10^{-5}$). Among hsFlt-1-e15a-treated mice, mice in the Ad-CMV-hsFlt-1-e15a group had the largest OR (3.9, $p=4.8x10^{-5}$) for glomerular damage (**Figure 24M)**.

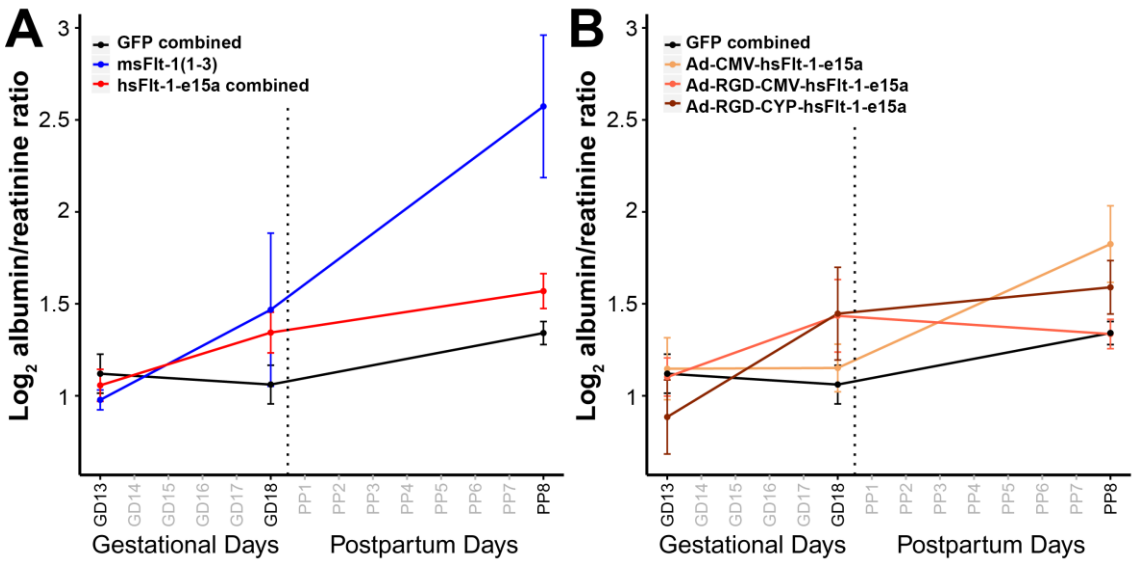

Figure 25. Functional evaluation of the kidneys. (**A**) Chart depicts albumin/creatinine ratios (in log scale) in urine specimens from mice in the GFP, msFlt-1(1-3) and hsFlt-1-e15a-treated groups. Mean urine albumin/creatinine ratios were higher in hsFlt-1-e15a-treated mice (GD18, p=0.04 and PPD8, p=0.03) and msFlt-1(1-3)-treated mice (PPD8, $p=4x10^{-5}$) than in controls. Proteinuria was extremely high in the mouse overexpressing msFlt-1(1-3) with chronic hypertension. (**B**) Subgroup analysis showed that hsFlt-1-e15a expressed under the CMV promoter in the adenovirus led to significant increase in albumin/creatinine ratio on PPD8 (p=0.003); hsFlt-1-e15a expressed under the CMV promoter in the fiber-mutant adenovirus led to significant increase in albumin/creatinine ratio on GD18 (p=0.04); while hsFlt-1-e15a expressed under the CYP promoter in the fiber-mutant adenovirus led to a marginally significant increase in albumin/creatinine ratio on GD18 (p=0.056) and a significant increase on PPD8 (p=0.04).

For functional evidence of kidney damage, we also determined albumin/creatinine ratios in urine samples obtained serially during pregnancy. As **Figure 25A** shows, mean urine albumin/creatinine ratios were higher in hsFlt-1-e15a treated mice (GD18, 1.9-fold, p=0.04 and PPD8, 1.7-fold, p=0.03) than in controls. The albumin/creatinine ratio was markedly

elevated in msFlt-1(1-3)-treated mice in the postpartum period (17-fold, $p=4x10^{-5}$). The dam in the msFlt-1(1-3)-treatment group with the constantly increasing blood pressure had extreme proteinuria with albumin/creatinine ratios of 3,070µg/mg on GD18 and 15,401µg/mg on PPD8. Subgroup analysis showed that Ad-CMV-hsFlt-1-e15a led to a significant increase in albumin/creatinine ratio on PPD8 (3-fold, p=0.003); Ad-RGD-CMV-hsFlt-1-e15a led to significant increase in albumin/creatinine ratio on GD18 (2.4-fold, p=0.04); while Ad-RGD-CYP-hsFlt-1-e15a led to a marginally significant increase in albumin/creatinine ratio on GD18 (2.4-fold, p=0.056) and a significant increase on PPD8 (1.8-fold, p=0.04) (**Figure 25B**). In summary, msFlt-1(1-3) had a stronger effect than hsFlt-1-e15a, and hsFlt-1-e15a expressed by the fiber-mutant adenovirus led to an earlier proteinuria than hsFlt-1-e15a expressed by the adenovirus.

4.2.6. Aortic endothelial dysfunction caused by hsFlt-1-e15a and msFlt-1

We found that the mean microvessel outgrowth volume was 77% reduced in hsFlt-1-e15a overexpressing mice than in controls (p=0.007), while the outgrowth volume was decreased by 66% in msFlt-1(1-3) overexpressing mice compared to controls (p=0.02) (**Figure 26**). Of interest, in the msFlt-1(1-3)-treated dam with the constantly increasing blood pressure, the microvessel outgrowth volume was only 53% of the mean microvessel outgrowth volume in other mice in this group, showing a strongly dysfunctional endothelium.

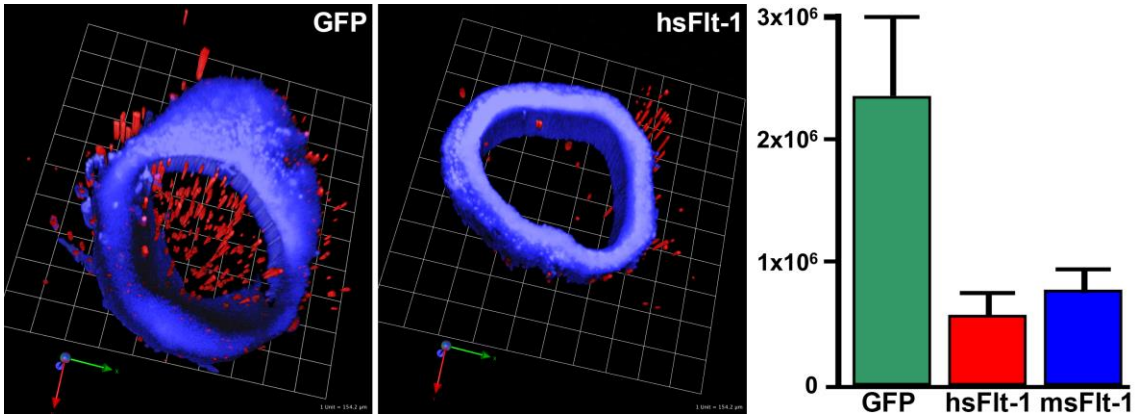

Figure 26. Aortic ring assays. Three dimensional reconstruction of confocal microscopic images of aortic rings from a mouse overexpressing GFP (left) or hsFlt-1-e15a (middle). Blue (4',6-diamidino-2-phenylindole, DAPI) depicts nuclei in the aortic rings, while red represents microvessel outgrowth volumes. The bar chart (right) depicts the differences in mean microvessel outgrowth volumes between the groups. Microvessel outgrowth from aortic rings was significantly decreased in hsFlt-1-e15a (p=0.007) and msFlt-1(1-3)-treated (p=0.02) mice compared to control animals.

DOI:10.14753/SE.2015.1828

4.2.7. Human sFlt-1-e15a but not msFlt-1(1-3) increases litter sizes

Fetal survival rate, average fetal weights, placental weights, and placental/fetal weight ratios were not affected by either hsFlt-1-e15a or msFlt-1(1-3) treatments (**Figure 27**).

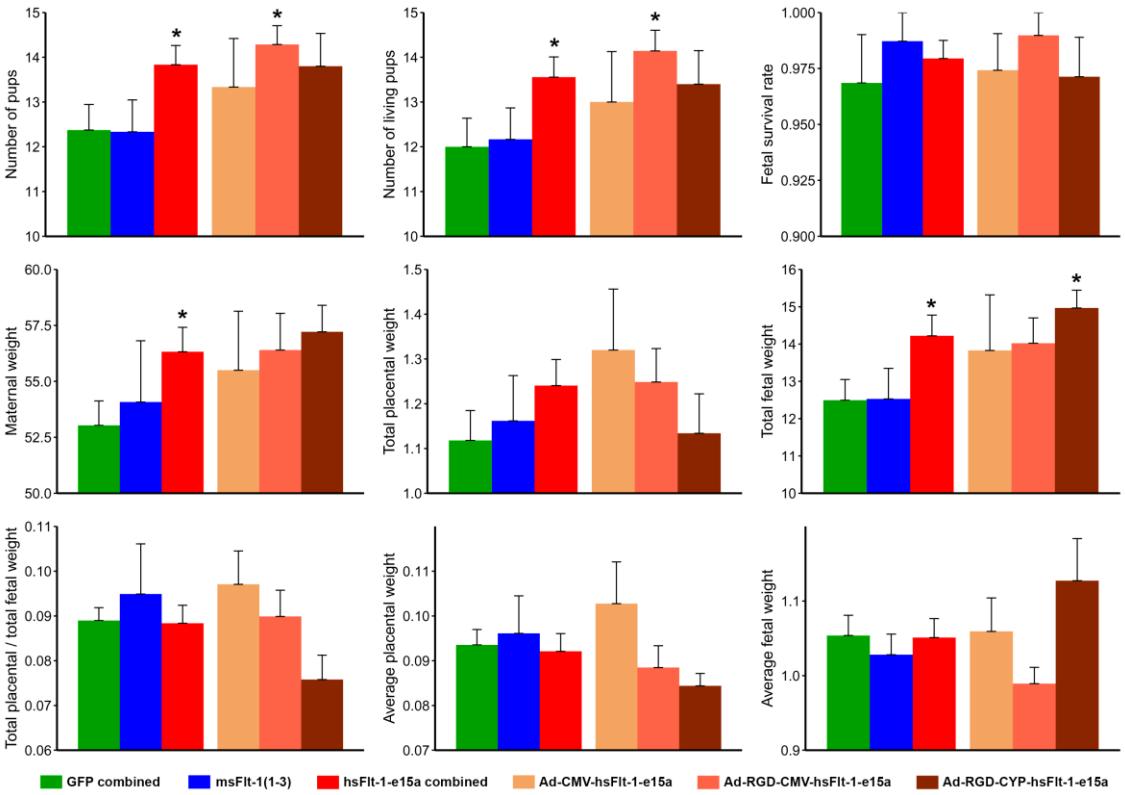

Figure 27. Litter sizes, maternal, placental and fetal weights, and placental/fetal weight ratios. Controls (n=17) and msFlt-1(1-3)-treated mice (n=6) had a litter size consistent with the strain average published by the vendor (n=11.5). The number of pups (13.8±0.4, p=0.046) and living pups (13.6±0.45, p=0.05) were higher in hsFlt-1-e15a-treated mice (n=18) than in controls. The total weight of living pups (14.2±0.56g, p=0.04) and maternal weights (56.3±1.1g, p=0.04) were also higher in hsFlt-1-e15a-treated mice than in controls. Truncated msFlt-1(1-3)-treated mice did not differ in any parameters from the controls. Among hsFlt-1-e15a-treated mice, the total weights of living pups was higher in the Ad-RGD-CYP-hsFlt-1-e15a treated mice than in controls (15±0.48g, p=0.043). The number of pups (14.3±0.42, p=0.047) and the number of living pups (14.1±0.46, p=0.039) was higher in the Ad-RGD-CMV-hsFlt-1-e15a treated mice than in controls. Stars denote statistical significance.

Controls (n=17) and msFlt-1(1-3)-treated mice (n=6) had a litter size consistent with the average published by the vendor (n=11.5). The number of pups (13.8±0.4, p=0.046) and living pups (13.6±0.45, p=0.05) were higher in hsFlt-1-e15a-treated mice (n=18) than in controls. The total weight of living pups (14.2±0.56g, p=0.04) and maternal weights (56.3±1.1g, p=0.04) were also higher in hsFlt-1-e15a-treated mice

DOI:10.14753/SE.2015.1828

than in controls. MsFlt-1(1-3)-treated mice did not differ in any parameters from the controls. When analyzing the subgroups of hsFlt-1-e15a-treated mice, the total weights of living pups was higher in the Ad-RGD-CYP-hsFlt-1-e15a treatment group than in controls (15±0.48g, p=0.043). The number of pups (14.3±0.42, p=0.047) and the number of living pups (14.1±0.46, p=0.039) was higher in the Ad-RGD-CMV-hsFlt-1-e15a-treated mice than in controls.

5. DISCUSSION

5.1. Principal findings

The principal findings of our first study included the followings: **1**) Ultrasound predicted pregnancy in 97% of the cases on GD7; **2**) Ultrasound determined telemetry catheter positions in all cases; **3**) The survival rate of the newly implemented, minimally invasive survival cesarean section was 100% and uteri showed complete healing at the incision site on PPD77; **4**) The hsFlt-1-e15a isoform was mainly expressed in the liver; **5**) The hsFlt-1-e15a isoform increased mean arterial blood pressure on GD18 compared to controls; **6**) The mean urine albumin/creatinine ratio on GD18 was higher in hsFlt-1-e15a-treated mice than in control mice; **7**) Glomerular changes were found in the kidneys of hsFlt-1-e15a-treated mice, including swollen capillary endothelial cells and occlusion of glomerular capillaries; **8**) Aortic ring assays showed lesser microvessel outgrowth in hsFlt-1-e15a-treated mice compared to control mice; **9**) There was no difference in placental and fetal weights between the treatment and control groups; and **10**) There was one hsFlt-1-e15a-treated mouse that had severe, early-onset preeclampsia-like symptoms associated with fetal growth restriction and multi-organ involvement.

The principal findings of our second study included the followings: **11**) The *in vivo* biological effects of full-length hsFlt-1-e15 and the truncated msFlt-1(1-3) could be directly compared; **12**) The full-length transmembrane mFlt-1 transcript was the most abundant in the placenta among six tissues investigated in mice; **13**) The soluble mFlt-1-i13 variant was only expressed in the placenta in mice. Its unique and high level of expression suggest an important role for this soluble variant in the placenta; **14**) The overexpression of the full-length hsFlt-1-e15a increased litter size, while the truncated msFlt-1(1-3) did not have this effect, underlining the important role of the full-length sFlt-1 in early pregnancy; **15**) In the second half of pregnancy, both the full-length human and the truncated mouse sFlt-1 promoted the development of preeclampsia, including blood pressure elevation, glomerular damage, proteinuria, and endothelial dysfunction; **16**) The truncated msFlt-1(1-3) also increased blood pressure and induced proteinuria similar to the full-length hsFlt-1-e15a; and **17**) One dam with msFlt-1(1-3)-treatment had constantly high blood pressure, severe proteinuria and extensive glomerular damage, suggesting an increased sensitivity to sFlt-1 of this animal.

5.2. Pregnancy status was accurately determined with high-resolution ultrasound

Timed-pregnant CD-1 mice arrived on GD5, when only a 75% pregnancy rate was guaranteed by the vendor. Therefore, we used a 55MHz ultrasound probe to determine the pregnancy status of each mouse before the implantation of a telemetry catheter. Initially, ultrasound scans were performed on GD6; however, positive signs of a pregnancy were limited to the detection of gestational sacs ≤2.7mm (**Figure 3A**). Therefore, later we continued the scans on GD7 when an advanced endometrial reaction and embryos were detectable in pregnant uteri (**Figure 3B**). These signs clearly distinguished pregnant uteri from non-pregnant uteri (**Figure 3C**). Among 35 mice scanned on GD7 in the first study, 32 were correctly diagnosed as pregnant and two as non-pregnant, while one mouse was falsely diagnosed as non-pregnant (**Figure 3D**). Thus, the accuracy of our method was 97% (34/35), showing that pregnancy could be identified with high confidence on GD7. In the case of the mouse with a false negative diagnosis, a very weak endometrial reaction could only be identified without signs of an embryo, which did not match our criteria for the diagnosis of pregnancy. Upon a cesarean delivery, we observed that this mouse had a highly compromised pregnancy and carried only three live fetuses, suggesting that high-frequency ultrasound may be useful for the early detection of pregnancy complications in mice.

5.3. Telemetric blood pressure monitoring provided accurate data acquisition in pregnant mice

Among blood pressure monitoring systems utilized in previous rodent preeclampsia models, the telemetric blood pressure monitoring system offers several advantages over non-invasive systems, including the tail-cuff method [262,264,301]. Telemetric blood pressure monitoring system supports continuous, validated, and reliable data acquisition from unrestricted, conscious mice in their physiological surroundings [302-306] (**Figure 28**).

DOI:10.14753/SE.2015.1828

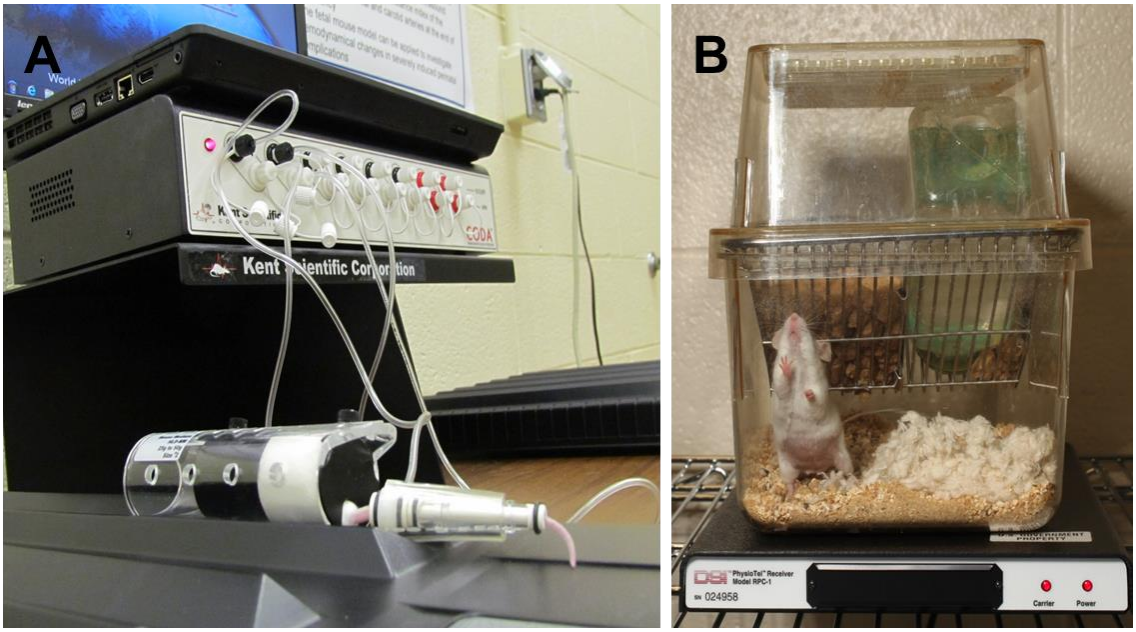

Figure 28. The tail-cuff and the telemetric blood pressure monitoring systems. (**A**) The tail-cuff blood pressure monitoring system is a non-invasive methodology, but mice are kept in a strain and stressful position during the measurement. (**B**) The telemetric blood pressure monitoring system supports continuous, validated, and reliable data acquisition from unrestricted, conscious mice in their physiological surroundings. The photos are courtesy of the Perinatology Research Branch, NICHD, NIH, DHHS.

The telemetric blood pressure monitoring enables the continuous, unstressful detection of circadian blood pressure changes in these very stress-sensitive rodents, and therefore it is the method recommended by the American Heart Association for the continuous blood pressure monitoring in unrestrained animals [307-309]. We aimed to implant telemetry catheters at an early stage of gestation so that recovery from surgery would occur before the expected time for blood pressure elevations during the second half of pregnancy. According to our initial results in the first study, the rate of uncomplicated carotid telemetry implantations in pregnant mice [79% (30/38)] were as high as in non-pregnant CD-1 mice in a previous study that compared the complication rates in carotid and abdominal aortic telemetry implantations [310]. The complication rate was higher in the case of the HD-X11 telemetry device [29% (5/17)] than in the case of the TA11PA-C10 transmitter [14% (3/21)]. Among these eight cases with complications, three mice implanted with the TA11PA-C10 devices and one mouse implanted with the HD-X11 device had abnormal body posture and seizures, suggesting ischemic brain damage, while four mice implanted with the HD-X11 devices had transmitter body exteriorization. Because the HD-X11 device is larger in weight and volume [311], the

decrease in subcutaneous space around the transmitter and the increase in abdominal circumference during pregnancy could lead to this higher frequency of HD-X11 transmitter exteriorization. These data suggest that the TA11PA-C10 device is more suitable than the HD-X11 device for blood pressure monitoring in pregnant mice.

As a malpositioned telemetry catheter (e.g. a catheter tip remaining in the carotid artery) can lead to thrombotic catheter occlusions and incorrect blood pressure readings [302,310,311], we investigated telemetry catheter positions in all mice. Since the evaluation of catheter positions after euthanization may be biased by accidental dislocation of catheter tips during autopsy, we used high-frequency (55MHz) ultrasound for the accurate, *in vivo* determination of catheter tip positions on GD13 (**Figure 5D**). According to the manufacturer's recommendation, their positions were treated as optimal when 2mm of the sensing region of the catheter was placed in the aortic arch [311]. These investigations assured us that blood pressure differences between animals did not occur due to malpositioned telemetry catheters.

5.4. A 100% survival rate was obtained with cesarean surgery

Preeclampsia is a syndrome originating from a dysfunctional placenta, since the clinical symptoms usually diminish within a couple of days after the delivery of this organ [19,46,53-57,61,109,185]. Intriguingly, preeclampsia can also develop postpartum, occurring in ~6% of cases; and thus, the monitoring of the symptoms of preeclampsia is recommended to continue in the early postpartum period [11,25]. Taking into account of these, a major limitation of most mouse preeclampsia models has been that fetuses and placentas were delivered via non-survival surgeries, disabling postpartum monitoring of these animals [262,263,312]. Although some mouse preeclampsia models included postpartum monitoring, in which animals were allowed to deliver naturally [191,265,313], the collection and evaluation of all placentas could have been problematic or impossible in these models, since mice usually deliver during the night and eat their placentas immediately after delivery [314]. Moreover, there is a natural variation in delivery dates of CD-1 pregnant mice according to the information from the vendor, which leads to variation in fetal and placental weights at the time of delivery [315], disabling accurate comparisons of these indices between the study groups.

Because of these facts, in the first study we developed a new survival cesarean surgery which enabled follow up on changes in blood pressure and urinary albumin during the postpartum period all along our experiments. In contrast to a previous survival uterine surgery performed in mice [298], we exteriorized only a short segment of one uterine horn at a time, and performed two or three small incisions on each horn (**Figure 9A-D**). The eight-day survival rate of this surgery was 100%, and histopathological examinations showed completely healed endometrium, as well as complete healing of the inner layer of the myometrium with only focal disruption of the outer layer at suture sites 77 days after surgery (**Figure 9J-L**). These results demonstrated that the aseptic, minimally invasive survival cesarean section offers an important advantage for rodent preeclampsia models: namely, the possibility of postpartum blood pressure and urine albumin monitoring after the delivery of fetuses and placentas.

5.5. A full-length, primate-specific sFlt-1-e15a isoform was selected to induce preeclampsia in mice

It is important to note that most anti-angiogenic rodent models of preeclampsia utilized adenoviruses overexpressing a truncated sFlt-1 mutant [msFlt-1(1-3)] comprising only 1-329 amino acids from Flt-1 [105,108,261,262,264,266,273-277,316]. This msFlt-1(1-3) mutant contains the first three Ig-like domains that are involved in VEGF binding, but it neither contains the additional Ig-like domains involved in receptor dimerization nor the unique tail region of sFlt-1-i13 [211]. This artificially truncated sFlt-1(1-3) mutant is naturally not expressed in any species. Therefore, the functional results of these animal studies may not entirely reflect the pathologic conditions in women with preeclampsia. Indeed, a recent mouse model of preeclampsia utilized the full-length, naturally expressed mouse sFlt-1-i13 (msFlt-1-i13) [263], which was less effective in inducing proteinuria than the truncated msFlt-1(1-3) mutant, suggesting that msFlt-1-i13 may have different bioavailability [263]. Another recent study of mice utilized the lentiviral overexpression of human sFlt-1-i13 (hsFlt-1-i13) isoform [265]. This isoform induced late-onset preeclampsia with only a moderate increase in urinary albumin excretion in mice [265].

Based on these previous experiences, we aimed to build a mouse model of preeclampsia in which we can better mimic the full spectrum of the human syndrome. We were interested in testing the *in vivo* pathologic effect of the predominant placental hsFlt-1-e15a transcript in preeclampsia [112,183,184], and whether it can induce the development of preeclampsia in mice. In the first study, our mouse model utilized adenoviruses overexpressing hsFlt-1-e15a or GFP under the CMV promoter, which was claimed to provide predominant gene expression in the liver [317,318]. In accord with these, we found that hsFlt-1-e15a and GFP mRNA expression was highest in the liver (**Figure 12A,B**). Although a viral dose-effect was not seen in GFP expression, a dose-effect was observed in the expression of hsFlt-1-e15a, which had an overall lower expression in all investigated tissues than GFP. These results suggested that the second injection of $1x10^9$ PFU Ad-CMV-hsFlt-1-e15a on GD11 led to a longer and persistent high viral load and hsFlt-1-e15a mRNA expression, and possibly longer persisting biological effects of hsFlt-1-e15a.

Previous studies of preeclampsia utilizing the overexpression of mouse or human sFlt-1-i13 did not aim to detect sFlt-1 protein expression in the placenta [263,265]. Besides the low placental sFlt-1 expression, another explanation may be the lack of suitable antibodies for immunostaining. Indeed, our search failed to find any commercially available antibody which would detect only hsFlt-1-e15a without the cross-reaction with the naturally expressed mouse sFlt-1 variants in the placenta. Because of this limitation, and to confirm the expression of hsFlt-1-e15a and GFP proteins, we infected BeWo human trophoblast-like cells with Ad-CMV-GFP or Ad-CMV-hsFlt-1-e15a, and used a human sFlt-1 specific antibody for Western blots or confocal microscopy for GFP detection. Western blots showed that non-infected BeWo cells expressed low amounts of the 185kDa Flt-1 membrane receptor, and two lower molecular weight (145kDa and 110kDa) sFlt-1 immunoreactive proteins (**Figure 13A**).

The size of these protein isoforms corresponded with the 130kDa and 115kDa protein isoforms expressed in HeLa cells by the sFlt1-14 (sFlt-1-e15a) transgene in the study of Sela et al. [112], and the 145kDa and 100kDa sFlt-1 isoforms detected in the plasma of patients with preeclampsia by the study of Rajakumar et al [319], which latter used the same antibody for Western blots as ours [319]. Of interest, Ad-CMVhsFlt-1-e15a-infected BeWo cells overexpressed both the 145kDa and the 110kDa sFlt-1

variants, which were shown to be glycoproteins of different peptide lengths rather than differentially glycosylated proteins [319]. Indeed, after deglycosylation, the ~145kDa and ~100kDa isoforms became ~80kDa and ~70kDa proteins, respectively [319]. Since the predicted molecular weights of the protein backbones of sFlt-1-i13 and sFlt-1-e15a are 77kDa and 82kDa respectively, it is possible that we and the two other research groups have detected these most abundant isoforms. This can occur if the sFlt-1-i13 isoform can be expressed from the sFlt-1-e15a transgene, which is theoretically possible based on the mode of alternative splicing resulting in this isoform. Confocal microscopy of BeWo cells infected with Ad-CMV-GFP revealed cytoplasmic GFP expression (**Figure 13B**). These results confirmed the functionality of the two adenoviral constructs at the protein level, and pointed out that different human sFlt-1 variants may be secreted into the circulation, complicating the blood concentration determinations with conventional techniques.

5.6. Human placental hsFlt-1-e15a increased blood pressure that normalized after delivery

In the same study we were able to show that the overexpression of the hsFlt-1-e15a isoform predominantly expressed in the human placenta in preeclampsia can induce blood pressure elevation in mice. Most anti-angiogenic models in rodents mimicked late-onset preeclampsia, with late-gestational blood pressure elevations and mild proteinuria in dams, and without growth restriction of the fetuses [263,276,277]. These models mostly did not include postpartum monitoring, making it impossible to confirm postpartum blood pressure elevation or normalization [105,261,262,264,266,277,312]. Since our model allowed for postpartum monitoring, we monitored blood pressures until PPD7. In the period between GD10 and the cesarean delivery, there was no significant change in blood pressures in the control mice; however, blood pressures significantly increased over time in response to hsFlt-1-e15a treatment, reaching a ΔMAP difference of 13.2 mmHg at parturition ($p=0.00107$) (**Figure 14**). After cesarean delivery, ΔMAP decreased in both the control group and in hsFlt-1-e15atreated mice. However, blood pressures decreased under baseline level in control mice, while these stayed above the baseline in hsFlt-1-e15a-treated mice. These results suggest that the overexpression of hsFlt-1-e15a leads to preeclampsia-like blood pressure elevation in

mice, which may stay beyond delivery. The postpartum decrease in blood pressures in hsFlt-1-e15a-treated mice was probably due to the decrease in viral load and hsFlt-1-e15a expression, including the effect of the delivery of the placenta. The delayed normalization of blood pressures may also reflect a conditioning effect of hsFlt-1-e15a on the vasculature.

Previous murine studies employing tail-vein injection of adenoviruses overexpressing sFlt-1 on GD8/GD9 and longitudinal blood pressure monitoring showed peak blood pressure elevations on GD17/GD18, eight to 10 days after adenovirus injection [261-264]. These previous observations were further substantiated by our findings, since mice that received one dose of Ad-CMV-hsFlt-1-e15a on GD8 had their peak MAP on GD18, similar to late-onset preeclampsia in humans. Interestingly, mice that received the second dose of Ad-CMV-hsFlt-1-e15a on GD11 in our study had their peak MAP postpartum (PPD3), similar to late-onset and/or postpartum preeclampsia in humans, suggesting that the extra dose of adenoviruses prolonged - but not heightened - the blood pressure elevation in these animals. This phenomenon suggests that one pathomechanism of postpartum preeclampsia may be that traces of placental tissues producing sFlt-1 and other toxic products may be left in the maternal body.

5.7. Human placental hsFlt-1-e15a impaired endothelial and kidney functions

One of the characteristics of preeclampsia is the generalized dysfunction and damage of the endothelium in the mother, including the morphological and functional changes in glomeruli [9,19,47,49,56,105,108,320,321]. It has been possible to recapitulate these findings in animal models of preeclampsia, especially in those employing the overexpression of anti-angiogenic factors [105,108,263,265], which would lead to a decrease in biological availability of angiogenic factors pivotal to endothelial functions [105,262-265,267,316]. Since aortic ring assays have been previously used to evaluate endothelial functions *in vitro* in some rodent models [292,293,322,323], we established this model in our first study to investigate endothelial functions in hsFlt-1-e15a overexpressing mice. We detected a large decrease in endothelial function measured by microvessel outgrowth in hsFlt-1-e15a overexpressing mice compared to controls (46%, p=0.012) (**Figure 17**). This result suggested that preeclampsia-like symptoms in our

mouse model also include endothelial dysfunction, which is a hallmark of preeclampsia in humans [47,56,320].

In most anti-angiogenic models of preeclampsia [105,263,264], glomerular endotheliosis could be detected in the kidneys, consistent with histopathological findings in women with preeclampsia [49,324,325]. In accord, histopathological examinations of the kidneys in this first study showed focal glomerular changes in mice overexpressing hsFlt-1-e15a (**Figure 18**). As expected, there were no significant morphological changes in the glomeruli of control mice. We also looked for *in vivo* functional evidence of kidney damage. The determination of the albumin/creatinine ratio for randomly collected human urine specimens has been proposed to replace the inconvenient 24-hour urine collection for the detection and monitoring of microalbuminuria, albuminuria and proteinuria. Although there are limitations of this ratio in clinical use, some animal models of preeclampsia utilized this method recently [108,263,265]. Here we also determined albumin/creatinine ratios in urine samples obtained longitudinally. In accord with the histopathological findings, mean urine albumin/creatinine ratios increased by GD18 and then dropped postpartum in hsFlt-1-e15a overexpressing mice, while these did not change in control mice (**Figure 18**). These results indicated that hsFlt-1-e15a overexpression led to endothelial damage in the kidneys besides endothelial dysfunction in the aorta, suggesting a generalized endothelial dysfunction in the dams.

5.8. Human placental hsFlt-1-e15a induced distinct preeclampsia phenotypes in CD-1 mice

Previous anti-angiogenic models of preeclampsia utilizing the overexpression of sFlt-1 in rodents could not recapitulate early-onset preeclampsia associated with fetal growth restriction. We found only a couple of studies where fetal growth restriction was associated with late-onset preeclampsia [108,262,265]. In our first study the fetal weights, placental weights, and placental/fetal weight ratios were not affected by hsFlt-1-e15a treatment, and the overexpression of hsFlt-1-e15a in mice mimicked late-onset and postpartum preeclampsia phenotype in humans. The close monitoring of mice during pregnancy and postpartum revealed that blood pressure peaks (GD18 and PPD3) occurred after 10 days following both the first (GD8) and second (GD11) Ad-CMV-

hsFlt-1-e15a injections in all mice but one ("EM35") (**Figure 29**). In these cases, the growth potential of the fetuses was not compromised because they had already reached the top of their growth curve [315] when the hsFlt-1-e15a effect reached its plateau. In the case of the "EM35" mouse, blood pressure elevations peaked at six and seven days after Ad-CMV-hsFlt-1-e15a injections (GD15 and PPD1). In this case, fetal growth restriction was similar to that observed in another mouse model [326]. In the "EM35" mouse, the fetal growth potential was severely compromised because the hsFlt-1-e15a effect was highest when fetuses reached only about one-third or one-fourth of their growth curve. These findings are in good accord with the angiogenic/anti-angiogenic imbalance that develops earlier in pregnancy, and fetal growth restriction occurs more frequently in early-onset preeclampsia than in late-onset preeclampsia [11,96,141,145,147,153,157,166,327].

Our histopathological findings suggested that the "EM35" mouse had cystic biliary hyperplasia, an infrequent but normal background lesion in CD-1 mice according to the information from Charles River Laboratories. As measured by qRT-PCR, this liver disease restricted the expression of hsFlt-1-e15a in the liver, allowing only shorter blood pressure elevations from the 5th to 10th days after Ad-CMV- hsFlt-1-e15a injections. However, this maternal liver disease probably sensitized this animal to any hsFlt-1-e15a effect, and promoted the development of a more severe and fulminant preeclampsia phenotype with heightened and early blood pressure elevation, generalized endothelial dysfunction, and generalized thrombotic disease, which affected the liver and the placenta, and consequent fetal growth restriction. We could not investigate maternal coagulation status in this mouse because we did not obtain maternal plasma specimens; however, since CD-1 is an outbred mouse strain with individual animals having a different genetic background [328-330], we hypothesize that the "EM35" mouse might have had a thrombotic disorder. This finding is consistent with the observation that inherited and acquired thrombophilias predispose for the development of severe preeclampsia and early-onset preeclampsia in humans [48,331-333], and also that women developing early-onset preeclampsia may have a pre-existing metabolic disease [30,334]. Of importance, among previous mouse models of preeclampsia, those which involved animals that had a maternal knock-out phenotype [e.g. eNOS(-/-), IL10(-/-), C1q(-/-)] were able to generate severe preeclampsia phenotype associated

with IUGR [103,267,313,335]. Based on these human and experimental animal data it seems that the phenotype of preeclampsia is fundamentally influenced by both fetal (placental factors released to the maternal circulation) and maternal (genetic and environmentally induced diseases) factors, and the parallel existence of certain maternal diseases to preeclampsia can promote the development of an early-onset preeclampsia phenotype.

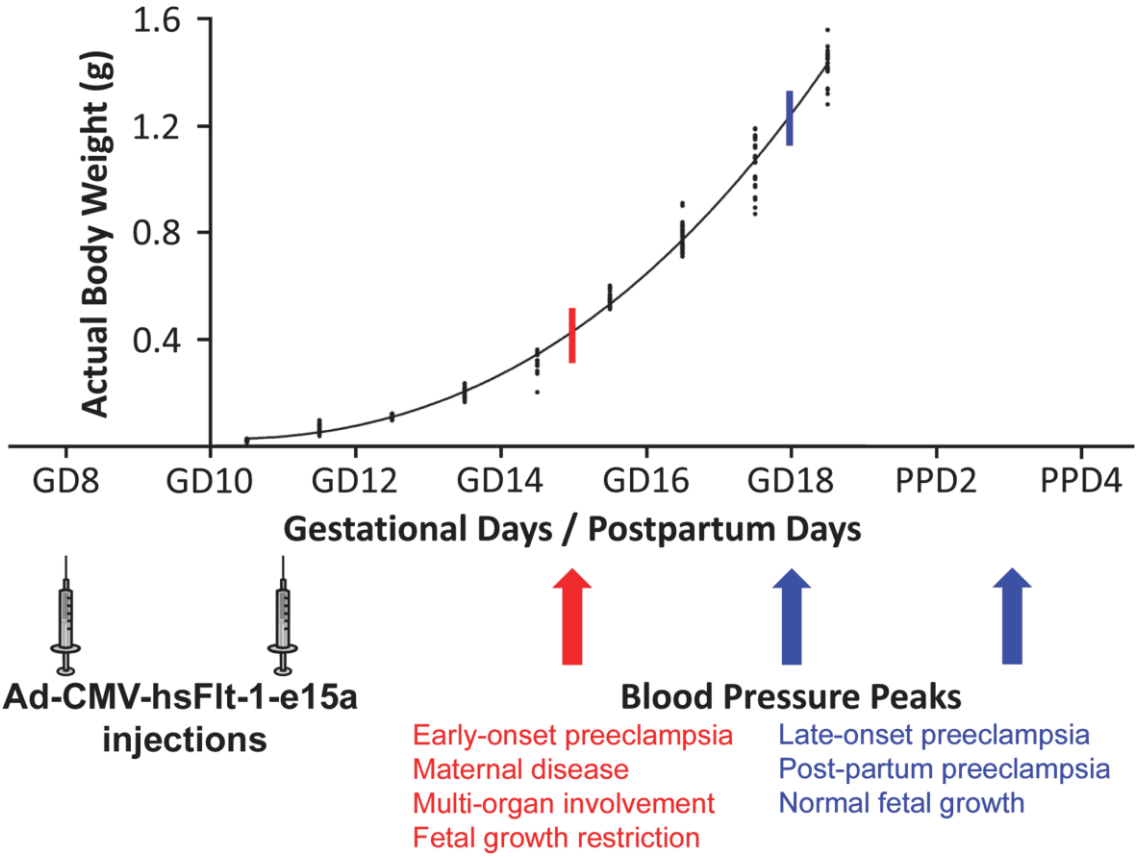

Figure 29. The possible mechanisms of distinct preeclampsia phenotypes induced by hsFlt-1-e15a. Blood pressure peaks (blue arrows) occurred after a ten-day-period following the first and second Ad-CMV-hsFlt-1-e15a injections in all but one mice that developed late-onset or postpartum preeclampsia without growth restriction. In these cases the growth potential of the fetuses was not compromised because they have already reached the top of their growth curve when hsFlt-1-e15a effect reached its plateau (blue stick crossing the curve). In case of "EM35" mouse, blood pressure elevations already peaked at six days after the first Ad-CMV- hsFlt-1-e15a injection (red arrow). In this case the fetal growth potential was severely compromised because the hsFlt-1-e15a effect was the highest when fetuses had reached only about one third or fourth of their growth curve (red stick crossing the curve). Preeclampsia phenotypes are described below the growth curve of CD-1 mouse embryos, which was adapted from a figure in a previous publication of Mu et al. [315]. Permission for reuse of this original figure was obtained from BioMed Central.

5.9. The preeclampsia-inducing effects of the full-length hsFlt-1-e15a are similar to those of the mouse truncated sFlt-1(1-3)

In our first study, similar to most previous anti-angiogenic murine models of preeclampsia, replication deficient adenoviruses with major tropism in the liver were used to overexpress sFlt-1, and thus, dominant placental sFlt-1 expression could not be achieved [105,263,264,317,336,337]. Interestingly, a couple of unrelated studies demonstrated that an "RGD fiber-mutant" adenovirus has a 10-100x higher placental tropism than the replication deficient adenovirus [295,299]. In another study, the human *CYP19A1* promoter was shown to drive placenta-specific gene expression in transgenic mice [300]. For these reasons, in our second study we chose different combinations of adeno- and "RGD fiber-mutant" adenoviruses as well as the common CMV promoter and the *CYP19A1* promoter to generate distinct tissue expression patterns of sFlt-1 (**Figure 11**). We also compared the effects of full-length hsFlt-1-e15a to those of the truncated msFlt-1(1-3) extensively used in previous studies [175]. Because of the high conservation between various, full-length and truncated isoforms of sFlt-1 in humans and mice [211,220] and the lack of immunoassays which could differentiate between these, we investigated the expression of these distinct isoforms at the RNA level.

In certain combinations we were able to reduce the expression of the transgene in the liver, and we could detect the highest expression of GFP in the placenta among all tissues. According to the GFP expression pattern, the "RGD fiber-mutant" adenovirus had a preference for the labyrinth zone of the placenta where most angiogenesis occurs. In spite of having the main expression of hsFlt-1-e15a and msFlt-1(1-3) in this zone, we could not observe any effect of the truncated msFlt-1(1-3) or the full-length hsFlt-1-e15a on fetal or placental growth either. Since a recent study that used lentiviral expression of sFlt-1 in the placenta could detect some effects of this decoy receptor on fetal growth [265], it might suggest that the local concentrations of sFlt-1 in the placenta expressed by the adenoviral delivery systems may not reach a certain level, which would severely affect placental angiogenesis.

However, the level of expression of the natural mouse sFlt-1-i13 in the current study was much higher in the placenta than the transgene in control mice, which had normal fetal growth. This observation suggests that sFlt-1 itself cannot have such a negative impact on placental angiogenesis, which would severely affect fetal growth in

mouse pregnancies. Indeed, a study that investigated the clinical effects of sFlt-1(1-3) and soluble endoglin in rats detected that the overexpression of sFlt-1(1-3) itself was not able to decrease birth-weights, only when coupled with the overexpression of soluble endoglin [108]. In fact, most of the studies in rodents recapitulated these results by not detecting decreased birth-weights in rodents overexpressing solely sFlt-1 [105,108,261,262,264,266,273-277].

Since our longitudinal study on human subjects previously demonstrated that sFlt-1 overexpression is a feature of both term and preterm preeclampsia, while soluble endoglin is overexpressed in cases of IUGR all along pregnancy and also in preterm preeclampsia [157], it is possible that soluble endoglin overexpression in parallel with that of sFlt-1 is a feature needed for the development of early-onset, IUGR-associated preeclampsia, if maternal or environmental factors otherwise do not exaggerate the phenotype of preeclampsia. This would mean that the phenotype of preeclampsia may depend on the angiogenic/anti-angiogenic molecule profile, which could be an interesting subject of later studies.

Similar to our first study, the plateaus in mean arterial blood pressures in both the msFlt-1 and hsFlt-1-treated animals in the second study occurred between GD15-18, seven to eight days after the adenovirus injections on GD8 and GD11. Since transient transgene expression by adenoviruses and the virus load decrease 7-10 days after virus injection [317,337,338], consistent with blood pressure peaks 8-10 days after injection of adenoviruses overexpressing sFlt-1 in rodents [261-264], our results corroborated that blood pressure plateaus occurred in parallel with the highest sFlt-1 transgene expression. The decrease in blood pressures was probably not only the result of the decrease in sFlt-1 transgene expression due to decreasing viral load, but also because of the delivery of the placentas expressing a considerable amount of sFlt-1. This is consistent with the findings in humans, where the delivery of the placenta, which produces the increased amounts of sFlt-1 variants almost exclusively [183], quickly decreases blood pressures and cures the clinical symptoms in preeclampsia [9,11]. Similarly, the extracorporeal removal of sFlt-1 from maternal blood leads to the decrease in blood pressures and the improvement of the clinical condition in women with preeclampsia [339].

Interestingly, the truncated msFlt-1(1-3) had a similar effect on blood pressure

elevation and proteinuria to the full-length hsFlt-1-e15a. Since the mouse placenta expresses levels of endogenous sFlt-1-i13 as high as in transgenic msFlt-1(1-3), the question occurred why this endogenous molecule did not cause severe preeclampsia-like symptoms in untreated animals. As has been discussed in previous publications [211,220], the truncated sFlt-1(1-3), which lacks three IgG-like domains and a conserved tail region compared to the hsFlt-1-e15a variant, may have different bioavailability, circulating half-life, and angiogenic factor sequestering capability than the full-length sFlt-1. Indeed, evidence from other studies suggests a milder effect of the overexpressed full-length mouse sFlt-1 compared to the truncated msFlt-1(1-3) on kidney functions [7,263,265].

5.10. sFlt-1 promotes the development of chronic disease following preeclampsia

Both of our studies provided evidence for the long-term maternal effects of sFlt-1. Indeed, preeclampsia does not only affect pregnant women and their offspring during pregnancy, but it also has long-term consequences on their morbidity and mortality later in life. Epidemiologic studies have revealed that preeclampsia confers an increased risk of cardiovascular and cerebrovascular complications, such as chronic hypertension, ischemic heart disease, or stroke [16-18,50,340,341]: 1) There is a two-fold risk of developing cerebrovascular or cardiovascular disease in women who had preeclampsia compared to normal pregnant women; 2) Twenty percent of women may develop cardiovascular disease within seven years of their pregnancy affected by preeclampsia; 3) Women with preeclampsia have a 2 to 10-fold risk of developing chronic hypertension postpartum than normal pregnant women; 4) Women with early-onset severe preeclampsia complicated by IUGR are at high risk of adverse long-term cardiovascular outcomes and an 8-fold increased risk of cardiovascular death compared to normal pregnant women; 5) Pregnant women with preeclampsia who delivered a low birth-weight neonate have an increased risk of chronic kidney disease later in life. Whether these long-term adverse outcomes result from the endothelial dysfunction and/or vascular damage in preeclampsia, or they point to pre-existing risk factors shared by preeclampsia and cardiovascular disease (chronic hypertension, diabetes,

dyslipidaemia, hypercoagulability, insulin resistance, metabolic syndrome, obesity, etc.) is still a topic of debate.

In this regard it was relevant to observe in both of our studies that mice in the hsFlt-1-e15a and msFlt-1(1-3) treatment groups had endothelial dysfunction one week after delivery as shown by the aortic ring assays, suggesting long-term maternal systemic vascular effects of sFlt-1 overexpression during pregnancy. Moreover, one mouse in the msFlt-1(1-3) treatment group had a very high blood pressure elevation, which was still increasing after one week postpartum. This mouse also had dramatic glomerular damage, extremely high proteinuria, and the most dysfunctional aortic endothelium among all mice in the study group. These results suggest that this dam developed chronic cardiovascular and kidney disease as a result of preeclampsia. In a similar mouse preeclampsia model, animals that received sFlt-1 treatment during pregnancy had characteristic changes in their plasma proteome six months after delivery with enrichment of proteins associated with cardiovascular and metabolic diseases, as well as inflammatory response [342]. That study and the current observations support the notion that some long-term adverse outcomes associated with preeclampsia may be the consequence rather than an underlying predisposition of this syndrome.

5.11. sFlt-1 supports embryonic survival in early pregnancy

Besides the observations on the detrimental effects of sFlt-1 in late pregnancy and postpartum, in our second study we have also revealed its positive effect in early pregnancy, in line with other *in vivo* and *in vitro* studies showing that anti-angiogenic molecules may support embryogenesis. This is somewhat surprising since angiogenesis, being strongly interconnected with inflammation and oxygen signaling [343-345], is key to successful implantation, embryogenesis and placentation [211,212,221,346-349].

Among various molecule families that regulate placental angiogenesis, the gene family of VEGFs and PlGF as well as their receptors have major regulatory roles [211,212,214,221,348]. The placenta itself is a rich source of these molecules [135,140,346,347], synthesizing them in characteristically changing amounts during gestation [135,153,157,159,221,347,348,350-354]. A growing body of evidence has shown that in early pregnancy VEGF is predominantly produced over PlGF in the

gestational sac [348,355-358], and VEGF promotes vascular endothelial cell proliferation, migration, survival, tube-formation, and branching angiogenesis *in vitro*, as well as vascular permeability *in vivo* [211,212,348,359]. Since *Plgf* null mice are healthy with no signs of embryonic maldevelopment, PlGF was suggested to indirectly promote angiogenesis by displacing VEGF from VEGFR-1 and making it available for VEGFR-2 binding, or by generating PlGF/VEGF heterodimers that are able to activate VEGFR-1 or to induce VEGFR-1/VEGFR-2 dimerization [360]. Further supporting the pivotal role of VEGF and its receptors in embryonic vasculogenesis and angiogenesis during early pregnancy, the knockout of *Vegf* or *Vegfr2* genes in mice leads to impaired angiogenesis, while the *Flt1* knockout embryos die on GD8.5-9 due to excessive blood vessel growth [211,212,214]. These data together suggest that the major signal transducer for VEGF is VEGFR-2, while Flt-1 and its soluble isoforms strongly bind and neutralize VEGF, and thus have negative effect on angiogenesis and vascular permeability [211,212,222,348]. Since the administration of VEGF in early pregnancy or endometrial overexpression lead to embryonic resorption in mice [8,221], it has been suggested that the most important role of the Flt-1/sFlt-1 system is to maintain a barrier and block excessive VEGF signaling during embryogenesis that would lead to vascular hyperpermeability, the leak of serum proteins, and embryonic death [8,212,221].

Strongly related to these, in our second study we found higher number of pups in hsFlt-1-e15a-treated mice. This result may support the above described concept if hsFlt-1-e15a reduced the bioavailability of mouse VEGF. Alternatively, this rescue effect of hsFlt-1-e15a might have been the result of its interference with the mouse Flt-1/msFlt-1 system and the bioavailability of mouse PlGF. In our study, circulating mouse PlGF and VEGF concentrations could not be measured; thus, this question needs to be addressed in a future study. Nevertheless, hsFlt-1-e15a was shown to be a predominant placental VEGF-inhibiting protein by functional experiments [112]. Moreover, human sFlt-1-i13 was shown to bind and sequester mouse PlGF *in vivo* since the parallel overexpression of these molecules in mice led to decreased circulating hsFlt-1-i13 concentrations compared to hsFlt-1-i13 overexpression alone [265]. These functional data along with the high sequential and functional conservation of sFlt-1 from birds to humans [211,212,361] support the relevance of the biological actions of human sFlt-1 on the VEGF/PlGF/VEGF receptor system in mice. Importantly, our treatments started on

GD8, exactly before the time-window (GD8.5-9) when *Flt1* knock-out embryos are lost, supporting the theory that the Flt-1/sFlt-1 system is important in embryonic development and the relevance of our findings on the biological effects of hsFlt-1-e15a treatment in early pregnancy in mice [211,212,214]. Since the same rescue-effect was not detected in the case of treatments with the truncated sFlt-1(1-3), the dimerization domain or the unique tail of hsFlt-1-e15a must play a key role in this rescue-effect, underlining the evolutionary conservation of these protein domains.

When looking at the different hsFlt-1-e15a treatment subgroups in our second study, an interesting association could be observed. The mean number of pups and living pups in a litter seemed to parallel hsFlt-1-e15a expression in the uterus (**Figures 22 and 27**). Moreover, the mean and total placental weights in a litter seem to parallel hsFlt-1-e15a expression in the placenta. These results suggest that the expression and the local availability of hsFlt-1-e15a in the uterus and placenta probably have a positive impact on decidual and placental angiogenesis, supporting successful embryonic and placental development in mice. In spite of the differences between human and mouse placentation [14,268-271], these results may be relevant to human pregnancy, as well. Indeed, decreased maternal blood concentrations of sFlt-1 in the first trimester are associated with miscarriages [168,362], supporting the idea that the protective mechanisms of Flt-1/sFlt-1 may also similarly function in early human pregnancy.

DOI:10.14753/SE.2015.1828

6. CONCLUSIONS

The principal developments and findings of our two studies included the followings:

1. A biologically relevant anti-angiogenic mouse model of preeclampsia was developed;
2. High-frequency ultrasound predicted pregnancy in 97% of the cases on GD7;
3. High-frequency ultrasound determined telemetry catheter positions in all cases;
4. Telemetry enabled non-stressed blood pressure monitoring in pregnancy and postpartum;
5. The survival rate of the newly developed survival cesarean section was 100%;
6. Ultrasound-guided cystocentesis was developed that enabled urine protein analysis;
7. The hsFlt-1-e15a transgene was mainly overexpressed in the liver by the adenovirus;
8. HsFlt-1-e15a treatment increased mean arterial blood pressure on GD18;
9. HsFlt-1-e15a treatment induced albuminuria on GD18;
10. Glomerular changes were found in the kidneys of hsFlt-1-e15a-treated mice;
11. Aortic ring microvessel outgrowth was inhibited in hsFlt-1-e15a-treated mice;
12. There was no effect of hsFlt-1-e15a on placental and fetal weights;
13. One hsFlt-1-e15a-treated mouse had severe, early-onset preeclampsia-like symptoms associated with fetal growth restriction and multi-organ involvement;
14. The in vivo biological effects of the full-length human sFlt-1-e15 and the truncated mouse sFlt-1(1-3) could be directly compared;
15. The full-length mouse transmembrane mFlt-1 was expressed most abundantly in the placenta, while the soluble mouse Flt-1-i13 was only expressed in the placenta;
16. Utilizing a fiber-mutant adenovirus and a placenta-specific promoter increased the placental expression of both the hsFlt-1-e15a and control transgenes;
17. Both hsFlt-1-e15a and msFlt-1(1-3) induced the symptoms of preeclampsia, including blood pressure elevation, glomerular damage, proteinuria and endothelial dysfunction;
18. One msFlt-1(1-3)-treated dam had constantly high blood pressure, severe proteinuria and extensive glomerular damage, suggesting increased sensitivity to sFlt-1 of this animal;
19. The overexpression of hsFlt-1-e15a increased litter size, while msFlt-1(1-3) did not have this effect, underlining the important role of the full-length sFlt-1 in early pregnancy;
20. These observations point to the difference in the biological effects of full-length and truncated sFlt-1 and the changes in the effect of full-length sFlt-1 during pregnancy, and thus, may have important implications in the management of preeclampsia.

DOI:10.14753/SE.2015.1828

7. SUMMARY

We created an accurate method for the early determination of pregnancy status in mice using high frequency ultrasound. The implication of microsurgery and high frequency ultrasound for the precise telemetry catheter positioning supported non-invasive blood pressure monitoring during pregnancy and postpartum. The development of the ultrasound-guided bladder puncture and the use of urine albumin and creatinine measurements helped the correct determination of proteinuria. The innovations in cesarean section promoted complete wound healing and full survival of the dams. Using these advanced methodologies and the adenoviral overexpression of hsFlt-1-e15a, a novel mouse model of preeclampsia was built to investigate the *in vivo* pathologic effects of this primate-specific, predominantly placental expressed sFlt-1 isoform.

We found that hsFlt-1-e15a could induce the full spectrum of symptoms of preeclampsia including high blood pressure and proteinuria. Using state-of-the art histopathological, immunohistochemical, molecular and cell biological as well as imaging techniques we could also show that hsFlt-1-e15a generated glomerular changes and endothelial damage characteristic for preeclampsia. Our findings support that this sFlt-1 isoform is central to the terminal pathway of preeclampsia. HsFlt-1-e15a induced late-onset preeclampsia in most cases, and promoted early-onset preeclampsia associated with IUGR and multi-organ involvement in one dam with liver disease, verifying that preeclampsia phenotype is influenced by both placental factors released to the maternal circulation and maternal genetic and environmentally induced diseases.

We also compared the effects of full-length hsFlt-1-e15a and the artificially truncated mouse sFlt-1(1-3) widely used in previous *in vivo* preeclampsia models. Both of these sFlt-1 variants promoted blood pressure elevation, glomerular damage, proteinuria and endothelial dysfunction, but neither of them affected placental or fetal weights. Of interest, full-length hsFlt-1-e15a increased litter size, while truncated msFlt-1(1-3) did not have this effect. It is in accord with the predominant placental expression of full-length hsFlt-1-e15a and mouse sFlt-1-i13 variants, underlining their important role in the regulation of embryonic development in early pregnancy. Our observations point to the difference in the biological effects of full-length and truncated sFlt-1 and the changes in the effects of full-length sFlt-1 during pregnancy. Therefore, our results may also have important implications in the clinical management of preeclampsia.

DOI:10.14753/SE.2015.1828

8. ÖSSZEFOGLALÁS

Magas frekvenciájú ultrahangot használva megbízható eljárást fejlesztettünk ki a terhesség korai megállapításához egerekben. A telemetriás vérnyomás monitor katéter mikrosebészeti beültetése és helyzetének ultrahangos ellenőrzése lehetővé tette az egerek stresszmentes, folyamatos vérnyomás monitorozását terhesség alatt és a szülés után. A proteinuria pontos meghatározásában fontos szerep jutott az újonnan fejlesztett ultrahang-vezérelt hólyagpunctionak és a vizelet albumin/kreatinin meghatározásának. Az újonnan kidolgozott császármetszés alkalmazása az összes egér túlélését és teljes sebgyógyulást eredményezett. Ezen módszerek használatával és adenovírus vektorral expresszált hsFlt-1-e15a segítségével új praeeclampsia modellt fejlesztettünk ki, mellyel vizsgálni tudtuk a főemlősökben többnyire placentában kifejeződő hsFlt-1-e15a *in vivo* hatásait.

A hsFlt-1-e15a a praeeclampsia összes klinikai tünetét, így magas vérnyomást és proteinuriát is kiváltotta. A legmodernebb szövettani, immunhisztokémiai, molekuláris és sejtbiológiai illetve képalkotó eljárásokat felhasználva igazolni tudtuk, hogy a hsFlt-1-e15a a praeeclampsiára jellemző generalizált endothel és vesekárosodást okozott. Eredményeink azt igazolják, hogy a sFlt-1 ezen variánsa központi szerepet játszik a praeeclampsia terminális útvonalában. A hsFlt-1-e15a késői praeeclampsiát okozott a legtöbb esetben, egy májbetegséggel rendelkező egérnél azonban méhenbelüli retardációval és többszervi elégtelenséggel társult korai praeeclampsia jelentkezett, ami azt igazolja, hogy a praeeclampsia kialakulását az anyai keringésbe került lepényi faktorok mellett az anya genetikai állománya és környezeti tényezők is befolyásolják.

Összehasonlítottuk az *in vivo* praeeclampsia állatmodellekben széleskörben használt, mesterségesen csonkított egér sFlt-1(1-3) és a teljes hosszúságú humán sFlt-1-e15a hatásit is. Mindkét sFlt-1 variáns vérnyomás emelkedést, vesekárosodást és endothel diszfunkciót okozott, de nem volt hatásuk a placenta vagy magzat súlyára. Érdekes, hogy a hsFlt-1-e15a növelte az egéralom nagyságát, míg a msFlt-1(1-3) nem. Ez alátámasztja, hogy a lepényi humán sFlt-1-e15a és egér sFlt-1-i13 fontos szerepet tölt be az embrió fejlődésében a terhesség korai fázisában. Megfigyeléseink rávilágítanak a teljes hosszúságú és a csonkított sFlt-1 variánsok biológiai hatásának különbségére, valamint a teljes hosszúságú sFlt-1 változó hatásaira a terhesség előrehaladtával. Így eredményeinknek fontos hatása lehet a praeeclampsia klinikai kezelésére is.

DOI:10.14753/SE.2015.1828

9. BIBLIOGRAPHY

1. Romero R, Espinoza J, Kusanovic JP, Gotsch F, Hassan S, Erez O, Chaiworapongsa T, Mazor M. (2006) The preterm parturition syndrome. BJOG 113 Suppl 3: 17-42.
2. Romero R. (2009) Prenatal medicine: the child is the father of the man. 1996. J Matern Fetal Neonatal Med 22: 636-639.
3. Di Renzo GC. (2009) The great obstetrical syndromes. J Matern Fetal Neonatal Med 22: 633-635.
4. Saftlas AF, Olson DR, Franks AL, Atrash HK, Pokras R. (1990) Epidemiology of preeclampsia and eclampsia in the United States, 1979-1986. Am J Obstet Gynecol 163: 460-465.
5. National High Blood Pressure Education Program Working Group. (2000) Report of the National High Blood Pressure Education Program Working Group on High Blood Pressure in Pregnancy. Am J Obstet Gynecol 183: S1-S22.
6. MacKay AP, Berg CJ, Atrash HK. (2001) Pregnancy-related mortality from preeclampsia and eclampsia. Obstet Gynecol 97: 533-538.
7. Sibai BM. (2003) Diagnosis and management of gestational hypertension and preeclampsia. Obstet Gynecol 102: 181-192.
8. WHO. The world health report 2005: make every mother and child count. WHO, Geneva, 2005.
9. Sibai B, Dekker G, Kupferminc M. (2005) Pre-eclampsia. Lancet 365: 785-799.
10. Khan KS, Wojdyla D, Say L, Gulmezoglu AM, Van Look PF. (2006) WHO analysis of causes of maternal death: a systematic review. Lancet 367: 1066-1074.
11. Than NG, Vaisbuch E, Kim CJ, Mazaki-Tovi S, Erez O, Yeo L, Mittal P, Hupuczi P, Varkonyi T, Hassan SS, Papp Z, Romero R. Early-onset preeclampsia and HELLP syndrome: an overview In: Preedy VR, editor. Handbook of Growth and Growth Monitoring in Health and Disease. Springer, Heidelberg, 2012: 1867-1891.
12. Stout C, Lemmon WB. (1969) Glomerular capillary endothelial swelling in a pregnant chimpanzee. Am J Obstet Gynecol 105: 212-215.

13. Baird JN, Jr. (1981) Eclampsia in a lowland gorilla. Am J Obstet Gynecol 141: 345-346.

14. Carter AM. (2007) Animal models of human placentation--a review. Placenta 28 Suppl A: S41-47.

15. Karumanchi SA, Lindheimer MD. (2007) Preeclampsia and the kidney: footprints in the urine. Am J Obstet Gynecol 196: 287-288.

16. Maynard S, Epstein FH, Karumanchi SA. (2008) Preeclampsia and angiogenic imbalance. Annu Rev Med 59: 61-78.

17. Irgens HU, Reisaeter L, Irgens LM, Lie RT. (2001) Long term mortality of mothers and fathers after pre-eclampsia: population based cohort study. BMJ 323: 1213-1217.

18. Ananth CV, Peltier MR, Kinzler WL, Smulian JC, Vintzileos AM. (2007) Chronic hypertension and risk of placental abruption: is the association modified by ischemic placental disease? Am J Obstet Gynecol 197: 273 e271-277.

19. Steegers EA, von Dadelszen P, Duvekot JJ, Pijnenborg R. (2010) Pre-eclampsia. Lancet 376: 631-644.

20. von Dadelszen P, Magee LA, Roberts JM. (2003) Subclassification of preeclampsia. Hypertens Pregnancy 22: 143-148.

21. Nishizawa H, Pryor-Koishi K, Kato T, Kowa H, Kurahashi H, Udagawa Y. (2007) Microarray analysis of differentially expressed fetal genes in placental tissue derived from early and late onset severe pre-eclampsia. Placenta 28: 487-497.

22. Valensise H, Vasapollo B, Gagliardi G, Novelli GP. (2008) Early and late preeclampsia: two different maternal hemodynamic states in the latent phase of the disease. Hypertension 52: 873-880.

23. Sibai BM. (2006) Preeclampsia as a cause of preterm and late preterm (near-term) births. Semin Perinatol 30: 16-19.

24. Hutcheon JA, Lisonkova S, Joseph KS. (2011) Epidemiology of pre-eclampsia and the other hypertensive disorders of pregnancy. Best Pract Res Clin Obstet Gynaecol 25: 391-403.

25. Matthys LA, Coppage KH, Lambers DS, Barton JR, Sibai BM. (2004) Delayed postpartum preeclampsia: an experience of 151 cases. Am J Obstet Gynecol 190: 1464-1466.

26. von Dadelszen P, Menzies JM, Payne B, Magee LA. (2009) Predicting adverse outcomes in women with severe pre-eclampsia. Semin Perinatol 33: 152-157.
27. Raymond D, Peterson E. (2011) A critical review of early-onset and late-onset preeclampsia. Obstet Gynecol Surv 66: 497-506.
28. Long PA, Abell DA, Beischer NA. (1980) Fetal growth retardation and pre-eclampsia. Br J Obstet Gynaecol 87: 13-18.
29. Weinstein L. (1982) Syndrome of hemolysis, elevated liver enzymes, and low platelet count: a severe consequence of hypertension in pregnancy. Am J Obstet Gynecol 142: 159-167.
30. Ness RB, Roberts JM. (1996) Heterogeneous causes constituting the single syndrome of preeclampsia: a hypothesis and its implications. Am J Obstet Gynecol 175: 1365-1370.
31. Sibai BM, Ewell M, Levine RJ, Klebanoff MA, Esterlitz J, Catalano PM, Goldenberg RL, Joffe G. (1997) Risk factors associated with preeclampsia in healthy nulliparous women. The Calcium for Preeclampsia Prevention (CPEP) Study Group. Am J Obstet Gynecol 177: 1003-1010.
32. Rath W, Faridi A, Dudenhausen JW. (2000) HELLP syndrome. J Perinat Med 28: 249-260.
33. Roberts JM, Lain KY. (2002) Recent Insights into the pathogenesis of pre-eclampsia. Placenta 23: 359-372.
34. Baxter JK, Weinstein L. (2004) HELLP syndrome: the state of the art. Obstet Gynecol Surv 59: 838-845.
35. Barton JR, Sibai BM. (2004) Diagnosis and management of hemolysis, elevated liver enzymes, and low platelets syndrome. Clin Perinatol 31: 807-833, vii.
36. Noris M, Perico N, Remuzzi G. (2005) Mechanisms of disease: Pre-eclampsia. Nat Clin Pract Nephrol 1: 98-114; quiz 120.
37. Haram K, Svendsen E, Abildgaard U. (2009) The HELLP syndrome: clinical issues and management. A Review. BMC Pregnancy Childbirth 9: 8.
38. Kim CJ, Romero R, Kusanovic JP, Yoo W, Dong Z, Topping V, Gotsch F, Yoon BH, Chi JG, Kim JS. (2010) The frequency, clinical significance, and pathological features of chronic chorioamnionitis: a lesion associated with spontaneous preterm birth. Mod Pathol 23: 1000-1011.

39. Hernandez-Andrade E, Serralde JA, Cruz-Martinez R. (2012) Can anomalies of fetal brain circulation be useful in the management of growth restricted fetuses? Prenat Diagn 32: 103-112.

40. Hernandez-Andrade E, Stampalija T, Figueras F. (2013) Cerebral blood flow studies in the diagnosis and management of intrauterine growth restriction. Curr Opin Obstet Gynecol 25: 138-144.

41. Caughey AB, Stotland NE, Washington AE, Escobar GJ. (2005) Maternal ethnicity, paternal ethnicity, and parental ethnic discordance: predictors of preeclampsia. Obstet Gynecol 106: 156-161.

42. Silva LM, Coolman M, Steegers EA, Jaddoe VW, Moll HA, Hofman A, Mackenbach JP, Raat H. (2008) Low socioeconomic status is a risk factor for preeclampsia: the Generation R Study. J Hypertens 26: 1200-1208.

43. Duley L. (2009) The global impact of pre-eclampsia and eclampsia. Semin Perinatol 33: 130-137.

44. Berg CJ, Mackay AP, Qin C, Callaghan WM. (2009) Overview of maternal morbidity during hospitalization for labor and delivery in the United States: 1993-1997 and 2001-2005. Obstet Gynecol 113: 1075-1081.

45. Wallis AB, Saftlas AF, Hsia J, Atrash HK. (2008) Secular trends in the rates of preeclampsia, eclampsia, and gestational hypertension, United States, 1987-2004. Am J Hypertens 21: 521-526.

46. Redman CW, Sargent IL. (2003) Pre-eclampsia, the placenta and the maternal systemic inflammatory response--a review. Placenta 24 Suppl A: S21-27.

47. Redman CW, Sargent IL. (2005) Latest advances in understanding preeclampsia. Science 308: 1592-1594.

48. Rigo J, Jr., Nagy B, Fintor L, Tanyi J, Beke A, Karadi I, Papp Z. (2000) Maternal and neonatal outcome of preeclamptic pregnancies: the potential roles of factor V Leiden mutation and 5,10 methylenetetrahydrofolate reductase. Hypertens Pregnancy 19: 163-172.

49. Karumanchi SA, Maynard SE, Stillman IE, Epstein FH, Sukhatme VP. (2005) Preeclampsia: a renal perspective. Kidney Int 67: 2101-2113.

50. Baumwell S, Karumanchi SA. (2007) Pre-eclampsia: clinical manifestations and molecular mechanisms. Nephron Clin Pract 106: c72-81.

51. Said J, Dekker G. (2003) Pre-eclampsia and thrombophilia. Best Pract Res Clin Obstet Gynaecol 17: 441-458.

52. Hupuczi P, Rigo B, Sziller I, Szabo G, Szigeti Z, Papp Z. (2006) Follow-up analysis of pregnancies complicated by HELLP syndrome. Fetal Diagn Ther 21: 519-522.

53. Page EW. (1948) Placental dysfunction in eclamptogenic toxemias. Obstet Gynecol Surv 3: 615-628.

54. Page EW. (1949) The physiologic basis of symptoms in eclampsia. Calif Med 70: 1-4.

55. Redman CW. (1991) Current topic: pre-eclampsia and the placenta. Placenta 12: 301-308.

56. Young BC, Levine RJ, Karumanchi SA. (2010) Pathogenesis of preeclampsia. Annu Rev Pathol 5: 173-192.

57. Eastabrook G, Brown M, Sargent I. (2011) The origins and end-organ consequence of pre-eclampsia. Best Pract Res Clin Obstet Gynaecol 25: 435-447.

58. Robertson WB, Brosens I, Dixon HG. (1967) The pathological response of the vessels of the placental bed to hypertensive pregnancy. J Pathol Bacteriol 93: 581-592.

59. Brosens IA. (1977) Morphological changes in the utero-placental bed in pregnancy hypertension. Clin Obstet Gynaecol 4: 573-593.

60. Gerretsen G, Huisjes HJ, Elema JD. (1981) Morphological changes of the spiral arteries in the placental bed in relation to pre-eclampsia and fetal growth retardation. Br J Obstet Gynaecol 88: 876-881.

61. Khong TY, De Wolf F, Robertson WB, Brosens I. (1986) Inadequate maternal vascular response to placentation in pregnancies complicated by pre-eclampsia and by small-for-gestational age infants. Br J Obstet Gynaecol 93: 1049-1059.

62. Zhou Y, Damsky CH, Fisher SJ. (1997) Preeclampsia is associated with failure of human cytotrophoblasts to mimic a vascular adhesion phenotype. One cause of defective endovascular invasion in this syndrome? J Clin Invest 99: 2152-2164.

63. Kaufmann P, Black S, Huppertz B. (2003) Endovascular trophoblast invasion: implications for the pathogenesis of intrauterine growth retardation and preeclampsia. Biol Reprod 69: 1-7.

64. Espinoza J, Romero R, Mee Kim Y, Kusanovic JP, Hassan S, Erez O, Gotsch F, Than NG, Papp Z, Jai Kim C. (2006) Normal and abnormal transformation of the spiral arteries during pregnancy. J Perinat Med 34: 447-458.

65. Brosens I, Derwig I, Brosens J, Fusi L, Benagiano G, Pijnenborg R. (2010) The enigmatic uterine junctional zone: the missing link between reproductive disorders and major obstetrical disorders? Hum Reprod 25: 569-574.

66. Brosens I, Pijnenborg R, Vercruysse L, Romero R. (2011) The "Great Obstetrical Syndromes" are associated with disorders of deep placentation. Am J Obstet Gynecol 204: 193-201.

67. Pineles BL, Romero R, Montenegro D, Tarca AL, Han YM, Kim YM, Draghici S, Espinoza J, Kusanovic JP, Mittal P, Hassan SS, Kim CJ. (2007) Distinct subsets of microRNAs are expressed differentially in the human placentas of patients with preeclampsia. Am J Obstet Gynecol 196: 261 e261-266.

68. Than NG, Abdul Rahman O, Magenheim R, Nagy B, Fule T, Hargitai B, Sammar M, Hupuczi P, Tarca AL, Szabo G, Kovalszky I, Meiri H, Sziller I, Rigo J, Jr., Romero R, Papp Z. (2008) Placental protein 13 (galectin-13) has decreased placental expression but increased shedding and maternal serum concentrations in patients presenting with preterm pre-eclampsia and HELLP syndrome. Virchows Arch 453: 387-400.

69. Singh H, Makino SI, Endo Y, Nie G. (2010) Inhibition of HTRA3 stimulates trophoblast invasion during human placental development. Placenta 31: 1085-1092.

70. Varkonyi T, Nagy B, Fule T, Tarca AL, Karaszi K, Schonleber J, Hupuczi P, Mihalik N, Kovalszky I, Rigo J, Jr., Meiri H, Papp Z, Romero R, Than NG. (2011) Microarray profiling reveals that placental transcriptomes of early-onset HELLP syndrome and preeclampsia are similar. Placenta 32 Suppl: S21-29.

71. Li Y, Puryer M, Lin E, Hale K, Salamonsen LA, Manuelpillai U, Tong S, Chan W, Wallace EM, Nie G. (2011) Placental HtrA3 is regulated by oxygen tension and serum levels are altered during early pregnancy in women destined to develop preeclampsia. J Clin Endocrinol Metab 96: 403-411.

72. Singh H, Endo Y, Nie G. (2011) Decidual HtrA3 negatively regulates trophoblast invasion during human placentation. Hum Reprod 26: 748-757.

73. Kliman HJ, Sammar M, Grimpel YI, Lynch SK, Milano KM, Pick E, Bejar J, Arad A, Lee JJ, Meiri H, Gonen R. (2012) Placental protein 13 and decidual zones of necrosis: an immunologic diversion that may be linked to preeclampsia. Reprod Sci 19: 16-30.

74. Dynon K, Heng S, Puryer M, Li Y, Walton K, Endo Y, Nie G. (2012) HtrA3 as an early marker for preeclampsia: specific monoclonal antibodies and sensitive high-throughput assays for serum screening. PLoS One 7: e45956.

75. Than NG, Romero R, Xu Y, Erez O, Xu Z, Bhatti G, Leavitt R, Chung TH, El-Azzamy H, LaJeunesse C, Wang B, Balogh A, Szalai G, Land S, Dong Z, Hassan SS, Chaiworapongsa T, Krispin M, Kim CJ, Tarca AL, Papp Z, Bohn H. (2014) Evolutionary origins of the placental expression of chromosome 19 cluster galectins and their complex dysregulation in preeclampsia. Placenta 35: 855-865.

76. Kim YM, Romero R, Oh SY, Kim CJ, Kilburn BA, Armant DR, Nien JK, Gomez R, Mazor M, Saito S, Abrahams VM, Mor G. (2005) Toll-like receptor 4: a potential link between "danger signals," the innate immune system, and preeclampsia? Am J Obstet Gynecol 193: 921-927.

77. Matthiesen L, Berg G, Ernerudh J, Ekerfelt C, Jonsson Y, Sharma S. (2005) Immunology of preeclampsia. Chem Immunol Allergy 89: 49-61.

78. Kim JS, Romero R, Cushenberry E, Kim YM, Erez O, Nien JK, Yoon BH, Espinoza J, Kim CJ. (2007) Distribution of CD14+ and CD68+ macrophages in the placental bed and basal plate of women with preeclampsia and preterm labor. Placenta 28: 571-576.

79. Dekker G, Robillard PY. (2007) Pre-eclampsia: Is the immune maladaptation hypothesis still standing? An epidemiological update. J Reprod Immunol 76: 8-16.

80. Redman CW, Sargent IL. (2010) Immunology of pre-eclampsia. Am J Reprod Immunol 63: 534-543.

81. Burke SD, Barrette VF, Gravel J, Carter AL, Hatta K, Zhang J, Chen Z, Leno-Duran E, Bianco J, Leonard S, Murrant C, Adams MA, Croy BA. (2010) Uterine NK cells, spiral artery modification and the regulation of blood pressure during mouse pregnancy. Am J Reprod Immunol 63: 472-481.

82. Leno-Duran E, Hatta K, Bianco J, Yamada AT, Ruiz-Ruiz C, Olivares EG, Croy BA. (2010) Fetal-placental hypoxia does not result from failure of spiral arterial modification in mice. Placenta 31: 731-737.

83. Girardi G, Prohaszka Z, Bulla R, Tedesco F, Scherjon S. (2011) Complement activation in animal and human pregnancies as a model for immunological recognition. Mol Immunol 48: 1621-1630.

84. Webster RP, Roberts VH, Myatt L. (2008) Protein nitration in placenta - functional significance. Placenta 29: 985-994.

85. Burton GJ, Woods AW, Jauniaux E, Kingdom JC. (2009) Rheological and physiological consequences of conversion of the maternal spiral arteries for uteroplacental blood flow during human pregnancy. Placenta 30: 473-482.

86. Burton GJ, Yung HW, Cindrova-Davies T, Charnock-Jones DS. (2009) Placental endoplasmic reticulum stress and oxidative stress in the pathophysiology of unexplained intrauterine growth restriction and early onset preeclampsia. Placenta 30 Suppl A: S43-48.

87. Myatt L, Webster RP. (2009) Vascular biology of preeclampsia. J Thromb Haemost 7: 375-384.

88. Romero R, Kusanovic JP, Chaiworapongsa T, Hassan SS. (2011) Placental bed disorders in preterm labor, preterm PROM, spontaneous abortion and abruptio placentae. Best Pract Res Clin Obstet Gynaecol 25: 313-327.

89. Moldenhauer JS, Stanek J, Warshak C, Khoury J, Sibai B. (2003) The frequency and severity of placental findings in women with preeclampsia are gestational age dependent. Am J Obstet Gynecol 189: 1173-1177.

90. Sebire NJ, Goldin RD, Regan L. (2005) Term preeclampsia is associated with minimal histopathological placental features regardless of clinical severity. J Obstet Gynaecol 25: 117-118.

91. Ogge G, Chaiworapongsa T, Romero R, Hussein Y, Kusanovic JP, Yeo L, Kim CJ, Hassan SS. (2011) Placental lesions associated with maternal underperfusion are more frequent in early-onset than in late-onset preeclampsia. J Perinat Med 39: 641-652.

92. Mayhew TM, Ohadike C, Baker PN, Crocker IP, Mitchell C, Ong SS. (2003) Stereological investigation of placental morphology in pregnancies complicated

by pre-eclampsia with and without intrauterine growth restriction. Placenta 24: 219-226.

93. Rasmussen S, Irgens LM. (2003) Fetal growth and body proportion in preeclampsia. Obstet Gynecol 101: 575-583.
94. Xiong X, Demianczuk NN, Saunders LD, Wang FL, Fraser WD. (2002) Impact of preeclampsia and gestational hypertension on birth weight by gestational age. Am J Epidemiol 155: 203-209.
95. Redman CW, Sargent IL, Staff AC. (2014) IFPA Senior Award Lecture: making sense of pre-eclampsia - two placental causes of preeclampsia? Placenta 35 Suppl: S20-25.
96. Levine RJ, Maynard SE, Qian C, Lim KH, England LJ, Yu KF, Schisterman EF, Thadhani R, Sachs BP, Epstein FH, Sibai BM, Sukhatme VP, Karumanchi SA. (2004) Circulating angiogenic factors and the risk of preeclampsia. N Engl J Med 350: 672-683.
97. Levine RJ, Karumanchi SA. (2005) Circulating angiogenic factors in preeclampsia. Clin Obstet Gynecol 48: 372-386.
98. Borzychowski AM, Sargent IL, Redman CW. (2006) Inflammation and pre-eclampsia. Semin Fetal Neonatal Med 11: 309-316.
99. Redman CW, Sargent IL. (2009) Placental stress and pre-eclampsia: a revised view. Placenta 30 Suppl A: S38-42.
100. Kalkunte S, Lai Z, Norris WE, Pietras LA, Tewari N, Boij R, Neubeck S, Markert UR, Sharma S. (2009) Novel approaches for mechanistic understanding and predicting preeclampsia. J Reprod Immunol 83: 134-138.
101. Roberts JM, Hubel CA. (2009) The two stage model of preeclampsia: variations on the theme. Placenta 30 Suppl A: S32-37.
102. Sharma S, Norris WE, Kalkunte S. (2010) Beyond the threshold: an etiological bridge between hypoxia and immunity in preeclampsia. J Reprod Immunol 85: 112-116.
103. Kalkunte S, Boij R, Norris W, Friedman J, Lai Z, Kurtis J, Lim KH, Padbury JF, Matthiesen L, Sharma S. (2010) Sera from preeclampsia patients elicit symptoms of human disease in mice and provide a basis for an in vitro predictive assay. Am J Pathol 177: 2387-2398.

104. Maynard SE, Karumanchi SA. (2011) Angiogenic factors and preeclampsia. Semin Nephrol 31: 33-46.

105. Maynard SE, Min JY, Merchan J, Lim KH, Li J, Mondal S, Libermann TA, Morgan JP, Sellke FW, Stillman IE, Epstein FH, Sukhatme VP, Karumanchi SA. (2003) Excess placental soluble fms-like tyrosine kinase 1 (sFlt1) may contribute to endothelial dysfunction, hypertension, and proteinuria in preeclampsia. J Clin Invest 111: 649-658.

106. Bdolah Y, Karumanchi SA, Sachs BP. (2005) Recent advances in understanding of preeclampsia. Croat Med J 46: 728-736.

107. Maynard SE, Venkatesha S, Thadhani R, Karumanchi SA. (2005) Soluble Fms-like tyrosine kinase 1 and endothelial dysfunction in the pathogenesis of preeclampsia. Pediatr Res 57: 1R-7R.

108. Venkatesha S, Toporsian M, Lam C, Hanai J, Mammoto T, Kim YM, Bdolah Y, Lim KH, Yuan HT, Libermann TA, Stillman IE, Roberts D, D'Amore PA, Epstein FH, Sellke FW, Romero R, Sukhatme VP, Letarte M, Karumanchi SA. (2006) Soluble endoglin contributes to the pathogenesis of preeclampsia. Nat Med 12: 642-649.

109. Wang A, Rana S, Karumanchi SA. (2009) Preeclampsia: the role of angiogenic factors in its pathogenesis. Physiology (Bethesda) 24: 147-158.

110. Sargent IL, Germain SJ, Sacks GP, Kumar S, Redman CW. (2003) Trophoblast deportation and the maternal inflammatory response in pre-eclampsia. J Reprod Immunol 59: 153-160.

111. Germain SJ, Sacks GP, Sooranna SR, Sargent IL, Redman CW. (2007) Systemic inflammatory priming in normal pregnancy and preeclampsia: the role of circulating syncytiotrophoblast microparticles. J Immunol 178: 5949-5956.

112. Sela S, Itin A, Natanson-Yaron S, Greenfield C, Goldman-Wohl D, Yagel S, Keshet E. (2008) A novel human-specific soluble vascular endothelial growth factor receptor 1: cell-type-specific splicing and implications to vascular endothelial growth factor homeostasis and preeclampsia. Circ Res 102: 1566-1574.

113. Balogh A, Pozsgay J, Matko J, Dong Z, Kim CJ, Varkonyi T, Sammar M, Rigo J, Jr., Meiri H, Romero R, Papp Z, Than NG. (2011) Placental protein 13

(PP13/galectin-13) undergoes lipid raft-associated subcellular redistribution in the syncytiotrophoblast in preterm preeclampsia and HELLP syndrome. Am J Obstet Gynecol 205: 156 e151-114.

114. Alasztics B, Gullai N, Molvarec A, Rigo J, Jr. (2014) [The role of angiogenic factors in preeclampsia]. Orv Hetil 155: 1860-1866.
115. Molvarec A, Szarka A, Walentin S, Szucs E, Nagy B, Rigo J, Jr. (2010) Circulating angiogenic factors determined by electrochemiluminescence immunoassay in relation to the clinical features and laboratory parameters in women with pre-eclampsia. Hypertens Res 33: 892-898.
116. Stenczer B, Molvarec A, Veresh Z, Gullai N, Nagy GR, Walentin S, Szijarto J, Rigo J, Jr. (2011) Circulating levels of the anti-angiogenic thrombospondin 2 are elevated in pre-eclampsia. Acta Obstet Gynecol Scand 90: 1291-1295.
117. Rigo J, Jr., Nagy B, Fintor L. (2002) Factor V Leiden mutation and preeclampsia. Am J Obstet Gynecol 186: 853; author reply 853-854.
118. Szarka A, Rigo J, Jr., Lazar L, Beko G, Molvarec A. (2010) Circulating cytokines, chemokines and adhesion molecules in normal pregnancy and preeclampsia determined by multiplex suspension array. BMC Immunol 11: 59.
119. Toldi G, Rigo J, Jr., Stenczer B, Vasarhelyi B, Molvarec A. (2011) Increased prevalence of IL-17-producing peripheral blood lymphocytes in pre-eclampsia. Am J Reprod Immunol 66: 223-229.
120. Redman CW, Sargent IL. (2000) Placental debris, oxidative stress and pre-eclampsia. Placenta 21: 597-602.
121. Gervasi MT, Chaiworapongsa T, Pacora P, Naccasha N, Yoon BH, Maymon E, Romero R. (2001) Phenotypic and metabolic characteristics of monocytes and granulocytes in preeclampsia. Am J Obstet Gynecol 185: 792-797.
122. Chaiworapongsa T, Gervasi MT, Refuerzo J, Espinoza J, Yoshimatsu J, Berman S, Romero R. (2002) Maternal lymphocyte subpopulations (CD45RA+ and CD45RO+) in preeclampsia. Am J Obstet Gynecol 187: 889-893.
123. Than NG, Romero R, Erez O, Kusanovic JP, Tarca AL, Edwin SS, Kim JS, Hassan SS, Espinoza J, Mittal P, Mazaki-Tovi S, Friel L, Gotsch F, Vaisbuch E, Camacho N, Papp Z. (2008) A role for mannose-binding lectin, a component of

the innate immune system in pre-eclampsia. Am J Reprod Immunol 60: 333-345.

124. Ogge G, Romero R, Chaiworapongsa T, Gervasi MT, Pacora P, Erez O, Kusanovic JP, Vaisbuch E, Mazaki-Tovi S, Gotsch F, Mittal P, Kim YM, Hassan SS. (2010) Leukocytes of pregnant women with small-for-gestational age neonates have a different phenotypic and metabolic activity from those of women with preeclampsia. J Matern Fetal Neonatal Med 23: 476-487.

125. Gu H, Pan Z, Duda C, Mann D, Kissinger C, Rohde C, Raftery D. (2007) 1H NMR study of the effects of sample contamination in the metabolomic analysis of mouse urine. J Pharm Biomed Anal 45: 134-140.

126. Roberts JM, Taylor RN, Musci TJ, Rodgers GM, Hubel CA, McLaughlin MK. (1989) Preeclampsia: an endothelial cell disorder. Am J Obstet Gynecol 161: 1200-1204.

127. Kraayenbrink AA, Dekker GA, van Kamp GJ, van Geijn HP. (1993) Endothelial vasoactive mediators in preeclampsia. Am J Obstet Gynecol 169: 160-165.

128. Higgins JR, Papayianni A, Brady HR, Darling MR, Walshe JJ. (1998) Circulating vascular cell adhesion molecule-1 in pre-eclampsia, gestational hypertension, and normal pregnancy: evidence of selective dysregulation of vascular cell adhesion molecule-1 homeostasis in pre-eclampsia. Am J Obstet Gynecol 179: 464-469.

129. Taylor RN, de Groot CJ, Cho YK, Lim KH. (1998) Circulating factors as markers and mediators of endothelial cell dysfunction in preeclampsia. Semin Reprod Endocrinol 16: 17-31.

130. Redman CW, Sacks GP, Sargent IL. (1999) Preeclampsia: an excessive maternal inflammatory response to pregnancy. Am J Obstet Gynecol 180: 499-506.

131. Erez O, Romero R, Kim SS, Kim JS, Kim YM, Wildman DE, Than NG, Mazaki-Tovi S, Gotsch F, Pineles B, Kusanovic JP, Espinoza J, Mittal P, Mazor M, Hassan SS, Kim CJ. (2008) Over-expression of the thrombin receptor (PAR-1) in the placenta in preeclampsia: a mechanism for the intersection of coagulation and inflammation. J Matern Fetal Neonatal Med 21: 345-355.

132. Erez O, Romero R, Hoppensteadt D, Than NG, Fareed J, Mazaki-Tovi S, Espinoza J, Chaiworapongsa T, Kim SS, Yoon BH, Hassan SS, Gotsch F, Friel L,

Vaisbuch E, Kusanovic JP. (2008) Tissue factor and its natural inhibitor in pre-eclampsia and SGA. J Matern Fetal Neonatal Med 21: 855-869.

133. Erez O, Romero R, Vaisbuch E, Mazaki-Tovi S, Kusanovic JP, Chaiworapongsa T, Than NG, Gotsch F, Kim CJ, Mittal P, Edwin S, Pacora P, Kim SK, Yeo L, Mazor M, Hassan SS. (2009) Maternal anti-protein Z antibodies in pregnancies complicated by pre-eclampsia, SGA and fetal death. J Matern Fetal Neonatal Med 22: 662-671.
134. Rigo J, Jr., Beke A, Papp Z, Paulin F. (1996) Neonatal outcome after preterm delivery for preeclampsia. Am J Obstet Gynecol 174: 1080-1081.
135. Clark DE, Smith SK, He Y, Day KA, Licence DR, Corps AN, Lammoglia R, Charnock-Jones DS. (1998) A vascular endothelial growth factor antagonist is produced by the human placenta and released into the maternal circulation. Biol Reprod 59: 1540-1548.
136. Nagy B, Toth T, Rigo J, Jr., Karadi I, Romics L, Papp Z. (1998) Detection of factor V Leiden mutation in severe pre-eclamptic Hungarian women. Clin Genet 53: 478-481.
137. Reuvekamp A, Velsing-Aarts FV, Poulina IE, Capello JJ, Duits AJ. (1999) Selective deficit of angiogenic growth factors characterises pregnancies complicated by pre-eclampsia. Br J Obstet Gynaecol 106: 1019-1022.
138. Vuorela P, Helske S, Hornig C, Alitalo K, Weich H, Halmesmaki E. (2000) Amniotic fluid--soluble vascular endothelial growth factor receptor-1 in preeclampsia. Obstet Gynecol 95: 353-357.
139. Koga K, Osuga Y, Yoshino O, Hirota Y, Ruimeng X, Hirata T, Takeda S, Yano T, Tsutsumi O, Taketani Y. (2003) Elevated serum soluble vascular endothelial growth factor receptor 1 (sVEGFR-1) levels in women with preeclampsia. J Clin Endocrinol Metab 88: 2348-2351.
140. Wang H, Li Q, Lin H, Yu X, Qian D, Dai J, Duan E, Zhu C. (2003) Expression of vascular endothelial growth factor and its receptors in the rhesus monkey (Macaca mulatta) endometrium and placenta during early pregnancy. Mol Reprod Dev 65: 123-131.
141. Chaiworapongsa T, Romero R, Espinoza J, Bujold E, Mee Kim Y, Goncalves LF, Gomez R, Edwin S. (2004) Evidence supporting a role for blockade of the

vascular endothelial growth factor system in the pathophysiology of preeclampsia. Young Investigator Award. Am J Obstet Gynecol 190: 1541-1547; discussion 1547-1550.

142. Hertig A, Berkane N, Lefevre G, Toumi K, Marti HP, Capeau J, Uzan S, Rondeau E. (2004) Maternal serum sFlt1 concentration is an early and reliable predictive marker of preeclampsia. Clin Chem 50: 1702-1703.

143. Thadhani R, Mutter WP, Wolf M, Levine RJ, Taylor RN, Sukhatme VP, Ecker J, Karumanchi SA. (2004) First trimester placental growth factor and soluble fms-like tyrosine kinase 1 and risk for preeclampsia. J Clin Endocrinol Metab 89: 770-775.

144. Bujold E, Romero R, Chaiworapongsa T, Kim YM, Kim GJ, Kim MR, Espinoza J, Goncalves LF, Edwin S, Mazor M. (2005) Evidence supporting that the excess of the sVEGFR-1 concentration in maternal plasma in preeclampsia has a uterine origin. J Matern Fetal Neonatal Med 18: 9-16.

145. Chaiworapongsa T, Romero R, Kim YM, Kim GJ, Kim MR, Espinoza J, Bujold E, Goncalves L, Gomez R, Edwin S, Mazor M. (2005) Plasma soluble vascular endothelial growth factor receptor-1 concentration is elevated prior to the clinical diagnosis of pre-eclampsia. J Matern Fetal Neonatal Med 17: 3-18.

146. Lam C, Lim KH, Karumanchi SA. (2005) Circulating angiogenic factors in the pathogenesis and prediction of preeclampsia. Hypertension 46: 1077-1085.

147. Levine RJ, Lam C, Qian C, Yu KF, Maynard SE, Sachs BP, Sibai BM, Epstein FH, Romero R, Thadhani R, Karumanchi SA. (2006) Soluble endoglin and other circulating antiangiogenic factors in preeclampsia. N Engl J Med 355: 992-1005.

148. Rigo J, Jr., Boze T, Derzsy Z, Derzbach L, Treszl A, Lazar L, Sobel G, Vasarhelyi B. (2006) Family history of early-onset cardiovascular disorders is associated with a higher risk of severe preeclampsia. Eur J Obstet Gynecol Reprod Biol 128: 148-151.

149. Staff AC, Braekke K, Johnsen GM, Karumanchi SA, Harsem NK. (2007) Circulating concentrations of soluble endoglin (CD105) in fetal and maternal serum and in amniotic fluid in preeclampsia. Am J Obstet Gynecol 197: 176 e171-176.

150. Vatten LJ, Eskild A, Nilsen TI, Jeansson S, Jenum PA, Staff AC. (2007) Changes in circulating level of angiogenic factors from the first to second trimester as predictors of preeclampsia. Am J Obstet Gynecol 196: 239 e231-236.

151. Berkane N, Lefevre G, Hertig A. (2007) Angiogenic factors in preeclampsia: so complex, so simple? Nephrol Dial Transplant 22: 2753-2756.

152. Chaiworapongsa T, Espinoza J, Gotsch F, Kim YM, Kim GJ, Goncalves LF, Edwin S, Kusanovic JP, Erez O, Than NG, Hassan SS, Romero R. (2008) The maternal plasma soluble vascular endothelial growth factor receptor-1 concentration is elevated in SGA and the magnitude of the increase relates to Doppler abnormalities in the maternal and fetal circulation. J Matern Fetal Neonatal Med 21: 25-40.

153. Erez O, Romero R, Espinoza J, Fu W, Todem D, Kusanovic JP, Gotsch F, Edwin S, Nien JK, Chaiworapongsa T, Mittal P, Mazaki-Tovi S, Than NG, Gomez R, Hassan SS. (2008) The change in concentrations of angiogenic and anti-angiogenic factors in maternal plasma between the first and second trimesters in risk assessment for the subsequent development of preeclampsia and small-for-gestational age. J Matern Fetal Neonatal Med 21: 279-287.

154. Chaiworapongsa T, Romero R, Gotsch F, Espinoza J, Nien JK, Goncalves L, Edwin S, Kim YM, Erez O, Kusanovic JP, Pineles BL, Papp Z, Hassan S. (2008) Low maternal concentrations of soluble vascular endothelial growth factor receptor-2 in preeclampsia and small for gestational age. J Matern Fetal Neonatal Med 21: 41-52.

155. Gotsch F, Romero R, Kusanovic JP, Chaiworapongsa T, Dombrowski M, Erez O, Than NG, Mazaki-Tovi S, Mittal P, Espinoza J, Hassan SS. (2008) Preeclampsia and small-for-gestational age are associated with decreased concentrations of a factor involved in angiogenesis: soluble Tie-2. J Matern Fetal Neonatal Med 21: 389-402.

156. Hertig A, Lefevre G, Toumi K, Rondeau E, Capeau J, Uzan S, Berkane N. (2008) Soluble endoglin levels during normotensive and hypertensive pregnancies. Eur J Obstet Gynecol Reprod Biol 140: 138-140.

157. Romero R, Nien JK, Espinoza J, Todem D, Fu W, Chung H, Kusanovic JP, Gotsch F, Erez O, Mazaki-Tovi S, Gomez R, Edwin S, Chaiworapongsa T, Levine RJ,

Karumanchi SA. (2008) A longitudinal study of angiogenic (placental growth factor) and anti-angiogenic (soluble endoglin and soluble vascular endothelial growth factor receptor-1) factors in normal pregnancy and patients destined to develop preeclampsia and deliver a small for gestational age neonate. J Matern Fetal Neonatal Med 21: 9-23.

158. Than NG, Romero R, Hillermann R, Cozzi V, Nie G, Huppertz B. (2008) Prediction of preeclampsia - a workshop report. Placenta 29 Suppl A: S83-85.
159. Kusanovic JP, Romero R, Chaiworapongsa T, Erez O, Mittal P, Vaisbuch E, Mazaki-Tovi S, Gotsch F, Edwin SS, Gomez R, Yeo L, Conde-Agudelo A, Hassan SS. (2009) A prospective cohort study of the value of maternal plasma concentrations of angiogenic and anti-angiogenic factors in early pregnancy and midtrimester in the identification of patients destined to develop preeclampsia. J Matern Fetal Neonatal Med 22: 1021-1038.
160. Smith GC, Wear H. (2009) The perinatal implications of angiogenic factors. Curr Opin Obstet Gynecol 21: 111-116.
161. Chaiworapongsa T, Romero R, Kusanovic JP, Mittal P, Kim SK, Gotsch F, Than NG, Mazaki-Tovi S, Vaisbuch E, Erez O, Yeo L, Hassan SS, Sorokin Y. (2010) Plasma soluble endoglin concentration in pre-eclampsia is associated with an increased impedance to flow in the maternal and fetal circulations. Ultrasound Obstet Gynecol 35: 155-162.
162. Chaiworapongsa T, Romero R, Tarca AL, Kusanovic JP, Gotsch F, Mittal P, Kim SK, Vaisbuch E, Mazaki-Tovi S, Erez O, Dong Z, Kim CJ, Yeo L, Hassan SS. (2010) A decrease in maternal plasma concentrations of sVEGFR-2 precedes the clinical diagnosis of preeclampsia. Am J Obstet Gynecol 202: 550 e551-510.
163. Ogge G, Romero R, Kusanovic JP, Chaiworapongsa T, Dong Z, Mittal P, Vaisbuch E, Mazaki-Tovi S, Gonzalez JM, Yeo L, Hassan SS. (2010) Serum and plasma determination of angiogenic and anti-angiogenic factors yield different results: the need for standardization in clinical practice. J Matern Fetal Neonatal Med 23: 820-827.
164. Powers RW, Jeyabalan A, Clifton RG, Van Dorsten P, Hauth JC, Klebanoff MA, Lindheimer MD, Sibai B, Landon M, Miodovnik M. (2010) Soluble fms-Like

tyrosine kinase 1 (sFlt1), endoglin and placental growth factor (PlGF) in preeclampsia among high risk pregnancies. PLoS One 5: e13263.

165. Hertig A, Fort J, Lefevre G, Chabbert-Buffet N, Uzan M, Rondeau E, Rozenberg P. (2010) Soluble endoglin in preeclamptic patients with or without HELLP syndrome. Am J Obstet Gynecol 202: 594 e591-594.
166. Chaiworapongsa T, Romero R, Savasan ZA, Kusanovic JP, Ogge G, Soto E, Dong Z, Tarca A, Gaurav B, Hassan SS. (2011) Maternal plasma concentrations of angiogenic/anti-angiogenic factors are of prognostic value in patients presenting to the obstetrical triage area with the suspicion of preeclampsia. J Matern Fetal Neonatal Med 24: 1187-1207.
167. Vaisbuch E, Whitty JE, Hassan SS, Romero R, Kusanovic JP, Cotton DB, Sorokin Y, Karumanchi SA. (2011) Circulating angiogenic and antiangiogenic factors in women with eclampsia. Am J Obstet Gynecol 204: 152 e151-159.
168. Muttukrishna S, Swer M, Suri S, Jamil A, Calleja-Agius J, Gangooly S, Ludlow H, Jurkovic D, Jauniaux E. (2011) Soluble Flt-1 and PlGF: new markers of early pregnancy loss? PLoS One 6: e18041.
169. Rana S, Powe CE, Salahuddin S, Verlohren S, Perschel FH, Levine RJ, Lim KH, Wenger JB, Thadhani R, Karumanchi SA. (2012) Angiogenic factors and the risk of adverse outcomes in women with suspected preeclampsia. Circulation 125: 911-919.
170. Eshkoli T, Holcberg G, Bronfenmacher B, Amash A, Huleihel M, Erez O. (2012) Perfusion with magnesium sulfate increases sFlt-1 secretion only in the fetal side of placenta of women with preeclampsia. J Matern Fetal Neonatal Med 26: 116-122.
171. Moore AG, Young H, Keller JM, Ojo LR, Yan J, Simas TA, Maynard SE. (2012) Angiogenic biomarkers for prediction of maternal and neonatal complications in suspected preeclampsia. J Matern Fetal Neonatal Med 25: 2651-2657.
172. Reimer T, Rohrmann H, Stubert J, Pecks U, Glocker MO, Richter DU, Gerber B. (2012) Angiogenic factors and acute-phase proteins in serum samples of preeclampsia and HELLP patients: a matched-pair analysis. J Matern Fetal Neonatal Med.

173. Verlohren S, Stepan H, Dechend R. (2012) Angiogenic growth factors in the diagnosis and prediction of pre-eclampsia. Clin Sci (Lond) 122: 43-52.

174. Weed S, Bastek JA, Anton L, Elovitz MA, Parry S, Srinivas SK. (2012) Examining the correlation between placental and serum placenta growth factor in preeclampsia. Am J Obstet Gynecol 207: 140 e141-146.

175. Szalai G, Xu Y, Romero R, Chaiworapongsa T, Xu Z, Chiang PJ, Ahn H, Sundell B, Plazyo O, Jiang Y, Olive M, Wang B, Jacques SM, Qureshi F, Tarca AL, Erez O, Dong Z, Papp Z, Hassan SS, Hernandez-Andrade E, Than NG. (2014) In vivo experiments reveal the good, the bad and the ugly faces of sFlt-1 in pregnancy. PLoS One 9: e110867.

176. Fan X, Rai A, Kambham N, Sung JF, Singh N, Petitt M, Dhal S, Agrawal R, Sutton RE, Druzin ML, Gambhir SS, Ambati BK, Cross JC, Nayak NR. (2014) Endometrial VEGF induces placental sFLT1 and leads to pregnancy complications. J Clin Invest 124: 4941-4952.

177. Szalai G, Romero R, Chaiworapongsa T, Xu Y, Wang B, Ahn H, Xu Z, Chiang PJ, Sundell B, Wang R, Jiang Y, Plazyo O, Olive M, Tarca AL, Dong Z, Qureshi F, Papp Z, Hassan SS, Hernandez-Andrade E, Than NG. (2015) Full-Length Human Placental sFlt-1-e15a Isoform Induces Distinct Maternal Phenotypes of Preeclampsia in Mice. PLoS One 10: e0119547.

178. Gullai N, Stenczer B, Molvarec A, Fugedi G, Veresh Z, Nagy B, Rigo J, Jr. (2013) Evaluation of a rapid and simple placental growth factor test in hypertensive disorders of pregnancy. Hypertens Res 36: 457-462.

179. Molvarec A, Gullai N, Stenczer B, Fugedi G, Nagy B, Rigo J, Jr. (2013) Comparison of placental growth factor and fetal flow Doppler ultrasonography to identify fetal adverse outcomes in women with hypertensive disorders of pregnancy: an observational study. BMC Pregnancy Childbirth 13: 161.

180. Gotsch F, Romero R, Friel L, Kusanovic JP, Espinoza J, Erez O, Than NG, Mittal P, Edwin S, Yoon BH, Kim CJ, Mazaki-Tovi S, Chaiworapongsa T, Hassan SS. (2007) CXCL10/IP-10: a missing link between inflammation and anti-angiogenesis in preeclampsia? J Matern Fetal Neonatal Med 20: 777-792.

181. Ahmed A. (2011) New insights into the etiology of preeclampsia: identification of key elusive factors for the vascular complications. Thromb Res 127 Suppl 3: S72-75.

182. Heydarian M, McCaffrey T, Florea L, Yang Z, Ross MM, Zhou W, Maynard SE. (2009) Novel splice variants of sFlt1 are upregulated in preeclampsia. Placenta 30: 250-255.

183. Jebbink J, Keijser R, Veenboer G, van der Post J, Ris-Stalpers C, Afink G. (2011) Expression of placental FLT1 transcript variants relates to both gestational hypertensive disease and fetal growth. Hypertension 58: 70-76.

184. Whitehead CL, Palmer KR, Nilsson U, Gao Y, Saglam B, Lappas M, Tong S. (2011) Placental expression of a novel primate-specific splice variant of sFlt-1 is upregulated in pregnancies complicated by severe early onset pre-eclampsia. BJOG 118: 1268-1271.

185. Silasi M, Cohen B, Karumanchi SA, Rana S. (2010) Abnormal placentation, angiogenic factors, and the pathogenesis of preeclampsia. Obstet Gynecol Clin North Am 37: 239-253.

186. Shah DM. (2005) Role of the renin-angiotensin system in the pathogenesis of preeclampsia. Am J Physiol Renal Physiol 288: F614-625.

187. Anguiano-Robledo L, Reyes-Melchor PA, Bobadilla-Lugo RA, Perez-Alvarez VM, Lopez-Sanchez P. (2007) Renal angiotensin-II receptors expression changes in a model of preeclampsia. Hypertens Pregnancy 26: 151-161.

188. Wallukat G, Homuth V, Fischer T, Lindschau C, Horstkamp B, Jupner A, Baur E, Nissen E, Vetter K, Neichel D, Dudenhausen JW, Haller H, Luft FC. (1999) Patients with preeclampsia develop agonistic autoantibodies against the angiotensin AT1 receptor. J Clin Invest 103: 945-952.

189. Dechend R, Muller DN, Wallukat G, Homuth V, Krause M, Dudenhausen J, Luft FC. (2005) Activating auto-antibodies against the AT1 receptor in preeclampsia. Autoimmun Rev 4: 61-65.

190. Zhou CC, Zhang Y, Irani RA, Zhang H, Mi T, Popek EJ, Hicks MJ, Ramin SM, Kellems RE, Xia Y. (2008) Angiotensin receptor agonistic autoantibodies induce pre-eclampsia in pregnant mice. Nat Med 14: 855-862.

191. Falcao S, Stoyanova E, Cloutier G, Maurice RL, Gutkowska J, Lavoie JL. (2009) Mice overexpressing both human angiotensinogen and human renin as a model of superimposed preeclampsia on chronic hypertension. Hypertension 54: 1401-1407.

192. Irani RA, Xia Y. (2008) The functional role of the renin-angiotensin system in pregnancy and preeclampsia. Placenta 29: 763-771.

193. Irani RA, Zhang Y, Blackwell SC, Zhou CC, Ramin SM, Kellems RE, Xia Y. (2009) The detrimental role of angiotensin receptor agonistic autoantibodies in intrauterine growth restriction seen in preeclampsia. J Exp Med 206: 2809-2822.

194. Irani RA, Zhang Y, Zhou CC, Blackwell SC, Hicks MJ, Ramin SM, Kellems RE, Xia Y. (2010) Autoantibody-mediated angiotensin receptor activation contributes to preeclampsia through tumor necrosis factor-alpha signaling. Hypertension 55: 1246-1253.

195. Hahn S, Lapaire O, Than NG. (2015) Biomarker development for presymptomatic molecular diagnosis of preeclampsia: feasible, useful or even unnecessary? Expert Rev Mol Diagn 15: 617-629.

196. Csuka D, Molvarec A, Derzsy Z, Varga L, Fust G, Rigo J, Jr., Prohaszka Z. (2010) Functional analysis of the mannose-binding lectin complement pathway in normal pregnancy and preeclampsia. J Reprod Immunol 87: 90-96.

197. Lynch AM, Salmon JE. (2010) Dysregulated complement activation as a common pathway of injury in preeclampsia and other pregnancy complications. Placenta 31: 561-567.

198. Derzsy Z, Prohaszka Z, Rigo J, Jr., Fust G, Molvarec A. (2010) Activation of the complement system in normal pregnancy and preeclampsia. Mol Immunol 47: 1500-1506.

199. Halmos A, Rigo J, Jr., Szijarto J, Fust G, Prohaszka Z, Molvarec A. (2012) Circulating ficolin-2 and ficolin-3 in normal pregnancy and pre-eclampsia. Clin Exp Immunol 169: 49-56.

200. Megyeri M, Jani PK, Kajdacsi E, Dobo J, Schwaner E, Major B, Rigo J, Jr., Zavodszky P, Thiel S, Cervenak L, Gal P. (2014) Serum MASP-1 in complex with MBL activates endothelial cells. Mol Immunol 59: 39-45.

201. Sacks G, Sargent I, Redman C. (1999) An innate view of human pregnancy. ImmunolToday 20: 114-118.

202. Gupta AK, Hasler P, Holzgreve W, Gebhardt S, Hahn S. (2005) Induction of neutrophil extracellular DNA lattices by placental microparticles and IL-8 and their presence in preeclampsia. Hum Immunol 66: 1146-1154.

203. Hahn S, Giaglis S, Hoesli I, Hasler P. (2012) Neutrophil NETs in reproduction: from infertility to preeclampsia and the possibility of fetal loss. Front Immunol 3: 362.

204. Sacks GP, Studena K, Sargent K, Redman CW. (1998) Normal pregnancy and preeclampsia both produce inflammatory changes in peripheral blood leukocytes akin to those of sepsis. Am J Obstet Gynecol 179: 80-86.

205. Romero R, Espinoza J, Goncalves LF, Kusanovic JP, Friel LA, Nien JK. (2006) Inflammation in preterm and term labour and delivery. Semin Fetal Neonatal Med 11: 317-326.

206. Romero R, Gotsch F, Pineles B, Kusanovic JP. (2007) Inflammation in pregnancy: its roles in reproductive physiology, obstetrical complications, and fetal injury. Nutr Rev 65: S194-202.

207. Fuchs TA, Brill A, Duerschmied D, Schatzberg D, Monestier M, Myers DD, Jr., Wrobleski SK, Wakefield TW, Hartwig JH, Wagner DD. (2010) Extracellular DNA traps promote thrombosis. Proc Natl Acad Sci U S A 107: 15880-15885.

208. Burton GJ, Jauniaux E. (2004) Placental oxidative stress: from miscarriage to preeclampsia. J Soc Gynecol Investig 11: 342-352.

209. Erez O, Gotsch F, Mazaki-Tovi S, Vaisbuch E, Kusanovic JP, Kim CJ, Chaiworapongsa T, Hoppensteadt D, Fareed J, Than NG, Nhan-Chang CL, Yeo L, Pacora P, Mazor M, Hassan SS, Mittal P, Romero R. (2009) Evidence of maternal platelet activation, excessive thrombin generation, and high amniotic fluid tissue factor immunoreactivity and functional activity in patients with fetal death. J Matern Fetal Neonatal Med 22: 672-687.

210. Shibuya M, Yamaguchi S, Yamane A, Ikeda T, Tojo A, Matsushime H, Sato M. (1990) Nucleotide sequence and expression of a novel human receptor-type tyrosine kinase gene (flt) closely related to the fms family. Oncogene 5: 519-524.

211. Shibuya M. (2001) Structure and function of VEGF/VEGF-receptor system involved in angiogenesis. Cell Struct Funct 26: 25-35.

212. Shibuya M. (2011) Involvement of Flt-1 (VEGF receptor-1) in cancer and preeclampsia. Proc Jpn Acad Ser B Phys Biol Sci 87: 167-178.

213. de Vries C, Escobedo JA, Ueno H, Houck K, Ferrara N, Williams LT. (1992) The fms-like tyrosine kinase, a receptor for vascular endothelial growth factor. Science 255: 989-991.

214. Fong GH, Rossant J, Gertsenstein M, Breitman ML. (1995) Role of the Flt-1 receptor tyrosine kinase in regulating the assembly of vascular endothelium. Nature 376: 66-70.

215. Keyt BA, Nguyen HV, Berleau LT, Duarte CM, Park J, Chen H, Ferrara N. (1996) Identification of vascular endothelial growth factor determinants for binding KDR and FLT-1 receptors. Generation of receptor-selective VEGF variants by site-directed mutagenesis. J Biol Chem 271: 5638-5646.

216. Shinkai A, Ito M, Anazawa H, Yamaguchi S, Shitara K, Shibuya M. (1998) Mapping of the sites involved in ligand association and dissociation at the extracellular domain of the kinase insert domain-containing receptor for vascular endothelial growth factor. J Biol Chem 273: 31283-31288.

217. Tanaka K, Yamaguchi S, Sawano A, Shibuya M. (1997) Characterization of the extracellular domain in vascular endothelial growth factor receptor-1 (Flt-1 tyrosine kinase). Jpn J Cancer Res 88: 867-876.

218. Thomas CP, Andrews JI, Liu KZ. (2007) Intronic polyadenylation signal sequences and alternate splicing generate human soluble Flt1 variants and regulate the abundance of soluble Flt1 in the placenta. Faseb J 21: 3885-3895.

219. Kendall RL, Thomas KA. (1993) Inhibition of vascular endothelial cell growth factor activity by an endogenously encoded soluble receptor. Proc Natl Acad Sci U S A 90: 10705-10709.

220. Kondo K, Hiratsuka S, Subbalakshmi E, Matsushime H, Shibuya M. (1998) Genomic organization of the flt-1 gene encoding for vascular endothelial growth factor (VEGF) receptor-1 suggests an intimate evolutionary relationship between the 7-Ig and the 5-Ig tyrosine kinase receptors. Gene 208: 297-305.

221. He Y, Smith SK, Day KA, Clark DE, Licence DR, Charnock-Jones DS. (1999) Alternative splicing of vascular endothelial growth factor (VEGF)-R1 (FLT-1) pre-mRNA is important for the regulation of VEGF activity. Mol Endocrinol 13: 537-545.

222. Kendall RL, Wang G, Thomas KA. (1996) Identification of a natural soluble form of the vascular endothelial growth factor receptor, FLT-1, and its heterodimerization with KDR. Biochem Biophys Res Commun 226: 324-328.

223. Thomas CP, Andrews JI, Raikwar NS, Kelley EA, Herse F, Dechend R, Golos TG, Liu KZ. (2009) A recently evolved novel trophoblast-enriched secreted form of fms-like tyrosine kinase-1 variant is up-regulated in hypoxia and preeclampsia. J Clin Endocrinol Metab 94: 2524-2530.

224. Helske S, Vuorela P, Carpen O, Hornig C, Weich H, Halmesmaki E. (2001) Expression of vascular endothelial growth factor receptors 1, 2 and 3 in placentas from normal and complicated pregnancies. Mol Hum Reprod 7: 205-210.

225. Thornton JG, Onwude JL. (1992) Convulsions in pregnancy in related gorillas. Am J Obstet Gynecol 167: 240-241.

226. Carter AM, Pijnenborg R. (2011) Evolution of invasive placentation with special reference to non-human primates. Best Pract Res Clin Obstet Gynaecol 25: 249-257.

227. Terio KA, Kinsel MJ, Raphael J, Mlengeya T, Lipende I, Kirchhoff CA, Gilagiza B, Wilson ML, Kamenya S, Estes JD, Keele BF, Rudicell RS, Liu W, Patton S, Collins A, Hahn BH, Travis DA, Lonsdorf EV. (2011) Pathologic lesions in chimpanzees (Pan trogylodytes schweinfurthii) from Gombe National Park, Tanzania, 2004-2010. J Zoo Wildl Med 42: 597-607.

228. Williams JM, Lonsdorf EV, Wilson ML, Schumacher-Stankey J, Goodall J, Pusey AE. (2008) Causes of death in the Kasekela chimpanzees of Gombe National Park, Tanzania. Am J Primatol 70: 766-777.

229. Wildman DE, Uddin M, Romero R, Gonzalez JM, Than NG, Murphy J, Hou ZC, Fritz J. (2011) Spontaneous abortion and preterm labor and delivery in nonhuman primates: evidence from a captive colony of chimpanzees (Pan troglodytes). PLoS One 6: e24509.

230. Than NG. (2012) PP13, decidual zones of necrosis, and spiral artery remodeling--preeclampsia revisited? Reprod Sci 19: 14-15.

231. McGowen MR, Erez O, Romero R, Wildman DE. (2014) The evolution of embryo implantation. Int J Dev Biol 58: 155-161.

232. McCarthy FP, Kingdom JC, Kenny LC, Walsh SK. (2011) Animal models of preeclampsia; uses and limitations. Placenta 32: 413-419.

233. Sunderland N, Hennessy A, Makris A. (2011) Animal models of pre-eclampsia. Am J Reprod Immunol 65: 533-541.

234. Davisson RL, Hoffmann DS, Butz GM, Aldape G, Schlager G, Merrill DC, Sethi S, Weiss RM, Bates JN. (2002) Discovery of a spontaneous genetic mouse model of preeclampsia. Hypertension 39: 337-342.

235. Woods AK, Hoffmann DS, Weydert CJ, Butler SD, Zhou Y, Sharma RV, Davisson RL. (2011) Adenoviral delivery of VEGF121 early in pregnancy prevents spontaneous development of preeclampsia in BPH/5 mice. Hypertension 57: 94-102.

236. Hodari AA. (1967) Chronic uterine ischemia and reversible experimental "toxemia of pregnancy". Am J Obstet Gynecol 97: 597-607.

237. Cavanagh D, Rao PS, Tsai CC, O'Connor TC. (1977) Experimental toxemia in the pregnant primate. Am J Obstet Gynecol 128: 75-85.

238. Clark KE, Durnwald M, Austin JE. (1982) A model for studying chronic reduction in uterine blood flow in pregnant sheep. Am J Physiol 242: H297-301.

239. Losonczy G, Brown G, Venuto RC. (1992) Increased peripheral resistance during reduced uterine perfusion pressure hypertension in pregnant rabbits. Am J Med Sci 303: 233-240.

240. Combs CA, Katz MA, Kitzmiller JL, Brescia RJ. (1993) Experimental preeclampsia produced by chronic constriction of the lower aorta: validation with longitudinal blood pressure measurements in conscious rhesus monkeys. Am J Obstet Gynecol 169: 215-223.

241. LaMarca BB, Bennett WA, Alexander BT, Cockrell K, Granger JP. (2005) Hypertension produced by reductions in uterine perfusion in the pregnant rat: role of tumor necrosis factor-alpha. Hypertension 46: 1022-1025.

242. Granger JP, LaMarca BB, Cockrell K, Sedeek M, Balzi C, Chandler D, Bennett W. (2006) Reduced uterine perfusion pressure (RUPP) model for studying cardiovascular-renal dysfunction in response to placental ischemia. Methods Mol Med 122: 383-392.

243. Gilbert JS, Babcock SA, Granger JP. (2007) Hypertension produced by reduced uterine perfusion in pregnant rats is associated with increased soluble fms-like tyrosine kinase-1 expression. Hypertension 50: 1142-1147.

244. Makris A, Thornton C, Thompson J, Thomson S, Martin R, Ogle R, Waugh R, McKenzie P, Kirwan P, Hennessy A. (2007) Uteroplacental ischemia results in proteinuric hypertension and elevated sFLT-1. Kidney Int 71: 977-984.

245. Sholook MM, Gilbert JS, Sedeek MH, Huang M, Hester RL, Granger JP. (2007) Systemic hemodynamic and regional blood flow changes in response to chronic reductions in uterine perfusion pressure in pregnant rats. Am J Physiol Heart Circ Physiol 293: H2080-2084.

246. Gilbert JS, Gilbert SA, Arany M, Granger JP. (2009) Hypertension produced by placental ischemia in pregnant rats is associated with increased soluble endoglin expression. Hypertension 53: 399-403.

247. Li J, LaMarca B, Reckelhoff JF. (2012) A model of preeclampsia in rats: the reduced uterine perfusion pressure (RUPP) model. Am J Physiol Heart Circ Physiol 303: H1-8.

248. Molnar M, Suto T, Toth T, Hertelendy F. (1994) Prolonged blockade of nitric oxide synthesis in gravid rats produces sustained hypertension, proteinuria, thrombocytopenia, and intrauterine growth retardation. Am J Obstet Gynecol 170: 1458-1466.

249. Huang PL, Huang Z, Mashimo H, Bloch KD, Moskowitz MA, Bevan JA, Fishman MC. (1995) Hypertension in mice lacking the gene for endothelial nitric oxide synthase. Nature 377: 239-242.

250. Salas SP, Altermatt F, Campos M, Giacaman A, Rosso P. (1995) Effects of long-term nitric oxide synthesis inhibition on plasma volume expansion and fetal growth in the pregnant rat. Hypertension 26: 1019-1023.

251. Shesely EG, Gilbert C, Granderson G, Carretero CD, Carretero OA, Beierwaltes WH. (2001) Nitric oxide synthase gene knockout mice do not become hypertensive during pregnancy. Am J Obstet Gynecol 185: 1198-1203.

252. Podjarny E, Bernheim J, Katz B, Green J, Mekler J, Bursztyn M. (1998) Chronic exogenous hyperinsulinemia in pregnancy: a rat model of pregnancy-induced hypertension. J Am Soc Nephrol 9: 9-13.

253. Kanasaki K, Palmsten K, Sugimoto H, Ahmad S, Hamano Y, Xie L, Parry S, Augustin HG, Gattone VH, Folkman J, Strauss JF, Kalluri R. (2008) Deficiency in catechol-O-methyltransferase and 2-methoxyoestradiol is associated with pre-eclampsia. Nature 453: 1117-1121.

254. Falcao S, Bisotto S, Gutkowska J, Lavoie JL. (2009) Hyperhomocysteinemia is not sufficient to cause preeclampsia in an animal model: the importance of folate intake. Am J Obstet Gynecol 200: 198 e191-195.

255. Doridot L, Chatre L, Ducat A, Vilotte JL, Lombes A, Mehats C, Barbaux S, Calicchio R, Ricchetti M, Vaiman D. (2014) Nitroso-redox balance and mitochondrial homeostasis are regulated by STOX1, a pre-eclampsia-associated gene. Antioxid Redox Signal 21: 819-834.

256. Alfaidy N, Chauvet S, Donadio-Andrei S, Salomon A, Saoudi Y, Richaud P, Aude-Garcia C, Hoffmann P, Andrieux A, Moulis JM, Feige JJ, Benharouga M. (2013) Prion protein expression and functional importance in developmental angiogenesis: role in oxidative stress and copper homeostasis. Antioxid Redox Signal 18: 400-411.

257. Takimoto E, Ishida J, Sugiyama F, Horiguchi H, Murakami K, Fukamizu A. (1996) Hypertension induced in pregnant mice by placental renin and maternal angiotensinogen. Science 274: 995-998.

258. Bohlender J, Ganten D, Luft FC. (2000) Rats transgenic for human renin and human angiotensinogen as a model for gestational hypertension. J Am Soc Nephrol 11: 2056-2061.

259. Orshal JM, Khalil RA. (2004) Reduced endothelial NO-cGMP-mediated vascular relaxation and hypertension in IL-6-infused pregnant rats. Hypertension 43: 434-444.

260. Zenclussen AC, Fest S, Joachim R, Klapp BF, Arck PC. (2004) Introducing a mouse model for pre-eclampsia: adoptive transfer of activated Th1 cells leads to pre-eclampsia-like symptoms exclusively in pregnant mice. Eur J Immunol 34: 377-387.

261. Li Z, Zhang Y, Ying Ma J, Kapoun AM, Shao Q, Kerr I, Lam A, O'Young G, Sannajust F, Stathis P, Schreiner G, Karumanchi SA, Protter AA, Pollitt NS. (2007) Recombinant vascular endothelial growth factor 121 attenuates hypertension and improves kidney damage in a rat model of preeclampsia. Hypertension 50: 686-692.

262. Lu F, Longo M, Tamayo E, Maner W, Al-Hendy A, Anderson GD, Hankins GD, Saade GR. (2007) The effect of over-expression of sFlt-1 on blood pressure and the occurrence of other manifestations of preeclampsia in unrestrained conscious pregnant mice. Am J Obstet Gynecol 196: 396 e391-397; discussion 396 e397.

263. Suzuki H, Ohkuchi A, Matsubara S, Takei Y, Murakami M, Shibuya M, Suzuki M, Sato Y. (2009) Effect of recombinant placental growth factor 2 on hypertension induced by full-length mouse soluble fms-like tyrosine kinase 1 adenoviral vector in pregnant mice. Hypertension 54: 1129-1135.

264. Bergmann A, Ahmad S, Cudmore M, Gruber AD, Wittschen P, Lindenmaier W, Christofori G, Gross V, Gonzalves A, Grone HJ, Ahmed A, Weich HA. (2010) Reduction of circulating soluble Flt-1 alleviates preeclampsia-like symptoms in a mouse model. J Cell Mol Med 14: 1857-1867.

265. Kumasawa K, Ikawa M, Kidoya H, Hasuwa H, Saito-Fujita T, Morioka Y, Takakura N, Kimura T, Okabe M. (2011) Pravastatin induces placental growth factor (PGF) and ameliorates preeclampsia in a mouse model. Proc Natl Acad Sci U S A 108: 1451-1455.

266. Mateus J, Bytautiene E, Lu F, Tamayo EH, Betancourt A, Hankins GD, Longo M, Saade GR. (2011) Endothelial growth factor therapy improves preeclampsia-like manifestations in a murine model induced by overexpression of sVEGFR-1. Am J Physiol Heart Circ Physiol 301: H1781-1787.

267. Li F, Hagaman JR, Kim HS, Maeda N, Jennette JC, Faber JE, Karumanchi SA, Smithies O, Takahashi N. (2012) eNOS deficiency acts through endothelin to

aggravate sFlt-1-induced pre-eclampsia-like phenotype. J Am Soc Nephrol 23: 652-660.

268. Rossant J, Cross JC. (2001) Placental development: lessons from mouse mutants. Nat Rev Genet 2: 538-548.

269. Adamson SL, Lu Y, Whiteley KJ, Holmyard D, Hemberger M, Pfarrer C, Cross JC. (2002) Interactions between trophoblast cells and the maternal and fetal circulation in the mouse placenta. Dev Biol 250: 358-373.

270. Georgiades P, Ferguson-Smith AC, Burton GJ. (2002) Comparative developmental anatomy of the murine and human definitive placentae. Placenta 23: 3-19.

271. Cox B, Kotlyar M, Evangelou AI, Ignatchenko V, Ignatchenko A, Whiteley K, Jurisica I, Adamson SL, Rossant J, Kislinger T. (2009) Comparative systems biology of human and mouse as a tool to guide the modeling of human placental pathology. Mol Syst Biol 5: 279.

272. Krishnamurthy U, Szalai G, Neelavalli J, Shen Y, Chaiworapongsa T, Hernandez-Andrade E, Than NG, Xu Z, Yeo L, Haacke M, Romero R. (2014) Quantitative T2 changes and susceptibility-weighted magnetic resonance imaging in murine pregnancy. Gynecol Obstet Invest 78: 33-40.

273. Lu F, Bytautiene E, Tamayo E, Gamble P, Anderson GD, Hankins GD, Longo M, Saade GR. (2007) Gender-specific effect of overexpression of sFlt-1 in pregnant mice on fetal programming of blood pressure in the offspring later in life. Am J Obstet Gynecol 197: 418 e411-415.

274. Byers BD, Betancourt A, Lu F, Hankins GD, Longo M, Saade GR, Bytautiene E. (2009) The effect of prepregnancy obesity and sFlt-1-induced preeclampsia-like syndrome on fetal programming of adult vascular function in a mouse model. Am J Obstet Gynecol 200: 432 e431-437.

275. Bytautiene E, Lu F, Tamayo EH, Hankins GD, Longo M, Kublickiene K, Saade GR. (2010) Long-term maternal cardiovascular function in a mouse model of sFlt-1-induced preeclampsia. Am J Physiol Heart Circ Physiol 298: H189-193.

276. Costantine MM, Tamayo E, Lu F, Bytautiene E, Longo M, Hankins GD, Saade GR. (2010) Using pravastatin to improve the vascular reactivity in a mouse model of soluble fms-like tyrosine kinase-1-induced preeclampsia. Obstet Gynecol 116: 114-120.

277. Fox KA, Longo M, Tamayo E, Kechichian T, Bytautiene E, Hankins GD, Saade GR, Costantine MM. (2011) Effects of pravastatin on mediators of vascular function in a mouse model of soluble Fms-like tyrosine kinase-1-induced preeclampsia. Am J Obstet Gynecol 205: 366 e361-365.

278. National Research Council of the National Academies: Guide for the Care and Use of Laboratory Animals. The National Academies Press, Washington DC, 2011.

279. Theiler K. The house mouse: atlas of embryonic development. Springer-Verlag, New York, 1989.

280. Turnbull DH. (1999) In utero ultrasound backscatter microscopy of early stage mouse embryos. Comput Med Imaging Graph 23: 25-31.

281. Foster FS, Zhang MY, Zhou YQ, Liu G, Mehi J, Cherin E, Harasiewicz KA, Starkoski BG, Zan L, Knapik DA, Adamson SL. (2002) A new ultrasound instrument for in vivo microimaging of mice. Ultrasound Med Biol 28: 1165-1172.

282. Zhou YQ, Foster FS, Qu DW, Zhang M, Harasiewicz KA, Adamson SL. (2002) Applications for multifrequency ultrasound biomicroscopy in mice from implantation to adulthood. Physiol Genomics 10: 113-126.

283. Brown SD, Zurakowski D, Rodriguez DP, Dunning PS, Hurley RJ, Taylor GA. (2006) Ultrasound diagnosis of mouse pregnancy and gestational staging. Comp Med 56: 262-271.

284. Slevin JC, Byers L, Gertsenstein M, Qu D, Mu J, Sunn N, Kingdom JC, Rossant J, Adamson SL. (2006) High resolution ultrasound-guided microinjection for interventional studies of early embryonic and placental development in vivo in mice. BMC Dev Biol 6: 10.

285. Pallares P, Gonzalez-Bulnes A. (2008) Non-invasive ultrasonographic characterization of phenotypic changes during embryo development in non-anesthetized mice of different genotypes. Theriogenology 70: 44-52.

286. Pallares P, Fernandez-Valle ME, Gonzalez-Bulnes A. (2009) In vivo virtual histology of mouse embryogenesis by ultrasound biomicroscopy and magnetic resonance imaging. Reprod Fertil Dev 21: 283-292.

287. Hernandez-Andrade E, Ahn H, Szalai G, Korzeniewski SJ, Wang B, King M, Chaiworapongsa T, Than NG, Romero R. (2014) Evaluation of utero-placental

and fetal hemodynamic parameters throughout gestation in pregnant mice using high-frequency ultrasound. Ultrasound Med Biol 40: 351-360.

288. Hoogstraten-Miller SL, Brown PA. (2008) Techniques in aseptic rodent surgery. Curr Protoc Immunol Chapter 1: Unit 1 12 11-11 12-14.

289. Arm JP, Peile EB, Rainford DJ, Strike PW, Tettmar RE. (1986) Significance of dipstick haematuria. 1. Correlation with microscopy of the urine. Br J Urol 58: 211-217.

290. Anders HJ, Dendorfer U, Schlondorff D. (2001) [Urine diagnosis: test strip analysis and urinary sediment]. Dtsch Med Wochenschr 126: 1269-1271.

291. Reine NJ, Langston CE. (2005) Urinalysis interpretation: how to squeeze out the maximum information from a small sample. Clin Tech Small Anim Pract 20: 2-10.

292. Nicosia RF, Ottinetti A. (1990) Growth of microvessels in serum-free matrix culture of rat aorta. A quantitative assay of angiogenesis in vitro. Lab Invest 63: 115-122.

293. Baker M, Robinson SD, Lechertier T, Barber PR, Tavora B, D'Amico G, Jones DT, Vojnovic B, Hodivala-Dilke K. (2012) Use of the mouse aortic ring assay to study angiogenesis. Nat Protoc 7: 89-104.

294. Jose Pinheiro DB, Saikat DebRoy, Deepayan Sarkar and the R Development Core Team (2013) nlme: Linear and Nonlinear Mixed Effects Models. R package version 3.1-108.

295. Mizuguchi H, Koizumi N, Hosono T, Utoguchi N, Watanabe Y, Kay MA, Hayakawa T. (2001) A simplified system for constructing recombinant adenoviral vectors containing heterologous peptides in the HI loop of their fiber knob. Gene Ther 8: 730-735.

296. Kliman HJ, Nestler JE, Sermasi E, Sanger JM, Strauss JF, 3rd. (1986) Purification, characterization, and in vitro differentiation of cytotrophoblasts from human term placentae. Endocrinology 118: 1567-1582.

297. Su AI, Wiltshire T, Batalov S, Lapp H, Ching KA, Block D, Zhang J, Soden R, Hayakawa M, Kreiman G, Cooke MP, Walker JR, Hogenesch JB. (2004) A gene atlas of the mouse and human protein-encoding transcriptomes. ProcNatlAcadSciUSA 101: 6062-6067.

298. Buhimschi CS, Zhao G, Sora N, Madri JA, Buhimschi IA. (2010) Myometrial wound healing post-Cesarean delivery in the MRL/MpJ mouse model of uterine scarring. Am J Pathol 177: 197-207.

299. Katayama K, Furuki R, Yokoyama H, Kaneko M, Tachibana M, Yoshida I, Nagase H, Tanaka K, Sakurai F, Mizuguchi H, Nakagawa S, Nakanishi T. (2011) Enhanced in vivo gene transfer into the placenta using RGD fiber-mutant adenovirus vector. Biomaterials 32: 4185-4193.

300. Kamat A, Smith ME, Shelton JM, Richardson JA, Mendelson CR. (2005) Genomic regions that mediate placental cell-specific and developmental regulation of human Cyp19 (aromatase) gene expression in transgenic mice. Endocrinology 146: 2481-2488.

301. Whitesall SE, Hoff JB, Vollmer AP, D'Alecy LG. (2004) Comparison of simultaneous measurement of mouse systolic arterial blood pressure by radiotelemetry and tail-cuff methods. Am J Physiol Heart Circ Physiol 286: H2408-2415.

302. Mills PA, Huetteman DA, Brockway BP, Zwiers LM, Gelsema AJ, Schwartz RS, Kramer K. (2000) A new method for measurement of blood pressure, heart rate, and activity in the mouse by radiotelemetry. J Appl Physiol 88: 1537-1544.

303. Kramer K, Voss HP, Grimbergen JA, Mills PA, Huetteman D, Zwiers L, Brockway B. (2000) Telemetric monitoring of blood pressure in freely moving mice: a preliminary study. Lab Anim 34: 272-280.

304. Van Vliet BN, Chafe LL, Antic V, Schnyder-Candrian S, Montani JP. (2000) Direct and indirect methods used to study arterial blood pressure. J Pharmacol Toxicol Methods 44: 361-373.

305. Kramer K, Kinter LB. (2003) Evaluation and applications of radiotelemetry in small laboratory animals. Physiol Genomics 13: 197-205.

306. Zhao X, Ho D, Gao S, Hong C, Vatner DE, Vatner SF. (2011) Arterial Pressure Monitoring in Mice. Curr Protoc Mouse Biol 1: 105-122.

307. Carlson SH, Wyss JM. (2000) Long-term telemetric recording of arterial pressure and heart rate in mice fed basal and high NaCl diets. Hypertension 35: E1-5.

308. Butz GM, Davisson RL. (2001) Long-term telemetric measurement of cardiovascular parameters in awake mice: a physiological genomics tool. Physiol Genomics 5: 89-97.

309. Kurtz TW, Griffin KA, Bidani AK, Davisson RL, Hall JE. (2005) Recommendations for blood pressure measurement in animals: summary of an AHA scientific statement from the Council on High Blood Pressure Research, Professional and Public Education Subcommittee. Arterioscler Thromb Vasc Biol 25: 478-479.

310. Kaidi S, Brutel F, Van Deun F, Kramer K, Remie R, Dewe W, Remusat P, Delaunois A, Depelchin O. (2007) Comparison of two methods (left carotid artery and abdominal aorta) for surgical implantation of radiotelemetry devices in CD-1 mice. Lab Anim 41: 388-402.

311. HD-X11 Device Surgical Manual. Data Science International, St.Paul, 2011: 32.

312. Siddiqui AH, Irani RA, Zhang Y, Dai Y, Blackwell SC, Ramin SM, Kellems RE, Xia Y. (2011) Recombinant vascular endothelial growth factor 121 attenuates autoantibody-induced features of pre-eclampsia in pregnant mice. Am J Hypertens 24: 606-612.

313. Singh J, Ahmed A, Girardi G. (2011) Role of complement component C1q in the onset of preeclampsia in mice. Hypertension 58: 716-724.

314. Kristal MB. (1980) Placentophagia: a biobehavioral enigma (or De gustibus non disputandum est). Neurosci Biobehav Rev 4: 141-150.

315. Mu J, Slevin JC, Qu D, McCormick S, Adamson SL. (2008) In vivo quantification of embryonic and placental growth during gestation in mice using micro-ultrasound. Reprod Biol Endocrinol 6: 34.

316. Sugimoto H, Hamano Y, Charytan D, Cosgrove D, Kieran M, Sudhakar A, Kalluri R. (2003) Neutralization of circulating vascular endothelial growth factor (VEGF) by anti-VEGF antibodies and soluble VEGF receptor 1 (sFlt-1) induces proteinuria. J Biol Chem 278: 12605-12608.

317. Xing A, Boileau P, Cauzac M, Challier JC, Girard J, Hauguel-de Mouzon S. (2000) Comparative in vivo approaches for selective adenovirus-mediated gene delivery to the placenta. Hum Gene Ther 11: 167-177.

318. Tal R, Shaish A, Barshack I, Polak-Charcon S, Afek A, Volkov A, Feldman B, Avivi C, Harats D. (2010) Effects of hypoxia-inducible factor-1alpha overexpression in pregnant mice: possible implications for preeclampsia and intrauterine growth restriction. Am J Pathol 177: 2950-2962.

319. Rajakumar A, Powers RW, Hubel CA, Shibata E, von Versen-Hoynck F, Plymire D, Jeyabalan A. (2009) Novel soluble Flt-1 isoforms in plasma and cultured placental explants from normotensive pregnant and preeclamptic women. Placenta 30: 25-34.

320. Roberts JM. (1999) Objective evidence of endothelial dysfunction in preeclampsia. Am J Kidney Dis 33: 992-997.

321. Khalil RA, Granger JP. (2002) Vascular mechanisms of increased arterial pressure in preeclampsia: lessons from animal models. Am J Physiol Regul Integr Comp Physiol 283: R29-45.

322. De P, Peng Q, Dmitry T, Li W, Yoder MC, March KL, Durden DL. (2009) Expression of RAC2 in endothelial cells is required for the postnatal neovascular response. Exp Cell Res 315: 248-263.

323. Conway BR, Rennie J, Bailey MA, Dunbar DR, Manning JR, Bellamy CO, Hughes J, Mullins JJ. (2012) Hyperglycemia and renin-dependent hypertension synergize to model diabetic nephropathy. J Am Soc Nephrol 23: 405-411.

324. Gaber LW, Spargo BH, Lindheimer MD. (1994) Renal pathology in pre-eclampsia. Baillieres Clin Obstet Gynaecol 8: 443-468.

325. Stillman IE, Karumanchi SA. (2007) The glomerular injury of preeclampsia. J Am Soc Nephrol 18: 2281-2284.

326. Kusinski LC, Stanley JL, Dilworth MR, Hirt CJ, Andersson IJ, Renshall LJ, Baker BC, Baker PN, Sibley CP, Wareing M, Glazier JD. (2012) eNOS knockout mouse as a model of fetal growth restriction with an impaired uterine artery function and placental transport phenotype. Am J Physiol Regul Integr Comp Physiol 303: R86-93.

327. Levine RJ, Qian C, Maynard SE, Yu KF, Epstein FH, Karumanchi SA. (2006) Serum sFlt1 concentration during preeclampsia and mid trimester blood pressure in healthy nulliparous women. Am J Obstet Gynecol 194: 1034-1041.

328. Chia R, Achilli F, Festing MF, Fisher EM. (2005) The origins and uses of mouse outbred stocks. Nat Genet 37: 1181-1186.

329. Aldinger KA, Sokoloff G, Rosenberg DM, Palmer AA, Millen KJ. (2009) Genetic variation and population substructure in outbred CD-1 mice: implications for genome-wide association studies. PLoS One 4: e4729.

330. Cao J, Gautier NM, Li MD. (2012) CD-1 mice Show Individual Differences in Nicotine Preference in a Modified Two-Bottle Oral Self-Administration Model. Front Psychiatry 3: 28.

331. Paidas MJ, Ku DH, Langhoff-Roos J, Arkel YS. (2005) Inherited thrombophilias and adverse pregnancy outcome: screening and management. Semin Perinatol 29: 150-163.

332. Girardi G. (2011) Role of tissue factor in pregnancy complications: crosstalk between coagulation and inflammation. Thromb Res 127 Suppl 3: S43-46.

333. Erez O, Hoppensteadt D, Romero R, Espinoza J, Goncalves L, Nien JK, Kusanovic JP, Fareed J, Gotsch F, Pineles B, Chaiworapongsa T. (2007) Preeclampsia is associated with low concentrations of protein Z. J Matern Fetal Neonatal Med 20: 661-667.

334. Ness RB, Sibai BM. (2006) Shared and disparate components of the pathophysiologies of fetal growth restriction and preeclampsia. Am J Obstet Gynecol 195: 40-49.

335. Agostinis C, Bulla R, Tripodo C, Gismondi A, Stabile H, Bossi F, Guarnotta C, Garlanda C, De Seta F, Spessotto P, Santoni A, Ghebrehiwet B, Girardi G, Tedesco F. (2010) An alternative role of C1q in cell migration and tissue remodeling: contribution to trophoblast invasion and placental development. J Immunol 185: 4420-4429.

336. Wilson JM. (1996) Adenoviruses as gene-delivery vehicles. N Engl J Med 334: 1185-1187.

337. Renaud SJ, Karim Rumi MA, Soares MJ. (2011) Review: Genetic manipulation of the rodent placenta. Placenta 32 Suppl 2: S130-135.

338. Katz AB, Keswani SG, Habli M, Lim FY, Zoltick PW, Midrio P, Kozin ED, Herlyn M, Crombleholme TM. (2009) Placental gene transfer: transgene

screening in mice for trophic effects on the placenta. Am J Obstet Gynecol 201: 499 e491-498.

339. Thadhani R, Kisner T, Hagmann H, Bossung V, Noack S, Schaarschmidt W, Jank A, Kribs A, Cornely OA, Kreyssig C, Hemphill L, Rigby AC, Khedkar S, Lindner TH, Mallmann P, Stepan H, Karumanchi SA, Benzing T. (2011) Pilot study of extracorporeal removal of soluble fms-like tyrosine kinase 1 in preeclampsia. Circulation 124: 940-950.
340. Ananth CV, Peltier MR, Chavez MR, Kirby RS, Getahun D, Vintzileos AM. (2007) Recurrence of ischemic placental disease. Obstet Gynecol 110: 128-133.
341. Drost JT, Maas AH, van Eyck J, van der Schouw YT. (2010) Preeclampsia as a female-specific risk factor for chronic hypertension. Maturitas 67: 321-326.
342. Bytautiene E, Bulayeva N, Bhat G, Li L, Rosenblatt KP, Saade GR. (2013) Long-term alterations in maternal plasma proteome after sFlt1-induced preeclampsia in mice. Am J Obstet Gynecol 208: 388 e381-388 e310.
343. Mole DR, Ratcliffe PJ. (2008) Cellular oxygen sensing in health and disease. Pediatr Nephrol 23: 681-694.
344. Kim YW, West XZ, Byzova TV. (2013) Inflammation and oxidative stress in angiogenesis and vascular disease. J Mol Med (Berl) 91: 323-328.
345. Scholz CC, Taylor CT. (2013) Targeting the HIF pathway in inflammation and immunity. Curr Opin Pharmacol 13: 646-653.
346. Sherer DM, Abulafia O. (2001) Angiogenesis during implantation, and placental and early embryonic development. Placenta 22: 1-13.
347. Charnock-Jones DS, Kaufmann P, Mayhew TM. (2004) Aspects of human fetoplacental vasculogenesis and angiogenesis. I. Molecular regulation. Placenta 25: 103-113.
348. Kaufmann P, Mayhew TM, Charnock-Jones DS. (2004) Aspects of human fetoplacental vasculogenesis and angiogenesis. II. Changes during normal pregnancy. Placenta 25: 114-126.
349. Mayhew TM, Charnock-Jones DS, Kaufmann P. (2004) Aspects of human fetoplacental vasculogenesis and angiogenesis. III. Changes in complicated pregnancies. Placenta 25: 127-139.

350. Jackson MR, Carney EW, Lye SJ, Ritchie JW. (1994) Localization of two angiogenic growth factors (PDECGF and VEGF) in human placentae throughout gestation. Placenta 15: 341-353.

351. Cooper JC, Sharkey AM, Charnock-Jones DS, Palmer CR, Smith SK. (1996) VEGF mRNA levels in placentae from pregnancies complicated by pre-eclampsia. Br J Obstet Gynaecol 103: 1191-1196.

352. Vuckovic M, Ponting J, Terman BI, Niketic V, Seif MW, Kumar S. (1996) Expression of the vascular endothelial growth factor receptor, KDR, in human placenta. J Anat 188 (Pt 2): 361-366.

353. Shiraishi S, Nakagawa K, Kinukawa N, Nakano H, Sueishi K. (1996) Immunohistochemical localization of vascular endothelial growth factor in the human placenta. Placenta 17: 111-121.

354. Romero R, Chaiworapongsa T, Erez O, Tarca AL, Gervasi MT, Kusanovic JP, Mittal P, Ogge G, Vaisbuch E, Mazaki-Tovi S, Dong Z, Kim SK, Yeo L, Hassan SS. (2010) An imbalance between angiogenic and anti-angiogenic factors precedes fetal death in a subset of patients: results of a longitudinal study. J Matern Fetal Neonatal Med 23: 1384-1399.

355. Sharkey AM, Charnock-Jones DS, Boocock CA, Brown KD, Smith SK. (1993) Expression of mRNA for vascular endothelial growth factor in human placenta. J Reprod Fertil 99: 609-615.

356. Ahmed A, Li XF, Dunk C, Whittle MJ, Rushton DI, Rollason T. (1995) Colocalisation of vascular endothelial growth factor and its Flt-1 receptor in human placenta. Growth Factors 12: 235-243.

357. Wheeler T, Elcock CL, Anthony FW. (1995) Angiogenesis and the placental environment. Placenta 16: 289-296.

358. Shore VH, Wang TH, Wang CL, Torry RJ, Caudle MR, Torry DS. (1997) Vascular endothelial growth factor, placenta growth factor and their receptors in isolated human trophoblast. Placenta 18: 657-665.

359. Wilting J, Birkenhager R, Eichmann A, Kurz H, Martiny-Baron G, Marme D, McCarthy JE, Christ B, Weich HA. (1996) VEGF121 induces proliferation of vascular endothelial cells and expression of flk-1 without affecting lymphatic vessels of chorioallantoic membrane. Dev Biol 176: 76-85.

360. De Falco S. (2012) The discovery of placenta growth factor and its biological activity. Exp Mol Med 44: 1-9.

361. Yamaguchi S, Iwata K, Shibuya M. (2002) Soluble Flt-1 (soluble VEGFR-1), a potent natural antiangiogenic molecule in mammals, is phylogenetically conserved in avians. Biochem Biophys Res Commun 291: 554-559.

362. Kaitu'u-Lino TJ, Whitehead CL, Ngian GL, Permezel M, Tong S. (2012) Serum concentrations of soluble Flt-1 are decreased among women with a viable fetus and no symptoms of miscarriage destined for pregnancy loss. PLoS One 7: e32509.

10. BIBLIOGRAPHY OF THE CANDIDATE'S PUBLICATIONS

10.1. Publications related to the PhD Thesis

Szalai G, Romero R, Chaiworapongsa T, Xu Y, Wang B, Ahn H, Xu Z, Chiang PJ, Sundell B, Wang R, Jiang Y, Plazyo O, Olive M, Tarca AL, Dong Z, Qureshi F, Papp Z, Hassan SS, Hernandez-Andrade E, Than NG:
Full-length human placental sFlt-1-e15a isoform induces distinct maternal phenotypes of preeclampsia in mice.
PLoS One, 2015, 10(4):e0119547. **IF: 3.234**

Szalai G, Xu Y, Romero R, Chaiworapongsa T, Xu Z, Chiang PJ, Ahn H, Sundell B, Plazyo O, Jiang Y, Olive M, Wang B, Jacques SM, Qureshi F, Tarca AL, Erez O, Dong Z, Papp Z, Hassan SS, Hernandez-Andrade E, Than NG:
In vivo experiments reveal the good, the bad and the ugly faces of sFlt-1 in pregnancy.
PLoS One, 2014, 9(11):e110867. **IF: 3.234, Citations: 5**

10.2. Publications unrelated to the PhD Thesis

Than NG, Romero R, Xu Y, Erez O, Xu Z, Bhatti G, Leavitt R, Chung TH, El-Azzamy H, LaJeunesse C, Wang B, Balogh A, **Szalai G**, Land S, Dong Z, Hassan SS, Chaiworapongsa T, Krispin M, Kim CJ, Tarca AL, Papp Z, Bohn H:
Evolutionary origins of the placental expression of chromosome 19 cluster galectins and their complex dysregulation in preeclampsia.
Placenta, 2014, 35, 855-865. **IF: 2.710, Citations: 6**

Krishnamurthy U, **Szalai G**, Neelavalli J, Shen Y, Chaiworapongsa T, Hernandez-Andrade E, Than NG, Xu Z, Yeo L, Haacke M, Romero R:
Quantitative T2 changes and susceptibility-weighted magnetic resonance imaging in murine pregnancy.
Gynecol. Obstet. Invest. 2014, 78, 33-40. **IF: 1.696, Citations: 2**

Hernandez-Andrade E, Ahn H, **Szalai G**, Korzeniewski SJ, Wang B, King M, Chaiworapongsa T, Than NG, Romero R:
Evaluation of utero-placental and fetal hemodynamic parameters throughout gestation in pregnant mice using high-frequency ultrasound.
Ultrasound Med. Biol., 2014, 40, 351-60. **IF: 2.214, Citations: 2**

Cumulative impact factor of peer-reviewed articles in the topic of the PhD Thesis: **6.468**

Cumulative impact factor of peer-reviewed articles: **13.088**

Number of citations: **15**

DOI:10.14753/SE.2015.1828

11. ACKNOWLEDGEMENTS

First of all, I would like to express my highest gratitude to *Professor Zoltán Papp* for supporting my PhD research work in the Doctoral Program that he leads at Semmelweis University. I highly appreciate his help in my admittance for the collaborative research program run at Wayne State University (WSU) and the Perinatology Research Branch of the *Eunice Kennedy Shriver* National Institute of Child Health and Human Development (NICHD), National Institutes of Health (NIH), Department of Health and Human Services (DHHS, Detroit, Michigan, USA). In addition, I am very grateful for his invaluable insights and critical feedback he has been providing all along my PhD research work and Thesis writing in the past four years.

I would also like to express my deepest gratitude to *Professor Roberto Romero*, Chief of the Perinatology Research Branch (NICHD, NIH), for his gracious support and the tremendous opportunity he provided for my research fellowship in Detroit. It was a privilege and a unique opportunity for me that not only enabled me to learn and expand my research skills and knowledge, but also supported the development of novel *in vitro* and *in vivo* methodologies and a new animal model of a human obstetrical syndrome. My collaborative works at the international, multi-disciplinary center of excellence he directs was highly stimulating and provided an exceptional experience from professional, intellectual and personal aspects.

I thank my supervisor, *Dr. Nándor Gábor Than* for his continuous supervision, support, guidance, advice and encouragement during my scientific endeavors in the past four years within the collaborative research program between Wayne State University, NIH and Semmelweis University. I am grateful for the opportunity to join the research group he directed, and I am thankful for my training and consultation in all research questions from designing experiments to writing manuscripts and this PhD Thesis, which had substantial impact on my scientific progress.

I would like to acknowledge the unhesitating support of *Professor András Vereczkei* and *Dr. Zalán Szántó* at the Surgical Clinic at the University of Pécs. This enabled my participation in a research program external to my home University, and thus, my professional and scientific development in frontier areas of surgery, obstetrics, imaging and molecular biology.

DOI:10.14753/SE.2015.1828

I take this opportunity to thank *Professors Sonia S. Hassan, Tinnakorn Chaiworapongsa (both WSU)* and *Offer Erez* (Ben Gurion University, Soroka, Israel) for their collaboration in the clinical part of our project, their helpful consultations regarding obstetrical aspects of the *in vivo* studies, useful advices, and support in summarizing and publication of our studies.

I express special thanks to *Drs. Yi Xu, Zhong Dong* and *Ted Price* (all WSU) for their helpful guidance and support in the *in vitro* laboratory work. I consider it a privilege to having worked with them, and their friendship and kindness have been a blessing.

I highly appreciated the guidance, support, insightful advices, and collaboration of *Drs. Edgar Hernandez-Andrade, Hyunyoung Ahn, Bing Wang* and *Mary King* (all NIH) in ultrasound examinations and the surgery of mice, as well as their friendship.

I am very grateful to *Dr. Adi L. Tarca, Zhonghui Xu* and *Gaurav Bhatti* (all WSU) for their unhesitating assistance with all kinds of statistical and bioinformatics issues, and the unforgettable, very helpful lunchtime and off-time discussions.

Special thanks go to *Drs. Faisal Qureshi* and *Suzanne M. Jacques* (all WSU) for their exceptional assistance with histopathological evaluations of the mouse tissues, and the useful training and consultations they provided in microscopic imaging.

I am indebted to *Rona Wang, Birgitta Sundell, Olesya Plazyo, Yang Jiang, Mary Olive, Lorrie McLuckie, Hong Meng, Stella Dewar, Jianhua Du,* and *Po Jen Chiang* (all NIH) for their help and technical assistance in *in vivo* and *in vitro* laboratory work.

I am appreciative for *Dr. Lisa J. Brossia-Root, Laura Lee McIntyre* (both WSU), *Angela Stoyanovitch* (Charles River Laboratories) for providing technical support for *in vivo* experiments, and for the staff at *Data Science International Inc.* (St. Louis, MN, USA) and *Visual Sonics Inc.* (Toronto, Canada) for the meticulous training in telemetry system implantation, microsurgical interventions and high-frequency ultrasound.

I also express my sincere thanks to *Valerie Richardson* (Yale University) and *Pat Schoff* (NIH) for artwork, to *Russ Price* (NIH) for technical assistance, and to *Sara Tipton* and *Maureen McGerty* (both WSU) for their critical reading of the manuscripts.

Last but not least, I am very thankful to my wonderful wife and our adorable sons. Without their continuous support my scientific and professional progress would not have been attainable. I also owe to express my gratitude to my parents and brother for the lifelong love and unconditional support they have been providing to me.